

Structure-Property Correlation as a Function of Donor and Acceptor Arrangement in Low Band Gap Materials

DISSERTATION

zur Erlangung des akademischen Grades
eines Doktors der Naturwissenschaften (Dr. rer. nat.)
im Promotionsprogramm

Fotophysik synthetischer und biologischer multichromophorer Systeme
der Bayreuther Graduiertenschule für Mathematik und Naturwissenschaften

vorgelegt von
Anne Neubig

Geboren in Pegnitz / Deutschland

Bayreuth, 2014

Die vorliegende Arbeit wurde in der Zeit von Januar 2010 bis Mai 2014 in der Arbeitsgruppe Angewandte Funktionspolymere am Lehrstuhl für Makromolekulare Chemie I der Universität Bayreuth unter der Betreuung von Herrn Prof. Dr. Mukundan Thelakkat angefertigt.

Vollständiger Abdruck der von der Bayreuther Graduiertenschule für Mathematik und Naturwissenschaften (BayNAT) der Universität Bayreuth genehmigten Dissertation zur Erlangung des akademischen Grades eines Doktors der Naturwissenschaften (Dr. rer. nat.).

Dissertation eingereicht am: 14.05.2014

Zulassung durch das Leitungsgremium: 15.05.2014

Wissenschaftliches Kolloquium: 27.06.2014

Amtierender Direktor: Prof. Dr. Franz Xaver Schmid

Prüfungsausschuss:

Prof. Dr. Mukundan Thelakkat (Erstgutachter)

Prof. Dr. Peter Strohriegl (Zweitgutachter)

Prof. Dr. Stephan Kümmel (Vorsitz)

Prof. Dr. Carlo Unverzagt

Meiner Familie

„Courage ist gut, aber Ausdauer ist besser“

Theodor Fontane

TABLE OF CONTENTS

| | |
|--|-----|
| 1. Summary | 1 |
| 2. Zusammenfassung | 5 |
| 3. Introduction | 9 |
| 3.1 <i>Low band gap materials</i> | 9 |
| 3.2 <i>Synthetic methods towards low band gap materials</i> | 21 |
| 3.3 <i>Charge carrier mobility in organic semiconductors</i> | 28 |
| 3.4 <i>Objectives of the thesis</i> | 36 |
| 4. Overview of the thesis | 47 |
| 5. Optical absorption in donor-acceptor polymers - alternating vs. random | 59 |
| 6. Random vs. alternating donor-acceptor copolymers: A comparative study of absorption and field effect mobility | 99 |
| 7. Optical gap tuning in thiophene-substituted naphthalenediimides | 119 |
| Danksagung | 143 |
| Erklärung | 147 |

1. SUMMARY

Low band gap (LBG) materials are of great interest since this class of compounds feature promising properties for application in a diversity of optoelectronic devices such as organic field effect transistors, organic light emitting displays or solar cells. A successful approach to extend the absorption to longer wavelength for LBG materials is the alternation of donor (D) and acceptor (A) units along a conjugated system. For a profound understanding of structure-property correlations in DA conjugated materials fundamental investigations are necessary.

This dissertation deals with the tailor-made syntheses and characterization of a variety of DA materials. Fundamental issues such as the specific arrangement of D and A units along the conjugated system, e.g. random or alternating, as well as the effect of increasing donor strength in donor-acceptor-donor systems are studied. The aim was to investigate the influences of such different DA arrangements on optical, electrochemical, and electronic properties. Therefore, a modular synthetic strategy was developed to achieve comparable DA systems. In particular this approach included the syntheses of novel bifunctional AB and AA/BB type monomers for the usage in Suzuki coupling reactions. Thus, directly comparable DA materials were synthesized. Due to this approach, we were able to obtain well-defined monodisperse low molecular weight compounds on the one hand and oligomers / polymers on the other hand. The fundamental question of charge transport in DA materials was examined by the preparation of organic field effect transistors (OFETs) and measuring typical output and transfer characteristics as well as by fabricating of single carrier devices using the space-charge limited current (SCLC) method.

The first part deals with well-defined monodisperse low molecular weight systems and oligomers with an alternating or random DA arrangement. DA materials consisting of 2,1,3-benzothiadiazole as acceptor unit and thiophenes as donor unit were synthesized. These compounds were investigated in a combined experimental and theoretical study. The latter was performed by using time-dependent density functional theory (TDDFT) based on non-empirically tuned range separated hybrid functionals. The fundamental question of whether the alternating or random arrangement of D and A units of conjugated materials have an impact on the optical absorption is addressed here. Due to its importance in light harvesting materials, the energy of the first electronic transition was studied. Our data suggests that the nature of the D and A arrangement has only little impact on the optical gap in such small molecular weight compounds.

The theoretical findings are in line with the experimental results. The first excitation energies for alternating and random systems vary no more than 0.09 eV in experiment and theory. Nevertheless, the interesting difference between experiment and theory lies in the absolute values of the excitation energies. We observed around 0.7 eV higher excitation energies in the experiment than for calculated ones for the oligomers. These differences for the excitation energies are larger than one would expect. However, in small molecular weight systems, a good agreement between experiment and theoretical calculations can be monitored. When the systems get larger, the difference between the experimental and calculated data increases. The excitation energy varies with the effective conjugation length. The experimental excitation energies start to saturate at $N = 15$, where N is the number of double bonds, whereas the saturation in calculation is at $N = 35$. This points out that different factors such as interactions between different chains, kinks and torsions in the structure can limit the effective conjugation length in real systems.

In the second part of the thesis, we extend our investigations on copolymers and their electrochemical as well as charge transport properties. For this, a target random copolymer was compared with two appropriate alternating copolymers, all consisting of 2,1,3-benzothiadiazole (B) as acceptor and hexylthiophene (T) as donor units. The aim was to evaluate the difference between random and alternating arranged conjugated copolymers in their properties. A randomly linked copolymer *r*-BTT was synthesized and compared with relevant alternating copolymers. The alternating copolymers are labeled as α -BTT where B units alternate with a bithiophene unit (TT) and α -BT in which one B unit is coupled with one thiophene unit (T). All copolymers show a high thermal stability ($T_{d-5\%} \geq 420$ °C) and *r*-BTT and α -BTT exhibit similar glass transition temperatures of 72 °C and 60 °C, while α -BT has a T_g of 122 °C. In chapter 6 *r*-BTT, α -BTT and α -BT are depicted as *r*-BT-2Th, α -BT-2Th and α -BT-1Th, respectively.

The solutions of copolymers *r*-BTT and α -BTT exhibit no considerable difference in absorption maximum in UV/Vis spectroscopy. In contrast, the copolymer α -BT shows a considerable red-shift of the absorption maximum indicating a better intra-chain delocalization / planarization. The corresponding absorption spectra in films are broadened for all copolymers. The copolymer α -BTT shows the most red-shifted absorption and a significantly reduced optical gap (1.75 eV) in thin films. This indicates stronger inter-chain interactions in α -BTT-H in solid state leading to an energetically more delocalized π -electron system than the other copolymers. The noticeable difference between both copolymers *r*-BTT and α -BTT is also reflected in the improved hole carrier mobility of $1.5 \times 10^{-3} \text{ cm}^2\text{V}^{-1}\text{s}^{-1}$ for copolymer α -BTT. This value is two

orders of magnitude higher than that for *r*-BTT. With this comparative study, we were thus able to elucidate the interdependence of the DA arrangement in donor-acceptor copolymer and material properties.

In the last chapter, low molecular weight donor-acceptor-donor materials were investigated. Herein, the relevant question of the influences of increasing the number of D units and thus the donor strength on optical, electronic and electrochemical properties was addressed. The goal was to decrease the optical gap to improve the absorption over a broad wavelength range. Therefore, the structure-property relationship for a series of donor-acceptor-donor model compounds was elucidated by a systematic study of optical and electrochemical properties. The donor-acceptor-donor materials were based on 1,4,5,8-naphthalenetetracarboxylic diimides (NDI) as acceptor and different thiophenes (T) as donor units. As a reference compound a NDI without any donor unit was synthesized. By extension of the NDI core with diverse thiophene donor units we were able to tune the donor strength within the T-NDI-T systems. In detail, the systematic increase of the donor strength was achieved by attaching substituents (thiophene, 3-hexylthiophene, bithiophene) at the acceptor core. The results show that the number of thiophene donor units does not affect the electrochemical reduction and thus the LUMO energy level. However, they drastically shift the HOMO energy level to higher values. Thus, with increasing donor strength we were able to selectively lower the band gap energies of T-NDI-T compounds by raising the HOMO energy level.

Altogether, new insights into structure-property relation of organic DA materials are presented in this work. By using novel monomers in a modular synthetic strategy, we were able to obtain directly comparable DA materials. These were examined in a precise manner and fundamental issues are clearly elucidated. As expected, the influence of the specific arrangement of donor and acceptor monomers on the optical gap in solution is limited. However, for copolymers in solid state, the charge transport properties and absorption are affected by the specific arrangement of D and A. It can be concluded that the multi-scale charge transport in solid state depends on inter-chain delocalization / coupling. Moreover, the detailed analysis of T-NDI-T low molecular weight systems helped to understand the influences of D and A in such systems and an approach towards lowering the optical gap via increasing the HOMO level is shown.

2. ZUSAMMENFASSUNG

Materialien mit kleiner Bandlücke (LBG) sind von hohem Interesse, da sie vielversprechende Eigenschaften aufweisen, die zur Anwendung in optoelektronischen Bauteilen, wie zum Beispiel Feldeffekttransistoren, organischen Leuchtdioden oder Solarzellen von Nöten sind. Eine erfolgreiche Strategie um eine Absorption auch im höheren Wellenlängenbereich zu ermöglichen, ist die Alternation von Donor (D) und Akzeptor (A) Einheiten entlang eines konjugierten Systems. Um die Struktur-Eigenschaftsbeziehungen von solchen konjugierten DA Materialien zu verstehen, sind fundamentale Untersuchungen erforderlich.

Diese Dissertation umfasst sowohl die maßgeschneiderte Synthese als auch die Charakterisierung und Untersuchung einer Vielzahl von DA Materialien. Es wurden grundlegende Aspekte untersucht, wie der Vergleich von konjugierten Systemen, die entweder statistisch oder alternierend angeordnete D und A Einheiten entlang des konjugierten Systems besitzen. Der Einfluss einer Zunahme der Donorstärke in Donor-Akzeptor-Donor Systemen ist ein weiteres Thema welches studiert wurde.

Ziel dieser Arbeit ist es die Einflüsse dieser unterschiedlichen DA Anordnungen auf die optischen, elektrochemischen und elektronischen Eigenschaften zu untersuchen. Um direkt vergleichbare DA Systeme zu erhalten wurde eine modulare Synthesestrategie entwickelt. Dazu wurden neuartige, bifunktionelle Monomere vom AB und AA/BB Typ synthetisiert und mittels Suzuki Kreuzkupplungsmethoden weiter umgesetzt. Dank dieser Strategie ist es gelungen einerseits wohldefinierte, monodisperse, niedermolekulare Verbindungen und andererseits sowohl Oligomere als auch Polymere zu synthetisieren und zum Vergleich heranziehen zu können. Der Ladungstransport der Materialien wurde mittels organischen Feldeffekttransistoren sowie der SCLC Methode („space-charge limited current“) und der Messung typischer Strom-Spannungs-Kennlinien grundlegend untersucht.

Der erste Teil dieser Dissertation beschäftigt sich mit wohldefinierten, monodispersen niedermolekularen und oligomeren Verbindungen mit einer alternierenden oder statistischen Anordnung der jeweiligen D und A Einheiten. Es wurden verschiedene DA Verbindungen synthetisiert, die als Akzeptoreinheit 2,1,3-Benzothiadiazol und als Donoreinheiten Thiophene besitzen. Verbindungen mit unterschiedlicher Länge wurden in einer kombinierten experimentellen und theoretischen Studie, die auf der zeitabhängigen Dichtefunktionaltheorie basiert, im Detail untersucht.

Die fundamentale Frage, ob statistische oder alternierende Anordnungen in DA

Systemen einen Einfluss auf die optische Absorption nehmen, wurde in diesem Teil der Arbeit gestellt. In lichtabsorbierenden Komponenten spielt die Energie der niedrigsten Anregung eine wichtige Rolle, daher stand diese bei unseren Untersuchungen im Fokus. Es konnte gezeigt werden, dass eine Variation der Anordnung der D und A Einheiten in solchen niedermolekularen Verbindungen lediglich einen geringen Einfluss auf die optische Lücke hat. Diese Ergebnisse sind sowohl für die theoretischen Berechnungen als auch für die experimentell bestimmten Energien der niedrigsten Anregung übereinstimmend, wobei die Differenz der alternierenden und statistischen Systeme im Bereich von 0.09 eV liegt.

Ein interessanter Unterschied zwischen Experiment und Theorie lässt sich in den Absolutwerten der Energien finden. Experimentell bestimmte Anregungsenergien liegen im Durchschnitt 0.7 eV höher als die theoretisch berechneten. Dieser Unterschied ist größer als erwartet, wobei die Werte der niedermolekularen Systeme sehr gut übereinstimmen. Durch Vergrößerung der Systeme wurde auch eine größere Differenz der Anregungsenergien zwischen Experiment und Theorie erkennbar. Die Anregungsenergien ändern sich mit der effektiven Konjugationslänge. Die experimentellen Anregungsenergien sättigen schon bei einer Anzahl von 15 Doppelbindungen, während die Sättigung in der Theorie erst bei 35 Doppelbindungen einsetzt. Dies weist darauf hin, dass verschiedene Einflüsse, wie zum Beispiel inter- und intramolekulare Wechselwirkungen, oder Verdrillungen innerhalb des Moleküls, die effektive Konjugationslänge in realen Systemen reduziert.

Im zweiten Teil dieser Arbeit wurden die Untersuchungen weiter auf die elektrochemischen und Ladungstransfereigenschaften von Copolymeren ausgedehnt. Für diese Studie wurde gezielt ein statistisches Copolymer mit zwei adäquaten alternierenden Copolymeren verglichen. Als Akzeptoreinheit diente 2,1,3-Benzothiadiazol (B) und als Donoreinheiten Hexylthiophene (T). Die Unterschiede der Eigenschaften zwischen statistischen und alternierenden Copolymeren, wurden gezielt untersucht. Dazu wurde ein statistisch verknüpftes Copolymer *r*-BTT synthetisiert und mit zwei alternierenden Copolymeren verglichen. Diese alternierenden Copolymere (*α*-BTT / *a*-BT) sind so verknüpft, dass sich eine Benzothiadiazoleinheit (B) entweder mit Bithiopheneinheiten (TT) oder mit einer Thiopheneinheit (T) abwechselt. In Kapitel 6 sind *r*-BTT, *α*-BTT und *a*-BT jeweils als *r*-BT-2Th, *α*-BT-2Th und *a*-BT-1Th bezeichnet.

Alle Copolymere weisen eine sehr hohe thermische Stabilität auf ($T_{d-5\%} \geq 420$ °C). Für *r*-BTT und *α*-BTT liegen die Glasübergangstemperaturen bei 72 °C und 60 °C, wobei *a*-BT einen T_g von 122 °C aufweist.

Während die Copolymere *r*-BTT und *α*-BTT keinen nennenswerten Unterschied im Absorptionsmaximum der jeweiligen Lösungen aufweisen, zeigt das Copolymer *α*-BT eine deutlich rotverschobene Absorption, was auf eine verbesserte intramolekulare Delokalisierung / Planarisierung schließen lässt. Im Vergleich zu den Absorptionsspektren in Lösung zeigen die UV/Vis-Spektren der Filme aller Copolymere eine Verbreiterung der Absorption. Hier weist das Copolymer *α*-BTT die größte Rotverschiebung in der Absorption, sowie eine signifikant verringerte optische Lücke (1.75 eV) auf. Dieses Resultat ist auf stärkere intermolekulare Wechselwirkungen in Filmen von *α*-BTT und damit auf ein größeres delokalisiertes π -Elektronensystem zurückzuführen. Dieser wesentliche Unterschied der Filmabsorption zwischen *r*-BTT und *α*-BTT wird auch in einem um zwei Größenordnungen verbesserten Lochtransport ($1.5 \times 10^{-3} \text{ cm}^2\text{V}^{-1}\text{s}^{-1}$) für das Copolymer *α*-BTT wiedergespiegelt. Durch diese Studie wurde erfolgreich die Wechselbeziehung zwischen der DA Anordnung in Donor-Akzeptor Copolymeren und deren Materialeigenschaften verdeutlicht.

Der letzte Teil dieser Dissertation behandelt niedermolekulare Donor-Akzeptor-Donor Verbindungen. Der Einfluss einer zunehmenden Anzahl an Donoreinheiten und dadurch veränderten optischen, elektrochemischen und elektronischen Eigenschaften wurde untersucht. Das Ziel war die optische Lücke zu verringern um dadurch die Absorption zu verbessern. Dies konnte anhand von einer Serie von Donor-Akzeptor-Donor Modellsystemen verwirklicht werden. Die Struktur-Eigenschaftsbeziehungen dieser Verbindungen wurden systematisch untersucht. Als Akzeptoreinheit dienten dabei 1,4,5,8-Naphthalintetracarboxyldiimide (NDI) und als Donoreinheiten verschiedene Thiophene (T). Ein am Kern unsubstituiertes NDI diente als Referenzverbindung. Durch die Erweiterung des NDI-Kerns mit verschiedenen Thiophenen war es möglich die Donorstärke innerhalb der T-NDI-T Systeme zu variieren. Durch die Anbringung von Donorsubstituenten (Thiophen, 3-Hexylthiophen, Bithiophen) wurde eine systematische Zunahme der Donorstärke erreicht.

Es konnte gezeigt werden, dass die Anzahl der Thiopheneinheiten am Kern zwar nicht die elektrochemische Reduktion und somit das LUMO Energielevel beeinflusst, jedoch das HOMO Energielevel drastisch erhöht. Durch eine Zunahme der Donorstärke konnte selektiv die optische Lücke verringert werden ohne das LUMO Energielevel merklich zu beeinflussen.

Zusammenfassend weist diese Arbeit neue fundamentale Erkenntnisse über Struktur-Eigenschaftsbeziehungen neuer organischer Donor-Akzeptor Verbindungen auf. Direkt vergleichbare DA Verbindungen wurden durch die Synthese neuartiger Monomere vom AB und AA/BB Typ und deren Einsatz in modularen Synthesestrategien erhalten. Diese Verbindungen wurden detailliert untersucht um neue

fundamentale Einblicke zu erhalten. Es zeigte sich, dass der Einfluss einer spezifischen Anordnung von Donor- und Akzeptoreinheiten auf die optische Lücke in Lösung limitiert ist. Erst in Filmen zeigte sich der Einfluss einer unterschiedlichen Anordnung der D und A Einheiten auf die Absorption und die Ladungstransporteigenschaften. Folglich hängt der Multiskalenladungstransport in diesen Systemen im Feststoff von inter-molekularer Delokalisierung / Kopplung ab. Zudem erweiterte die detaillierte Analyse von niedermolekularen T-NDI-T Systemen das Verständnis der Einflüsse von D und A und ein Ansatz in Richtung Verringerung der optischen Lücke mittels Zunahme des HOMO Energielevels wurde gezeigt.

3. INTRODUCTION

In the last decade low band gap (LBG) materials also called donor-acceptor (DA) materials have attracted much interest due to their promising properties for application in optoelectronic devices like solar cells^[1-3], organic field effect transistors (OFETs)^[4, 5], organic light emitting displays (OLEDs)^[6], electrochromic devices^[7-9] as well as imaging and sensing applications.^[10, 11] The origin of the term low band gap is discussed in the first part of this chapter together with the concept to achieve such low band gap materials. After a brief description of the state-of-the art of DA materials, a selection of acceptor units is presented in more detail. In the second part typical synthesis routes for obtaining LBG materials such as Suzuki or Stille coupling techniques are demonstrated. Afterwards, important device characterization methods for measuring charge carrier mobility are presented with focus on OFETs. As a last point, the objectives of this thesis are presented briefly.

3.1 Low band gap materials

Historical and theoretical background

The key experiment for the basis of quantum physics was the study of the photoelectric effect. The Nobel Prize in physics 1921 was awarded to Albert Einstein for the discovery of the law of this photoelectric effect.^[12] He postulated 1905 at first the particle nature of light and is one of the founders of the wave-particle dualism.^[13] His explanation resulted in Einsteins photoelectric equation, meaning that a photon that runs through a metal surface can transfer its whole energy ($h\nu$) to an electron. If the work function (ϕ) is the minimal amount of energy that is necessary to remove an electron from the surface of the metal, the maximal kinetic energy of the electrons which leave the surface is $h\nu - \phi$.^[14]

$$(E_{kin})_{max} = (\frac{1}{2} m v^2)_{max} = h\nu - \phi \quad (1)$$

where m is the electron mass, v the velocity, h Planck's constant and ν the frequency. The work function ϕ is illustrated in Figure 1. It is a characteristic parameter for metals that corresponds to the energy difference between Fermi level and vacuum level at zero Kelvin. The theoretically established differentiation between a conductor, an insulator, and a semiconductor was given in 1931 by Wilson.^[15] A

schematic picture of electronic band structures of these classes is depicted in Figure 1. Concerning semiconductors or insulators, the Fermi level lies in a forbidden band between the filled valence band and the empty conducting band. In the conductor, electrons can be easily excited to higher states and conductivity is possible. In semiconductors a gap has to be overcome. This energy gap is also called band gap and is relatively high for insulators. Thus, the electrons cannot pass this gap.^[14]

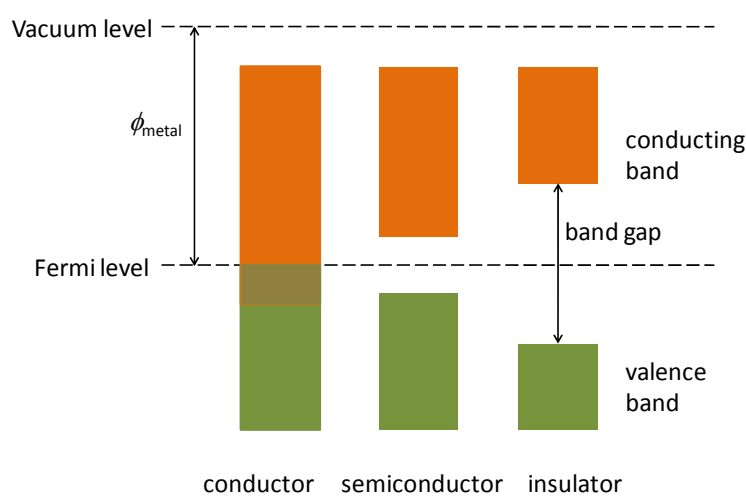


Figure 1: Three possible band structures of a solid. Conductor: permitted bands overlap. Semiconductor: A small energy gap exists between the permitted valence and conducting band. Insulator: The energy gap between the filled valence band and the empty conducting band is large. Adapted from Ref.^[14, 16]

The electronic band structure theory was the basis for modern semiconductor physics. When the 2000 Chemistry Nobel Laureates H. Shirakawa, A. G. MacDiarmid, and A. Heeger^[17] discovered and developed in 1977 conductive doped polyacetylene (PA), they opened the research area to organic materials that behave like semiconductors or even as conductors in contrast to the traditional insulators. Additionally, they represent the possibilities of inexpensive, flexible, and light-weight devices made from organic semiconductors. For this novel kind of materials the transitions between the different states have to be described. Therefore, as a simplification terms of the classical solid state physics were adapted. As a result, e.g. the band gap known from solid state physics is used for the difference in HOMO (highest occupied molecular orbital) and LUMO (lowest unoccupied molecular orbital) in semiconducting polymers.

In the literature, the term energy gap is widely used for a variety of gaps e.g.

fundamental gap, optical gap, HOMO-LUMO gap etc. This leads to confusion because it does not differentiate between the terms. Brédas^[18] recently addressed this problem in a focus article where he gave information about the concept behind the variety of energy gaps. The next section briefly summarizes this concept:

At the molecular level the vertical ionization potential (IP) corresponds to the HOMO level whereas the LUMO energy level can be considered as the vertical electron affinity (EA). The fundamental gap (E_{fund}) is the difference between the ionization potential and electron affinity ($E_{\text{fund}} = \text{IP} - \text{EA}$) as depicted in Figure 2a). The optical gap (E_{opt}) can be measured by absorption of a single photon which correlates to the energy of the lowest electronic transition. This energy is lower than the fundamental gap because a coulombically bound electron-hole pair is created by excitation. In Figure 2a) the difference between these E_{opt} and E_{fund} is illustrated as electron-hole pair binding energy E_{B} .

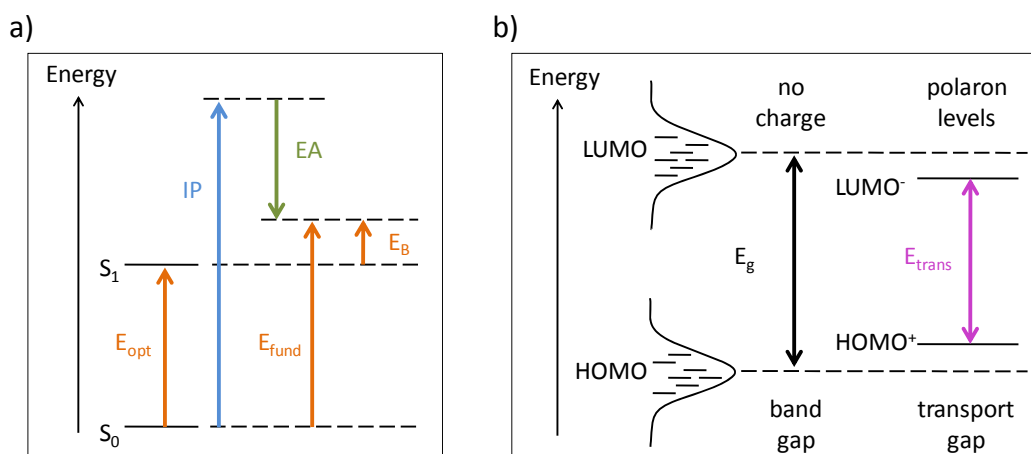


Figure 2: Illustration of schematic energy diagrams. **(a)** The molecular case: the energy difference between the electronic ground state (S_0) and the lowest excited state (S_1) is referred to the optical gap E_{opt} . The magnitude of the ionization potential IP and the electron affinity EA is shown in blue and green, respectively. The fundamental gap E_{fund} is the IP-EA energy difference. E_{B} is correlated to the electron-hole pair binding energy. Reproduced from Ref.^[18] **(b)** In polymeric materials in the ground-state and during charge transport: E_{g} is the ground-state band gap between uncharged HOMO-LUMO levels. The charged polaronic levels (HOMO⁺ and LUMO⁻) are separated by the transport gap E_{trans} that is shown in violet. Because of disorder, a Gaussian distribution of energy levels is assumed. Adapted from Ref.^[19]

Due to intermolecular interactions as well as energetic and structural disorder in polymeric materials, molecular energy levels are broadened leading to a Gaussian distribution of energy levels. The energy levels in the ground-state and during charge

transport are depicted in Figure 2b). The optical gap (E_{opt}) can be experimentally achieved by optical absorption whereas the ground-state band gap (E_g) and the uncharged HOMO-LUMO levels cannot be obtained directly. During charge transport positive or negative polaronic levels (HOMO^+ and LUMO^-) are separated by the transport gap E_{trans} ; they can be determined by a combination of ultraviolet photoelectron spectroscopy (UPS) and inverse photo-emission spectroscopy (IPES).^[19, 20] A more practicable and cheaper measurement used in many laboratories is cyclic voltammetry (CV). One must consider that with these methods (UPS, CV, etc.) the measurement conditions are completely different. For example CV measurements are often performed in solution and under diverse polar conditions, whereas UPS and IPES provide solid-state values. Hence, values obtained from several sources under diverse conditions are difficult to compare and have to be handled carefully.

Originally, the band structure engineering in organic conductive materials was motivated by the expectation, that π -conjugated polymers with narrow band gaps are promising materials for the use as an intrinsically conductive polymer and nonlinear optical devices.^[21-24] After the discovery of the conductive doped PA, the search for new organic semiconductors that have a non-degenerated ground-state was promoted to overcome the disadvantages of the PAs, such as their instability in atmosphere and insolubility.^[22] New heteroaromatic polymers such as polythiophene, polypyrrole and polyisothianaphthene were introduced in the early 1980s.^[25] As one important parameter for reducing the band gap E_g the bond length alternation (BLA) was identified. Soon it was pointed out that, electronic and optical properties are adjustable by controlling the polymer structure.^[21, 26]

The BLA is defined as the average difference between C-C single and C=C double bonds in a polyene chain. Introducing an energetically less stabilized quinoid resonance form in the conjugated polymer chain, leads to transfer of the C-C single bonds into C=C double bonds resulting in a decreasing BLA (*cf.* Fig. 3a)). Thus, the band gap can be lowered linearly as a function of increasing quinoid character.^[23, 26, 27]

Bearing in mind the importance of quinoid monomer segments along the chain, different copolymers were synthesized in the early 1990s by a combination of aromatic and quinoid monomer units that exhibit different electronic structures.^[21, 24, 28] Havinga *et al.*^[29, 30] showed 1992 the successful strategy to lower the band gap by alternation of electron-deficient (acceptor) and electron-rich (donor) units along the conjugated polymer chain. This concept uses the introduction of strong push-pull driving forces that facilitate electron delocalization along the polymer chain and thus enhancing the quinoid character in these systems. Besides the energy related to BLA

($E^{\delta r}$) other factors determine the band gap energy, such as torsion angle E^{θ} , resonance energy E^{Res} , substituents E^{Sub} and intra- and intermolecular interactions E^{Int} (cf. Fig 3b))^[23, 31].

$$E_g = E^{\delta r} + E^{\theta} + E^{Res} + E^{Sub} + E^{Int} \quad (2)$$

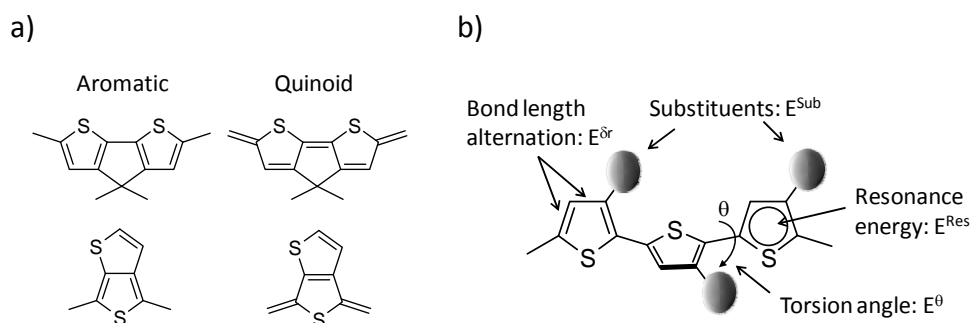


Figure 3: (a) Comparison of aromatic and quinoid resonance structures along a polymer section. (b) Factors influencing the band gap (E_g) in linear conjugated systems: bond length alternation ($E^{\delta r}$), substituents (E^{Sub}), torsion angle (E^{θ}) and resonance energy (E^{Res}). Intra- and intermolecular interaction are not shown here. Adapted from Ref.^[22]

State-of-the art

Based on the pioneering work of Havinga *et al.*^[29] exactly this successful DA approach was used to tune the properties of a huge number of LBG molecules for a variety of applications. The research field of organic semiconductors has grown enormously because their optoelectronic properties are tunable by well-defined, convenient change in chemical structure, promising a great potential for these materials. Moreover, semiconducting materials possess a large processing versatility. With solution-based processing, a high-throughput fabrication at low temperatures and thus, flexible, large-area and low cost devices are achievable. Yan *et al.*^[32] utilized in 2009 the donor-acceptor copolymer poly{[*N,N'*-bis(2-octyldodecyl)-naphthalene-1,4,5,8-bis(dicarboximide)-2,6-diyl]-alt-5,5'-(2,2'-bithiophene)} (P(NDI2OD-T2)) for the first gravure printed n-type transistor under ambient conditions with an extraordinary high-mobility up to $0.85 \text{ cm}^2 \text{ V}^{-1} \text{ s}^{-1}$ (cf. Fig. 4).

Regarding organic photovoltaic (OPV) devices, cost-effective manufacturing printing techniques (inkjet-, roll-to-roll, flexo-printing, etc.) on flexible substrates are successfully shown mainly with the well-studied poly(3-hexylthiophene) (P3HT) as the p-type moiety in combination with fullerene (PCBM) as acceptor. In recent years,

some low band gap π -conjugated polymers have been used for large area modules.^[33, 34] The large scale processed modules are so far not competitive with lab scale organic solar cells that predict certified thin film solar cell efficiencies of up to 9.2 %.^[35]

One of the most prominent low band gap polymer for bulk heterojunction solar cells is the thieno[3,4-b]thiophene / benzodithiophene based p-type polymer PTB7 (cf. Fig. 5) which is usually blended with [6,6]-phenyl C₇₁-butyric acid methyl ester (PC₇₁BM). Applying PTB7 in conventional-type BHJ solar cells, power conversion efficiencies of 8.37 % were obtained.^[36] Changing the solar cell type to an inverted structure led to a further increased certified efficiency of 9.2 %.^[35]

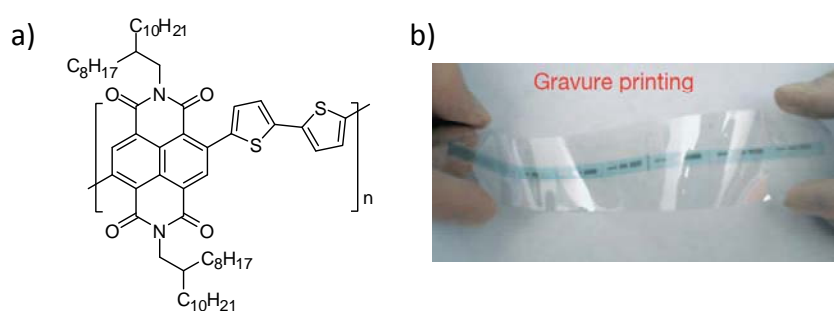


Figure 4: (a) Chemical structure of n-type polymer P(NDI2OD-T2) (b) Optical image of gravure-printed n-channel polymeric TFT on a plastic substrate (PET, polyethyleneterephthalat) before top-gate contact deposition. Reproduced from Yan et al.^[32]

Amb *et al.* demonstrated successfully different spray-processable DA π -conjugated polymers for the application in electrochromics and as ambipolar polymers in organic field effect transistors.^[5, 37] Impressive record hole-mobilities in OFETs as high as 23.7 cm²V⁻¹s⁻¹ were achieved recently via macroscopic alignment of the low band gap polymer PCDTPT into oriented fibers by Tseng *et al.* (cf. Fig. 5).^[4] To give a short overview over the great variety of DA materials a selection of different prominent DA low band gap polymers is given in Figure 5.

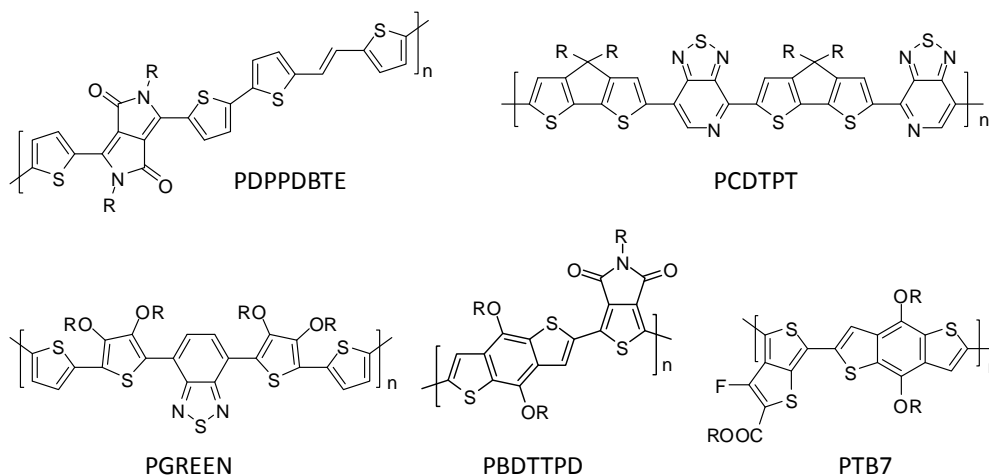


Figure 5: Illustration of important low band gap donor-acceptor polymers based on diketopyrrolopyrrole- (PDPPDBTE)^[38], thiadiazolo[3,4-c]pyridine- (PCDTPT)^[4], benzothiadiazole- (PGREEN)^[34], thieno[3,4-c]pyrrole-4,6-dione- (PBDTTPD)^[39] and thienothiophene- (PTB7) acceptor units.^[35] R= alkyl.

In comparison to low band gap polymers applied in different devices by solution-processing, small-molecules have received attention in multilayer devices prepared by vapor deposition. The semiconductor polymers exhibit batch-to-batch variations in terms of molecular weight, polydispersity, solubility as well as purity that influence processability and thus the performance.^[3, 40] In contrast, small molecule semiconductors are easy to scale up and exhibit a higher batch-to-batch reproducibility as well as a well-defined molecular structure and they are monodisperse.^[41] Due to these striking properties the research in the low molecular weight field has also moved to the donor-acceptor approach for the successful application in OPVs^[1, 2, 42, 43] and OFETs^[40, 44] (cf. Figure 6).

Within the last years, increasing number of solution-processed DA small molecules as donor material in OPVs led to remarkable power conversion efficiencies up to 7%.^[1-3] Furthermore, DA small molecules were also implemented in OFETs. Recently, a donor-acceptor-donor type small molecule (DHB-QDTB) utilized in a n-type OFET showed a high electron mobility ($0.88 \text{ cm}^2\text{V}^{-1}\text{s}^{-1}$) under ambient conditions.^[44] A relatively high hole mobility ($1.4 \text{ cm}^2\text{V}^{-1}\text{s}^{-1}$) was shown for a Pechmann dye based solution processed donor-acceptor-donor molecule in OFETs (BTBPD).^[40] A selection of successfully applied low molecular weight DA materials into OPVs and OFETs is depicted in Figure 6.

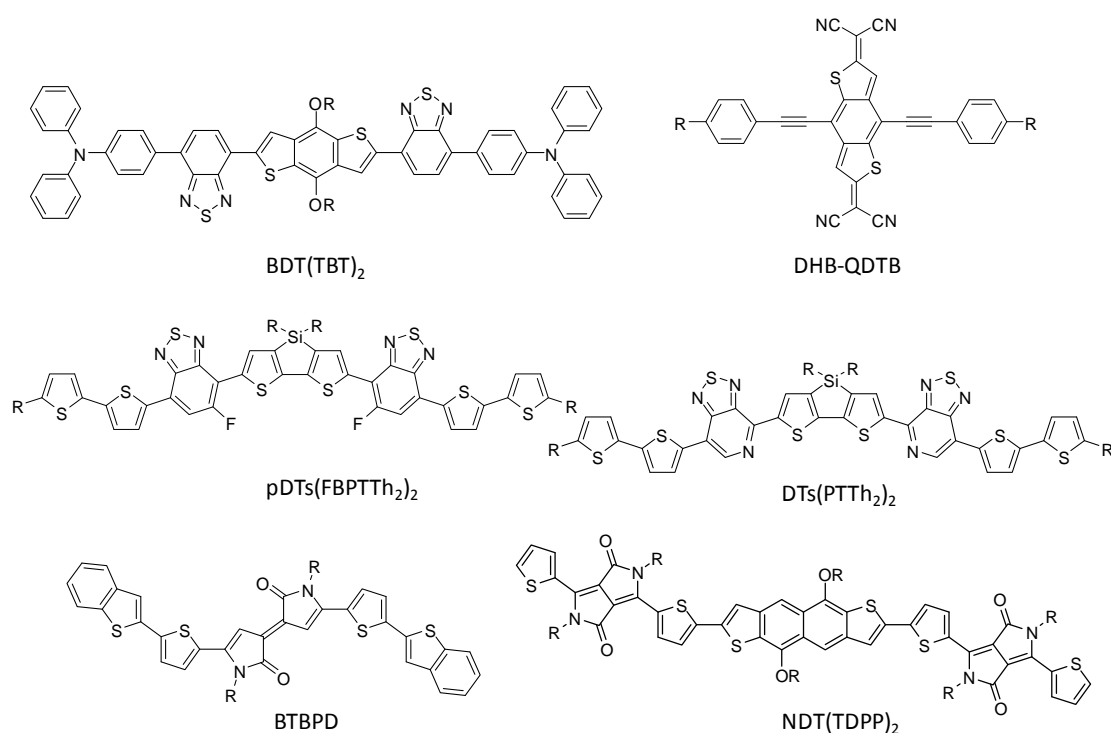


Figure 6: Illustration of solution-processable DA small molecules: $\text{BDT}(\text{TBT})_2$ ^[2] with dialkoxy-substituted benzo[1,2-b:4,5-b']dithiophene (BDT) as central donor unit; DHB-QDTB ^[44] with a quinoidal BTD acceptor; $\text{pDTs}(\text{FBPTTh}_2)_2$ ^[1] comprised of a silolo[3,2-b:4,5-b']dithiophene central unit and a 5-fluorobenzo[c][1,2,5]thiadiazole acceptor in contrast to $\text{DTs}(\text{PTh}_2)_2$ ^[3] that exhibits a pyridyl[2,1,3]-thiadiazole acceptor unit. BTBPD ^[40] with a [3,3'-bipyrrrolylidene]-2,2'(1H,1'H)-dione acceptor and $\text{NDT}(\text{TDPP})_2$ ^[43] with a naphtha[2,3-b:6,7-b']dithiophene donor. R = alkyl.

In the next section I emphasize some prominent acceptor units in more detail, namely 2,1,3-benzothiadiazoles (B) and 1,4,5,8-naphthalenetetracarboxylic diimides (NDI). The characteristic properties as well as synthetic structures based on these units towards DA low molecular weight and polymeric materials are presented.

2,1,3-Benzothiadiazole (B) based donor- acceptor materials

2,1,3-Benzothiadiazole derivatives gained increased attention within the last decade. They were successfully applied as antibacterials, fluorescent dyes, organic conductors as well as biosensors and others.^[45] As described above, with incorporation of D and A units that possess a quinoid resonance structure in a conjugated DA material, the BLA can be lowered. 2,1,3-benzothiadiazole (B) derivatives are well suited for the application in such DA materials since the B building block has a strong tendency to impose a quinoid resonance structure on the ground

state of the conjugated system (*cf.* Fig.7).^[46] Moreover, two electron-withdrawing imine nitrogen atoms are present in B units, leading to high electron affinity. 2,1,3-Benzothiadiazole derivatives are important compounds for organic light emitting devices e.g. OLEDs, as they possess a relatively high electron affinity, reversible electrochemical reduction and strong fluorescence.^[45] The following section gives a short overview of 2,1,3-benzothiadiazole based DA polymers and DA low molecular weight materials.^[45]

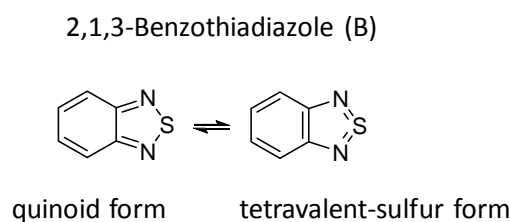


Figure 7: Resonance structures of 2,1,3-benzothiadiazole (B).^[45]

Recently, Mathew *et al.*^[47] published a broadly absorbing porphyrin dye (SM315; *cf.* Fig. 8) that depicts a donor- π -bridge-acceptor structure. Incorporation of a proquinoidal B unit into the porphyrin structure lead to strong perturbations within the electronic structure that improved light harvesting in dye sensitized solar cells resulting in a record power conversion efficiency of 13 %. Furthermore, 2,1,3-benzothiadiazole based DA materials have the potential to serve as an emitter for OLEDs. They provide high emission quantum yields as well as photoluminescence emission in solution that can be tuned from a bluish-green to a dark red emission by structural variation. With a non-doped solution-processable molecular B based emitter, a pure red electroluminescence without the necessity for a hole-blocker was achieved, showing the importance of this class of materials.^[48]

Some of the most popular DA low band gap polymers for the use in luminescent devices contain B as acceptor units. Their inherent properties can be varied by a clever combination with different comonomers resulting in a wide applicability. For example, polymers consisting of more than one electron accepting unit show excellent OFET electron mobilities of $0.02 \text{ cm}^2\text{V}^{-1}\text{s}^{-1}$ (*cf.* Fig. 8, P1).^[49] 2,1,3-Benzothiadiazole containing polymers are also used in organic light-emitting field-effect transistors (LEFETs) as well. LEFETs provide the advantage of a combination of the light-emitting ability of OLEDs with the electrical switching characteristics of organic transistors. In particular, LEFET devices are of great interest e.g. for organic electrical injection lasers.

They may be brighter and more efficient than OLEDs, hence could act as alternative in displays or optoelectronic switches.^[50] Gwinner *et al.*^[51] utilize single, solution-processed layers of the DA copolymer F8BT (*cf.* Fig. 8) for an ambipolar LEFET showing external quantum efficiency (EQE) values $> 8\%$ and luminance efficiencies $> 28 \text{ cdA}^{-1}$.

Moreover, polymers containing 2,1,3-benzothiadiazole units are suitable for electrochromic devices (*cf.* Fig. 8, P7) and as semiconducting polymer dots in water for imaging and sensor applications.^[7, 9, 10] Regarding OPVs, B based polymers are investigated by many groups. Worth mentioning are PGREEN and PCDTBT. PGREEN (*cf.* Fig. 5) is one of the first low band gap polymer used in roll-to-roll (R2R) printed large area solar cells instead of utilizing P3HT as active donor material.^[34] PCDTBT (*cf.* Fig. 8) is one of the best performing low band gap polymers used in BHJ devices with power conversion efficiencies as high as 7.1%. Furthermore, PCDTBT is able to reach an internal quantum efficiency of 100% at around 450 nm.^[52]

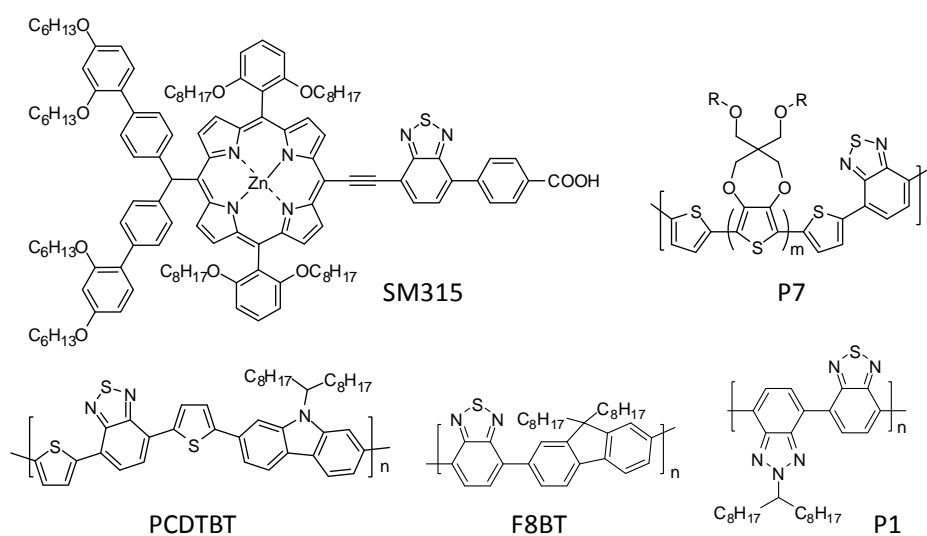


Figure 8 : Illustration of important 2,1,3-benzothiadiazole based DA materials: SM315^[47] a panchromatic porphyrin sensitizer with a bis-(2',4'-bis(hexyloxy)-[1,1'-biphenyl]-4-yl)amine donor; P7^[9] a polymer electrochrome consisting of 3,4-propylenedioxy-bridged thiophene units; PCDTBT^[52] a high-performance polymer in solar cells features a 2,7-carbazole donor; F8BT^[51] consists of 9,9-dioctylfluorene donor; P1^[49] made solely of electron-accepting units (B and benzotriazole).

1,4,5,8-Naphthalenetetracarboxylic diimide (NDI) based donor-acceptor materials

A further important acceptor building block in DA compounds is 1,4,5,8-naphthalenetetracarboxylic diimide, also called naphthalene diimide (NDI). This section refers to the literature survey about the chemistry and application of NDIs as well as NDI based copolymers.^[53] An illustration of different interesting NDI derivatives is given in Figure 9.

The compact, aromatic NDIs are characterized by their highly electron deficient character that results from two electron-withdrawing imide groups. Hence, they exhibit low lying LUMO energy levels and exhibit high electron mobilities. Additionally, their chemical and photochemical stability makes them interesting candidates for the application in supramolecular chemistry, electron transfer systems and organic electronic devices. Adjustable absorption and emission properties by functionalization at carbons 2,3,6,7 of the NDI core lead to highly colored, functional materials that have attracted more and more interest during the last years. The substituents on the nitrogens have in general less influence on the electronic properties due to the presence of a nodal plane on the nitrogen of the diimide groups. Functionalization through the imide nitrogens is frequently used to introduce solubility enhancing substituents.

Porphyrin donor - NDI acceptor dyads are excellent model systems to study the electron transfer dynamics. Mimicking the process of photosynthesis, or at least parts thereof is of particular interest to gain insight into photosynthetic reaction centre processes. The electron transfer from photo-excited porphyrin derivatives to a linked NDI moiety is energetically similar to the natural porphyrin-quinone system.^[54, 55] Photo-induced ultrafast electron transfer was reported in a covalently linked zinc(II) tetraphenylporphyrin-amino naphthalene diimide dyad (ZnTPP-ANDI), revealing an efficient electron transfer process occurring from the initially excited S₂ state of the donor (*cf.* Fig 9).^[54]

NDIs were used in dyads (DPP-NDI) for NiO p-type dye-sensitized solar cells as well (*cf.* Fig 9). A diketopyrrolopyrrole (DPP), as a common acceptor unit, linked to a secondary electron acceptor (NDI) demonstrated a power conversion efficiency of 0.18 % with a cobalt complex as redox shuttle.^[56] Polander *et al.* published n-channel OFETs based on solution-processed small molecule NDI₂-X derivatives with conjugated fused heterocycle ring systems. OFETs fabricated of NDI₂-DTP (*cf.* Fig 9) exhibit electron mobilities as high as 1.5 cm²V⁻¹s⁻¹.^[57] The excellent electron transport property of this class of materials was also exploited to replace the fullerene acceptor

in BHJ solar cells. NDI substituted with oligothiophenes in the core position were combined with P3HT as donor material resulting in a PCE of 1.5 %.^[58]

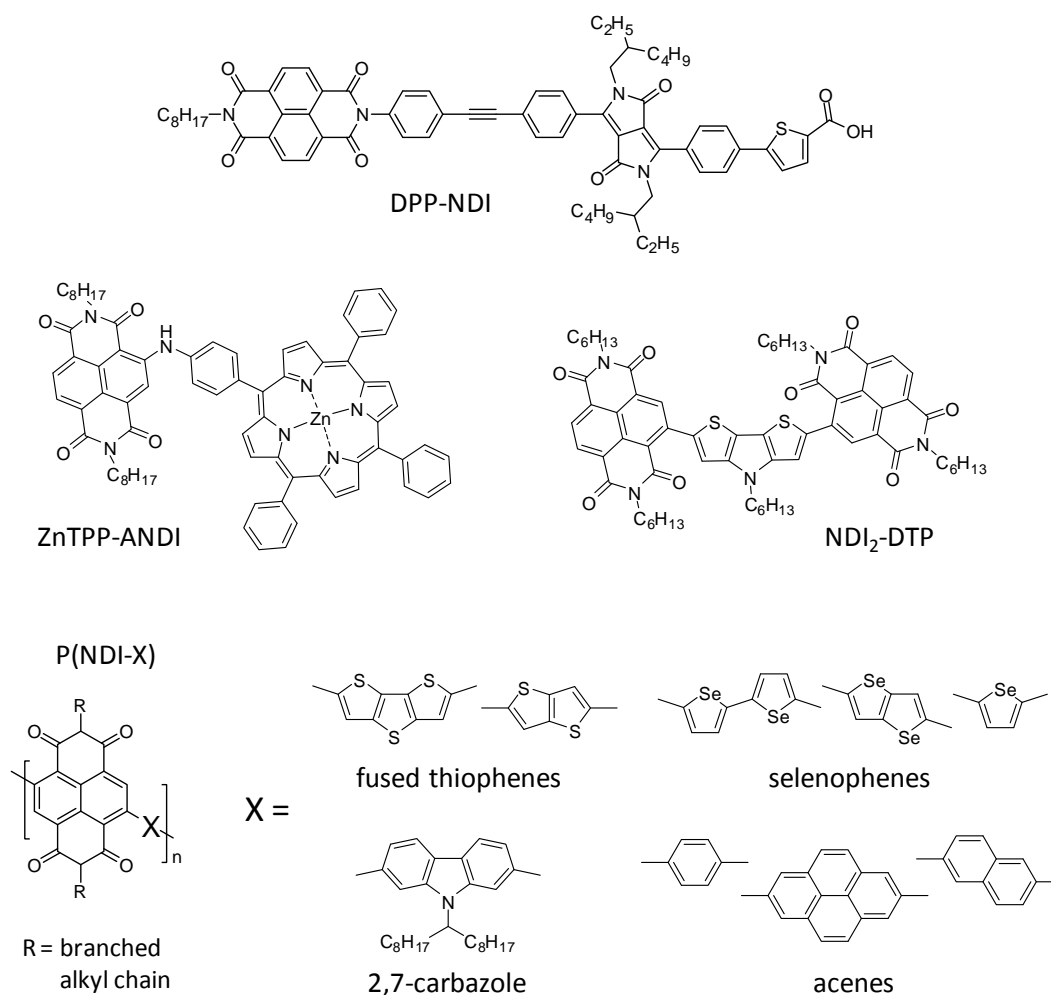


Figure 9: Illustration of important naphthalene diimide (NDI) based DA materials: DPP-NDI a diketopyrrolopyrrole-based dyad; ZnTPP-ANDI^[54] a zinc(II) tetraphenylporphyrin-amino NDI dyad; NDI₂-DTP^[57] with dithieno[3,2-b:2',3'-d]pyrrole as central unit; polymers of NDI P(NDI-X) with different comonomers in the main chain such as fused thiophenes^[59], selenophenes^[60, 61], 2,7-carbazole^[62] or acene-based comonomers^[63].

As described above, one of the most prominent NDI based DA copolymer is P(NDI2OD-T2) (*cf.* Fig 4). Besides its outstanding electron mobility ($0.85 \text{ cm}^2\text{V}^{-1}\text{s}^{-1}$) as measured in an OFET under ambient conditions, it also provides excellent electron mobilities ($\approx 5 \times 10^{-3} \text{ cm}^2\text{V}^{-1}\text{s}^{-1}$) in bulk which were measured with time of flight (ToF) and space charge limited current (SCLC) techniques.^[64] Meanwhile, several other conjugated copolymers consisting of NDI with different aromatic donor comonomers

in the main chain are published. In order to shine light on this kind of systems, systematic studies of copolymers based on NDIs coupled with oligothiophenes, fused thiophenes and also with “thiophene-free” donors were performed.^[59, 62, 63]

Not only low molecular weight NDIs but also NDI based acceptor copolymers were used for replacing the fullerenes in BHJ solar cells. All-polymer solar cells consisting of alternating DA copolymers of NDI and 2,7-carbazole as acceptor material and a PTB7 based copolymer modified with tris(thienylenevinylene) side chains as donor material show a record PCE of 3.64 %.^[65] Additionally, DA copolymers comprised of NDI and selenophene units provide electron field-effect mobilities of $0.24 \text{ cm}^2\text{V}^{-1}\text{s}^{-1}$ and in combination with a thiazolothiazole copolymer donor delivered all-polymer solar cells with a PCE of 3.3 %.^[60] Figure 9 illustrates a selection of NDI based DA small molecules and polymers. In conclusion, low band gap systems are an extraordinary interesting class of materials. With these materials impressive performances in devices were achieved which may be also contributed to the great variety of LBG systems. This diversity is obtained by just combining different D and A units. Usually the D and A units are arranged in an alternating fashion, but in this thesis the effect of a random arrangement on the properties should be studied as well. The different synthetic methods to achieve LBG materials are therefore presented in the next chapter.

3.2 Synthetic methods towards low band gap materials

For the synthesis of LBG materials several methods are available as described in the literature. Especially transition metal catalyzed carbon-carbon coupling reactions are of particular interest since they provide a great variety of complex compounds from readily accessible reactants.^[66] Among them, palladium (Pd) - catalyzed cross-coupling reactions are a powerful tool in monomer and polymer synthesis. The most commonly used palladium-catalyzed carbon-carbon coupling reactions are Heck, Sonogashira, Negishi, Stille, and Suzuki(-Miyaura) reactions.^[67] These coupling reactions are presented in detail in the following and an overview of the reactions is illustrated in Figure 10.^[67]

The palladium-catalyzed coupling of alkenyl or aryl halides or triflates with alkenes is called Heck reaction. It is a robust and efficient method for generating carbon-carbon bonds. The coupling of terminal alkynes with vinyl or aryl halides catalyzed by palladium and a cocatalytic Cu(I) salt is titled Sonogashira reaction which is a method for the synthesis of conjugated acetylenic systems. When highly reactive organozinc reagents as nucleophilic compounds are used, the reaction is called Negishi coupling.

Since the organozinc reagents exhibit a low toxicity, the Negishi coupling is an alternative to other cross-coupling reactions. One of the most widely applied palladium-catalyzed reactions to form carbon-carbon bonds is known as Stille reaction. The Stille reaction features a mild and versatile reaction with tolerance of a wide variety of functional groups. It includes the cross-coupling of organic electrophiles with organotin compounds. An extraordinarily useful coupling method that involves organoborane derivatives is the Suzuki(-Miyaura) coupling. In the next section I want to focus on this coupling reaction since it is the method of choice for obtaining conjugated donor (D) - acceptor (A) materials in this work.^[68-71]

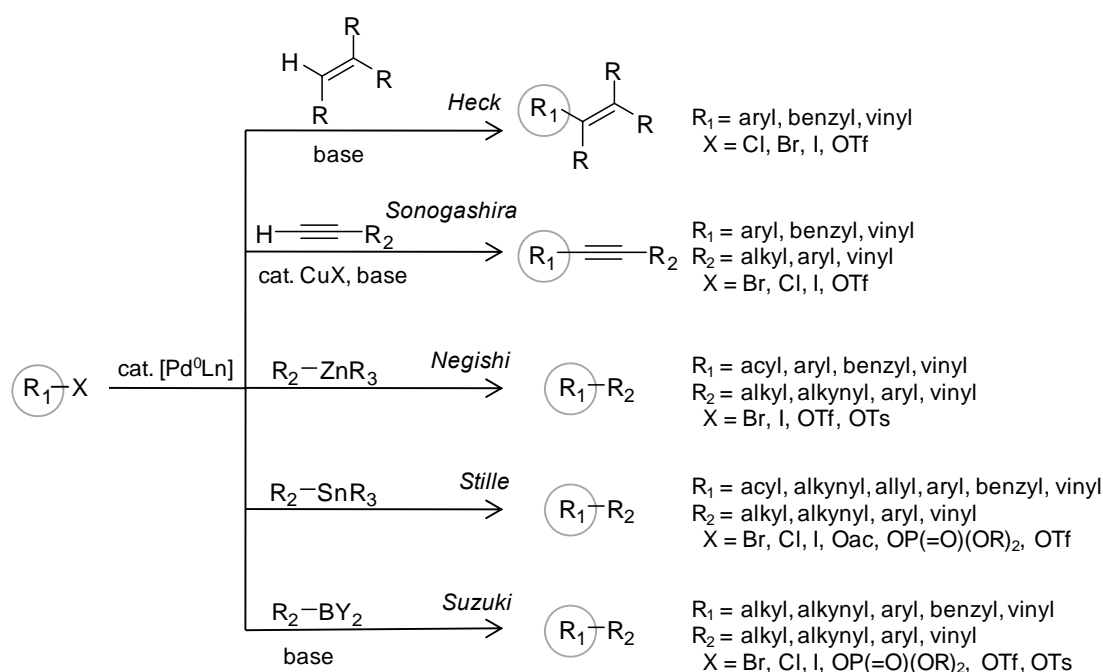


Figure 10: Overview of selected palladium-catalyzed carbon-carbon cross-coupling reactions. Adapted from Ref.^[67]

Suzuki(-Miyaura) cross coupling reaction

The palladium-catalyzed cross-coupling of alkenyl and aryl halides with organoborane derivatives in the presence of a base is a well-established procedure for generating carbon-carbon single bonds. The Suzuki coupling features mild reaction conditions, stereoselectivity as well as regioselectivity. Easily accessible reagents which exhibit low toxicity, in particular compared to tin-containing derivatives used in Stille reaction, can be utilized. The mechanism of the Suzuki coupling reaction which

involves oxidative addition-transmetalation-reductive elimination sequences is depicted in Figure 11.

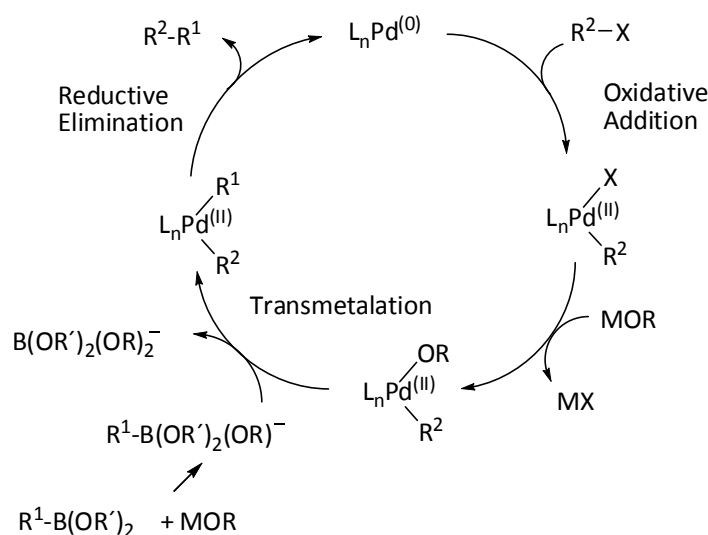


Figure 11: The mechanism of the Suzuki coupling reaction. $MOR = e.g. NaOH$; $MX: X = I, Br, Cl$. Adapted from Ref.^[68]

In the first step of the catalytic cycle the organic halide is added to the coordinative unsaturated palladium(0) complex achieving a palladium(II) complex (oxidative addition). The weak carbanion character of the boron compound has to be enhanced by adding a base. With base the boron-containing reagent forms a more nucleophilic tetravalent boron derivative. Therefore, the transmetalation of the carbon from boron to the $R^2-Pd(II)L_n-OR$ complex is facilitated. This more reactive $R^2-Pd(II)L_n-OR$ complex is formed with help of the base from the $R^2Pd(II)L_n-X$ complex. The reductive elimination as final step lead to the desired product by regeneration of the palladium catalyst to its initial oxidation state Pd(0) (cf. Fig. 11). The oxidative addition is often the rate-determining step. The reaction rate is dependent on the utilized halide whose relative reactivity decreases in the order of $R^2-I > R^2-Br \gg R^2-Cl$.

The most common and cheap bases that are employed for such reactions are $NaOH$, K_2CO_3 , Et_3N or Na_2CO_3 . Moreover, water as cosolvent can be utilized with a variety of solvents such as DMF, toluene, $MeOH$, THF or dioxane. The use of pure water shows the potential of the Suzuki coupling to be a very eco-friendly reaction. Commonly used catalysts are e.g. $Pd(PPh_3)_4$ or $Pd_2(dba)_3$ which are already in the zerovalent Pd state. Also precatalyst systems in the Pd(II) state in combination with respective reducing agents have attracted attention. In such systems a Pd(II) source e.g. $PdCl_2$ or $Pd(OAc)_2$

is used for in-situ generation of the active Pd(0) species.^[72] Widely used reducing agents are phosphines, among them triphenylphosphine (PPh₃) is by far the most frequently used, which also works as ligand.

A huge effort was made in the development of catalyst systems for Suzuki coupling reactions targeting mild conditions, higher turn-over numbers as well as higher efficiencies. They were successfully demonstrated especially for the use of less reactive aryl chlorides and even for sterically hindered substrates under mild conditions e.g. by the combination of bulky, electron-rich phosphine ligands (PCy₃, P(*t*-Bu)₃) with PdCl₂ or Pd₂(dba)₃.^[73]

One example for a catalyst system with wide application, reactivity and stability is using Buchwald's biaryl based phosphine ligands.^[74] Since phosphine ligands are expensive and difficult to recover, Suzuki cross coupling reactions without phosphine ligands are desirable. One strategy to avoid phosphine ligands is the application of colloidal Pd nanoparticles as active catalyst that provides a large surface area and therefore a high activity. In order to avoid agglomeration, stabilizing agents which offer either electrostatic or steric stabilization are needed.^[72, 75] Reetz *et al.*^[76] reported Pd nanoparticles stabilized with tetraalkylammonium salts for the Suzuki coupling reaction. Another attractive strategy is to use palladium on carbon (Pd/C) in aqueous medium without any ligand.^[77]

From an environmental point of view it is desirable to carry out the reactions in water. Therefore water-soluble precatalysts and ligands are needed. Liu *et al.*^[78] showed a new Pd(0)/ligand system with water-soluble ligands in a Suzuki polycondensation in a THF/water reaction medium. They demonstrated higher molecular weights compared to Pd(PPh₃)₄. Especially, they were able to decrease the residual Pd in the final products after scavenger extraction. It has to be considered that reactive catalysts used in the Suzuki coupling reaction for single C-C bond formation are not automatically usable for the Suzuki polycondensation reaction which is described in the following.

Suzuki polycondensation (SPC)

Employing the Suzuki cross-coupling reaction to synthesize a conjugated polymer – poly(*p*-phenylene) – was first reported by Schlüter and coworkers in 1989.^[79] This opens the research field towards numerous polyarylenes and other unsaturated polymers via the so-called Suzuki polycondensation (SPC) method. The polymers can be usually built up from monomers either by the AA/BB or the AB type monomers via

step-growth polycondensation. These two different approaches are illustrated in Figure 12.

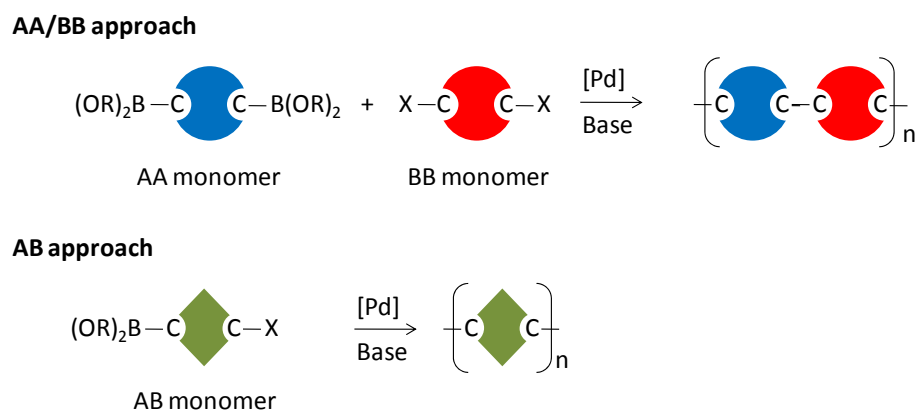


Figure 12: The two different approaches for Suzuki polycondensation based on AA/BB type monomers (top) and AB type monomers (bottom). As the A functionality boronic acids or acid esters (e.g. pinacol esters) are typically used. Commonly, the leaving group X is Br, but it can also be I, OTf or Cl. Adapted from Ref.^[80]

In the AA/BB strategy, typically two types of monomers are coupled together, each of them bearing either two boron or two halide functionalities. This strategy leads to conjugated polymers consisting of two aromatic units arranged in an alternating fashion. In contrast, the AB approach utilizes only one kind of an aromatic monomer carrying both the functional groups, boronic acid and halide, in one molecule. Hence, they are non-symmetric and need to be synthesized via multi-step procedures. The AA/BB monomers are easier to synthesize since they exhibit in many cases a symmetrical structure, which is a main reason for the popularity of the AA/BB approach.

For the purpose of accessing high-molar mass polymers, the two AA/BB monomers have to be applied in perfect stoichiometric balance of a 1 : 1 mole ratio, while AB type monomers feature intrinsically this balance between the functional groups. Using both the AA/BB type and AB type approaches usually alternating copolymers can be obtained. In order to achieve copolymers with a random arrangement of donor (D) and acceptor (A) units, two different AB monomers (of D and A) are needed. However, the two monomers are statistically incorporated into the polymer backbone with this strategy.

According to a typical step-growth profile bifunctional monomers react with each other to form first oligomers. They grow by stepwise reaction of monomers to oligomers and finally to polymers.^[81] Carothers equation^[82] describes the dependence of the number average degree of polymerization P_n on monomer conversion p .

$$P_n = \frac{1}{1-p} \quad \text{with } p = \frac{N_0 - N_t}{N_0} \quad (3)$$

where N_0 is the initial number of molecules and N_t the number of molecules at a time t . As shown in Figure 13 as soon as 90 % conversion (p) is achieved the average degree of polymerization (P_n) reaches the value 10. To obtain a P_n of 50 a conversion of 98 % has to be guaranteed. For obtaining high molar mass polymers extremely high conversion and no side-reactions are required. Consequently, the purity of monomers is of special importance and storage, weighing, transfer to the flask etc. has to be carried out with great care. When the monomers are not present in stoichiometric quantities the Carothers equation is extended by a stoichiometric ratio r .

$$P_n = \frac{1+r}{1+r-2rp} \quad \text{with } r = \frac{N_A}{N_B} \leq 1 \quad (4)$$

where r is the stoichiometric ratio of reactants. N_A and N_B the initial number of the respective functional groups A or B. In the case of $r = 1$ (i.e. for exact stoichiometry) equation (4) simplifies to the Carothers equation (3). For non-stoichiometric reactants the ratio of reactants get below 1, means that this results in a drastic decrease of molecular weight. Since the step-growth reactivity of functional groups is not dependent on the chain length and P_n increases linearly with the reaction time, one ensures higher conversions by applying longer reaction times up to several days. Therefore, under the assumption that side reactions are suppressed, one would expect that high molar mass polymer chains can be achieved.

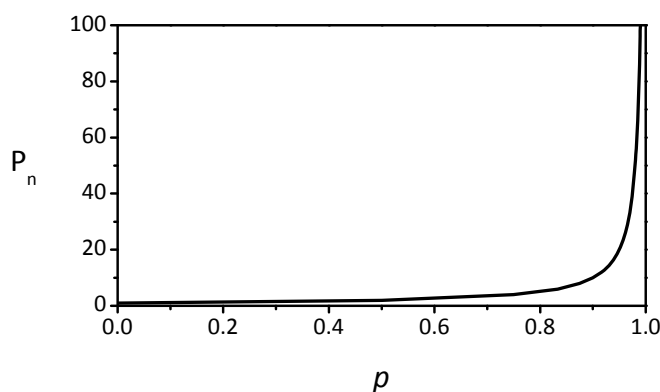


Figure 13: Dependence of number average degree of polymerization P_n with conversion p according to Carothers equation.

In order to avoid by-products the reaction should be carried out under conditions of inert atmosphere since a frequently investigated side-reaction is a oxygen promoted homocoupling process.^[70, 83] Hence, no oxygen should enter the reaction accidentally, e.g. by incomplete degassing of the solvents. Adamo *et al.*^[84] showed that this homocoupling of two arylboronic acids proceeds via a palladium(II) peroxo complex. Another possible side-reaction is the protodeboronation.^[85] The hydrolysis of the boronic acid can proceed in water and is catalyzed by base, acid and even by metal salts resulting in a B-C bond cleavage. This side reaction is facilitated by using strong aqueous bases. Further by-products can emerge via palladium-catalyzed dehalogenation of aromatic halides.^[86] Undesirable hydrodehalogenation products (Ar-Pd(II)-H) often arise in the presence of a Pd catalyst and a hydride donor. Especially, when alcohols are used, an alkoxide can attack at the metal center. Then β -hydride elimination leads to the corresponding Pd(II) hydride complex. It is essential that side-reactions have to be minimized because they would lead to a mismatch of the number of functional groups and as a consequence can terminate the propagation. Hence, a thorough optimization of reaction conditions and parameters like palladium source, ligand, solvent, temperature, etc. is necessary for SPC.

There are enabling techniques to further improve the reaction conditions for the syntheses of low molecular weight compounds, namely the application of microwaves and the microreactor technique. These modifications make it possible to shorten the reaction time drastically. With microwave-assisted Suzuki coupling, reaction times of minutes instead of days are achievable. This very attractive methodology was also applied to Suzuki polycondensation but with limited success, the products were more or less in an oligomeric regime.^[69] For up-scaling procedures and enabling a specific level of reaction control, continuous production techniques are desirable to avoid the problems that are present in a batch synthesis such as heat transfer and reproducibility. Thus, microreactors and continuous-flow methods have been developed.^[87] In recent years the application of microwave heated continuous flow syntheses were also shown to be efficient in the synthesis of conjugated polymers via Suzuki polycondensation as well as Stille polycondensation.

Conjugated polymers prepared by Suzuki polycondensation also follow a classical step-growth mechanism as described above. In recent years reports indicate that the Suzuki polycondensation reaction via the AB approach may also occur in a chain-growth polymerization mechanism.^[88, 89]

A controlled chain-growth Suzuki type polymerization reaction leading to well-defined polyfluorenes was first reported by Yokoyama *et al.* in 2007.^[90] This report showed the linear dependence of the molar mass on the conversion following typical chain-growth

kinetics. Chain propagation in this polymerization was initiated by an initiator unit derived from an arylpalladium(II) halide catalyst. If the polymerization proceeded in a chain-growth manner, the Pd(0) species would move intramolecularly from its last reaction site to the C-Br bond at the end of the chain.

Such a polymerization method would provide the ability to introduce reactive chain-end functionalities enhancing the general scope of this methodology. Indeed, Fischer *et al.*^[89] recently published heterodifunctional polyfluorenes by controlled chain-growth Suzuki AB type polymerization. They derived reactive functional end groups at both chain ends from a functionalized initiator and a reactive end-capped chain end. Research results on chain-growth Suzuki polycondensation was reported by different groups showing nicely that low polydispersities < 1.2 can be achieved. However, mostly polymers with low molecular weights up to 10.000 gmol⁻¹ were obtained.^[91, 92] This is probably due to the slow transfer of the catalyst to the monomer over time during the polymerization. Therefore, chain-growth polymerization can just be ensured at the beginning of the polymerization.^[88] In contrast, Zhang *et al.*^[91] applied ArPd(*t*-Bu₃P)I complexes as efficient initiators in 2012. They achieved higher molecular weights ($M_n > 30.000 \text{ gmol}^{-1}$) by using smaller amounts of the robust initiator demonstrating the great potential of this methodology.

In conclusion, Suzuki chain-growth polycondensation is an interesting alternative to classical chain-growth polycondensations, but further improvements have to be accomplished in future work. Thus, this thesis considers the syntheses of copolymers via the classical Suzuki polycondensation method.

3.3 Charge carrier mobility in organic semiconductors

In organic semiconductor devices such as OFETs, OLEDs, and OPVs the efficient and well controlled transport of charge carriers has a direct impact on their performance. Hence, a fundamental understanding of operation mechanism like charge injection and transport in π -conjugated systems is of basic necessity and thereby gained great attention recently by both academia and industry.^[93]

The velocity of charge carriers in a given electric field affects the response time of optoelectronic devices. Therefore the improvement of charge carrier mobility of organic semiconductors (μ) is of special importance and can be considered as important task.^[94] It is empirically defined as:

$$\mu = \frac{v}{E} \quad (5)$$

where v is the drift velocity of charge carriers and E is the applied electrical field. The charge carrier mobility is typically expressed in $\text{cm}^2\text{V}^{-1}\text{s}^{-1}$ and linked to the electrical conductivity (σ) of materials by the equation:

$$\sigma = n \cdot e \cdot \mu \quad (6)$$

where n is the number of charge carriers and e is the electronic charge. The conductivity is usually given in Scm^{-1} . In contrast to inorganic semiconductors the charge carrier mobility of organic solids is orders of magnitude less, caused mainly by disorder effects.^[94] In organic materials positional and conformational disorder such as twists and kinks along conjugated backbones of polymers or conjugated cores of small molecules is present.^[95]

Different transport theories are used to explain the electrical properties of organic semiconductors. A commonly used model for describing charge transport in organic solids is the Gaussian disorder model (GDM) suggested by BäSSLER in 1993.^[96] In this model charge transport occurs via incoherent hopping of charge carriers between strongly localized states. A hole (positive charge) or electron (negative charge) hops from site-to-site in a Gaussian distribution of density of states (DOS) and neglects any polaron effects. The assumption of weak electron-phonon coupling is used in the well-known Miller–Abrahams^[97] formalism to determine the hopping rate. This model was originally developed for inorganic disordered materials and it is valid in the weak electron-phonon coupling regime and at low temperatures.^[98, 99]

In contrast, Marcus approximation describes the regime of strong electron-phonon coupling at high temperatures. In this polaron model, Marcus formalism can be used to determine the transfer rate where any polaron effects are included. Recently, Fishchuk *et al.*^[99] developed a model based on a Marcus jump rate model and Gaussian disorder, to describe charge hopping in organic semiconductors with incorporation of both energetic disorder and polaronic contributions.

The classical Gaussian disorder model was further improved to describe the charge carrier mobility in dependence of temperature, electric field, and carrier density.^[100] Especially, when including carrier concentration, the classical model is extended to the so called extended Gaussian disorder model (EGDM).^[99-101] This is usually adapted for the description of organic light emitting diodes and organic field-effect transistors in which current is space-charge limited. The model formalisms (disorder and polaron) for the description of charge transport properties of organic solids were refined during the last decade. However, the charge transport phenomena in organic semiconductors are not yet completely understood and it is still under investigation.

Furthermore, the relationship between microstructure and electrical properties of conjugated polymers is intensively discussed at the moment. To mimic the high performance of inorganic semiconductors, it is attempted to get higher crystallinity also in conjugated polymers.

It is generally believed that the degree of crystallinity plays a very important role for the charge carrier mobility. Actually, donor-acceptor polymers with increased crystallinity were successfully applied in OFETs to get the record hole-mobility of $23.7 \text{ cm}^2\text{V}^{-1}\text{s}^{-1}$ (cf. chapter 3.1; PCDTPT).^[4] Nevertheless, highly disordered LBG polymers which exhibit less or even undetectable long-range order, also possess mobilities higher than $1 \text{ cm}^2\text{V}^{-1}\text{s}^{-1}$.^[102] These results show that understanding the correlation of structure and charge transport in conjugated polymers is challenging. For conjugated polymers a model that takes the complex macromolecular nature of materials into consideration is missing.^[103] Therefore, a general relationship between structure and charge transport within such disordered materials is necessary.

Recently, more and more investigations regarding this topic are published.^[104] Noriega *et al.*^[103, 105] presented a theory which combines well-known models to describe multiscale charge transport with respect to chain conformations. Kinetics of intramolecular (within an individual polymer chain) and intermolecular charge transport (among adjacent chains) are discussed. They conclude, for getting high mobilities, polymers with high molecular weights and, most notably, the existence of interconnected aggregates are required and not necessarily a high crystallinity. In such disordered polymers intermolecular charge transport occurs through these ordered aggregates.

On the contrary, a detailed study of crystallinity, long period of lamellae and SCLC mobility in a series of P3HT samples clearly proves that no high molecular weights are required for obtaining the maximum mobility.^[106] This is due to the fact that after a certain length, the polymer chains start folding resulting in saturation of lamellar thickness and charge carrier mobility. Additionally, recent reports on the widely studied n-type polymer P(NDI2OD-T2) (cf. chapter 3.1 Figure 4) have demonstrated that the field-effect mobility can be controlled over two orders of magnitude (up to $1 \text{ cm}^2\text{V}^{-1}\text{s}^{-1}$) by controlling the extension of orientated domains.^[107] Long-range order with domains in the dimension of hundreds of micrometers, showing successfully the connection of better transport properties by increasing length scales from meso- to macro-scale.

In conclusion, charge transport processes in disordered materials are of great interest and it is a subject matter of intensive investigation. Theoretical models are developed to gain further insight into these phenomena. However, there are several

methods to experimentally determine the charge carrier mobility (μ). The most common ones are the time of flight technique (ToF), space-charge limited current (SCLC), carrier extraction by linearly increasing voltage (CELIV), photogenerated charges in CELIV (photo-CELIV) as well as field-effect transistors (FETs).^[108] In the following, SCLC and FET methods are described in more detail since these methods are mainly used in this thesis.

Space-charge limited current (SCLC)

The space-charge limited current (SCLC) technique is often used to determine the charge carrier mobility of organic semiconductors in a diode geometry.^[93, 108, 109] The device setup is a diode where the organic material is sandwiched between two electrodes. With this method, current-voltage characteristics are measured and analyzed. A space-charge limited current can be achieved in devices wherein the organic semiconductor is in contact with ohmic electrodes.^[109] In these devices the current is only limited by the bulk mobility and not by charge injection. The electrode has to be chosen in a way enabling injection of enough charge carriers (only holes or electrons) so that the electric field at this electrode disappears ($E = 0$). The space-charge limited current J is described by equation 7, which is also known as Mott-Gurney equation, assuming that any trapping effects are absent:^[108]

$$J = \frac{9}{8} \varepsilon_0 \varepsilon_r \mu \frac{V^2}{L^3} \quad (7)$$

where ε_0 is the vacuum permittivity, ε_r is the relative permittivity. V is the voltage applied and L the thickness of the active layer. The charge carrier mobility can be calculated from equation 7 if the current J has a quadratic dependence on voltage (V). Moreover, the thickness scaling should also be taken into account to prevent incorrectly data interpretation.

In cases, where the charge carrier mobility is field dependent, the J - V characteristics can be better described by equation 8, which is a modified Mott-Gurney equation developed by Murgatroyd:^[108, 110]

$$J = \frac{9}{8} \varepsilon_0 \varepsilon_r \mu_0 e^{0.89 \cdot \gamma} \sqrt{V/L} \cdot \frac{V^2}{L^3} \quad (8)$$

where μ_0 is the zero-field mobility and γ is the field activation parameter. The charge carrier mobility at zero field μ_0 as well as the activation parameter γ are obtained by plotting J vs. V and fitting the data according to equation 8. The charge carrier

mobilities μ , depending on the electric field within the device, can be then calculated by inserting μ_0 and γ into equation 9:^[111]

$$\mu = \mu_0 e^{\gamma \cdot \sqrt{E}} \quad (9)$$

In contrast to the above described steady state SCLC method, one can also apply a step voltage leading at first to an increase of current with time (Dark injection, DI-SCLC). The current reaches a maximum at time t_{max} ($= 0.78 \cdot t_{tr}$) which is related to the respective space-charge limited transient time (t_{tr}), and then gradually decays to a constant current.^[93] The charge carrier mobility can then be extracted by equation 10:

$$\mu = 0.78 \cdot \frac{L^2}{V \cdot t_{max}} \quad (10)$$

Field effect transistors (FETs)

In contrast to the method above, charge transport in organic field effect transistors (OFETs)^[108, 112, 113] occurs generally in a thin layer laterally and not vertically as in sandwich devices. This is due to a device setup which consists of a thin semiconductor film embedded between three electrodes: the source (S), drain (D), and gate (G) electrode, where the latter is separated by an insulating layer. These elements can be arranged in several ways. The bottom gate, bottom contact configuration is mainly used and shown in Figure 16a). The distance between source and drain is called channel length (L) and the width (W) is referred to the length of the conducting channel.

The operating principle of an organic field effect transistor is illustrated in Figure 16b). An electrical current in transistors depends on gate and drain voltage. By applying a voltage (V_g) to the gate electrode an accumulation layer (shown in red) is formed at the insulator-semiconductor interface which connects source and drain. A second voltage (V_d) applied to the drain electrode, leads to charge injection at the source. At first charge traps, if present, have to be filled. Hence, a threshold voltage (V_{th}) must be overcome to enable an efficient current from source to drain. Following Ohm's law, at a given V_g (higher than V_{th}) the current increases linearly with the drain voltage and defines the linear region ($V_d \ll V_g - V_{th}$) in a typical output characteristic shown in Figure 16c) and 16b I).^[114]

As the drain voltage increases the conductivity of the channel decreases and the current gradually levels-off to a point at which the charge concentration at the drain electrode is diminished to nearly zero, because the charge is reduced by the channel potential.^[113] The transistor is pinched-off ($V_d = V_g - V_{th}$) at the so called "pinch-off

point” (cf. Fig.16b II)). From now on the voltage applied to the channel remains the same by further increasing of V_d , since the “pinch-off point” moves towards the source. A depletion region between the “pinch-off point” and the drain electrode is formed at such high voltages ($V_d > V_g - V_{th}$). Here, the transistor acts in the saturation region, which is illustrated in Figure 16b III) and in the output characteristics shown in Figure 16c). An organic semiconductor can be classified in n-type or p-type according to whether electrons or holes are injected at the source electrode in its LUMO or HOMO level. Moreover, some organic materials show ambipolar transport behavior, which means they conduct electrons as well as holes.

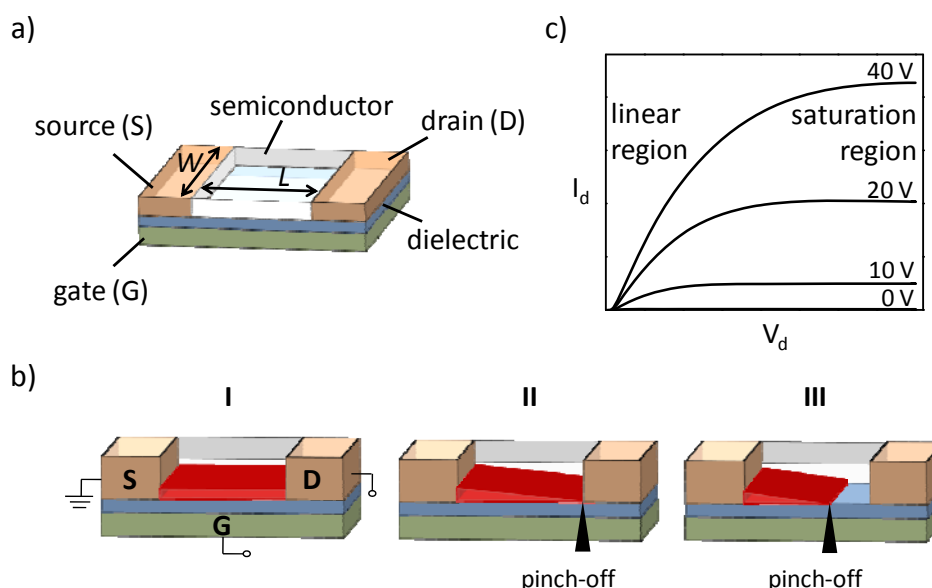


Figure 16: Schematic illustration of (a) a bottom-gate, bottom-contact field effect transistor. The gate electrode (G) is separated by a dielectric from the semiconductor as well as the source (S) and drain (D) electrodes. The n- or p-type semiconductor is placed between the source and drain electrode. The width (W) is the length of the conducting channel and the length (L) defines the distance between source and drain. (b) Different operation regimes of a transistor at different voltages: I) as soon as V_g exceeds the threshold voltage V_{th} an accumulation layer of charges (red) is formed where $V_d \ll V_g - V_{th} \neq 0$; the transistor works in the linear region. II) The transistor is pinched-off ($V_d = V_g - V_{th} \neq 0$); the “pinch-off point” is shown with a black triangle. III) The transistor works in the saturation regime ($V_d > V_g - V_{th} \neq 0$). (c) A typical current-voltage (I_d - V_d) plot (output characteristic) for various constant gate voltages ranging from 0 V to 40 V. The linear and saturation region are well-separated. Adapted from Ref. ^[114]

The charge carrier mobility μ is calculated with the assumption that the electric field across the channel is much larger than along the channel.^[114] This gradual channel

approximation is a widely used model proposed by Shockley and requires the transport of all charges at the semiconductor-dielectric interface.^[115] When a gate voltage is applied, charges accumulate on the semiconductor-dielectric interface. This charge density is uniform along the channel when the applied source-drain bias is zero. By applying a source voltage the spatial density of charge at the position x , $q_{ind(x)}$, is proportional to the voltage difference $V_g - V(x)$:

$$q_{ind(x)} = n(x) et = C_{ox}(V_g - V(x)) \quad (11)$$

where C_{ox} is the capacitance of the dielectric capacitor, $n(x)$ corresponds to the number of charges in the channel, e is the fundamental unit of charge and the thickness of the charged layer is written as t . Taking the threshold voltage V_{th} into account leads to:

$$q_{ind(x)} = n(x) et = C_{ox}(V_g - V_{th} - V(x)). \quad (12)$$

With the gradual channel approximation equation 12 becomes:

$$q_{ind(x)} = n(x) et = C_{ox} \left(V_g - V_{th} - \frac{V_d}{2} \right). \quad (13)$$

If the transistor works in the linear regime ($V_d \ll V_g - V_{th} \neq 0$) the current increases linearly with V_d following Ohm's law. Using the electrical conductivity σ (equation 6) gives:

$$\frac{I_d}{tW} = \sigma \frac{V_d}{L} \rightarrow I_d = \frac{W}{L} (n_{ind,av} et) \mu V_d \quad (14)$$

where $n_{ind,av}$ relates to the average carrier concentration in the channel. By putting equation 13 into 14 leads to:

$$I_d = \frac{W}{L} C_{ox} \mu \left[(V_g - V_{th}) - \frac{V_d}{2} \right] V_d. \quad (15)$$

Equation 15 can be simplified by writing

$$I_d = \frac{W}{L} C_{ox} \mu \left[(V_g - V_{th}) V_d - \frac{V_d^2}{2} \right], \quad (16)$$

showing that the current not only scales linearly with V_g but also quadratically with V_d . In the linear regime $V_d \ll V_g - V_{th} \neq 0$, the $V_d/2$ term can be neglected. It becomes

$$I_d = \frac{W}{L} C_{ox} \mu (V_g - V_{th}) V_d. \quad (17)$$

At this point the channel transconductance g_m is defined as:

$$g_m = \frac{\partial I_d}{\partial V_g} = \frac{W}{L} C_{ox} \mu V_d. \quad (18)$$

Substituting $V_d = V_g - V_{th}$ in equation 16 describes the current-voltage characteristic in the saturation region:

$$I_{d,sat} = \frac{W}{2L} C_{ox} \mu_{sat} (V_g - V_{th})^2. \quad (19)$$

The charge carrier mobility in the saturation regime is determined by plotting $I_d^{1/2}$ versus V_g . With help of the first derivative of $I_d^{1/2}$ and respect to V_g the charge carrier mobility is calculated by using:

$$\mu_{sat} = \left(\frac{\partial \sqrt{I_{d,sat}}}{\partial V_g} \right)^2 \frac{2L}{WC_{ox}}. \quad (20)$$

The current-voltage (I_d - V_g) plot is called transfer characteristic where V_d is constant and V_g is swept. A schematic transfer characteristic is shown in Figure 17. By a semi-logarithmic plot of I_d vs. V_g , the on/off current ratio of the device can be extracted. This ratio specifies the ability of the transistor to shut down. It is desirable to achieve a high on/off ratio, especially for applications in displays or logic circuits.^[116] Plotting $I_d^{1/2}$ vs. V_g the threshold voltage V_{th} can be determined with the help of the intercept of a linear fit in the saturation region. The charge carrier mobility can be calculated with equation 20 using the slope of the $I_d^{1/2}$ vs. V_g plot in the saturation regime.^[114]

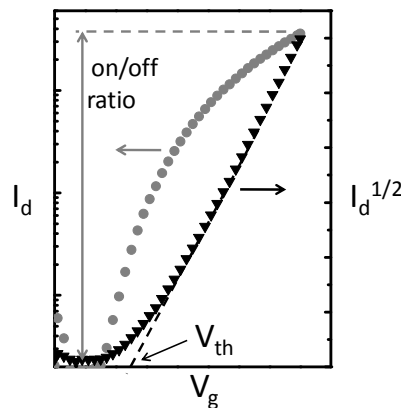


Figure 17: Schematic illustration of a transfer characteristic. From the logarithmic transfer plot on the left-hand side the on/off current ratio can be extracted. Whereas the threshold voltage V_{th} and the charge carrier mobility μ can be determined using the $I_d^{1/2}$ vs. V_g plot on the right-hand side.

In the following part the above mentioned techniques for determining the charge carrier mobility are briefly compared to each other.^[108] Generally, the charge carrier mobility in FETs is measured in the film laterally, so that the use of relatively thin films is possible. This is in contrast to CELIV, ToF, or SCLC, where the mobility is measured

vertically in a sandwich device. Especially for SCLC measurements, film thicknesses of around 200 nm up to 500 nm are required. The charge carrier mobilities obtained from SCLC measurements are comparable to those of ToF, whereas the FET mobility is usually some orders of magnitude higher. This is due to the higher charge concentration in an OFET device induced by the gate which fill up tail states of the DOS distribution, leading to a narrowing of activation energy.^[109] In contrast to ToF mobility, the charge carrier mobility derived from CELIV method is related to intrinsic carriers. Differentiation between holes and electrons is not possible here, and it is a drawback when ambipolar materials are used.^[109] However, it turns into an advantage, because electron and hole mobilities can be measured utilizing the same sample. Moreover, the CELIV technique can be utilized to characterize charge transport in semiconductors with high bulk conductivity.

In general the determination of charge carrier mobility with different techniques requires a careful selection of electrode materials and experimental conditions. The used technique as well as device preparation and storage can have a remarkable impact on the measured parameters. This has to be kept in mind when preparing devices and comparing results.

3.4 Objectives of this thesis

Although a huge number of low band gap (LBG) materials has been synthesized and successfully applied into semiconductor devices, there is lack of fundamental understanding why especially just few LBG materials show extraordinary performance. For instance it is believed that high degree of crystallinity and long-range order of the semiconductor material are of great importance for providing high carrier mobilities and thus a high performance in devices. However, highly disordered materials predict good mobilities as well, like already discussed in chapter 3.3.^[104] Now the question arises why? This example of the relationship between microstructure and electrical properties demonstrates the need for further work to describe consistent structure-function relationships. I am interested in providing meaningful conclusions of comparative studies concerning LBG materials. Therefore, fundamental issues such as donor (D) - acceptor (A) arrangements along the conjugated system are considered in this work.

The aim is to investigate the impact of different DA arrangements in relation to the optical, electrochemical, thermal and electronic properties.

In detail, it shall be investigated how a random ordering of the respective D and A units differs from an alternating ordering of these units. To provide a comparative study, the ratio of D and A units should stay constant in both arrangements. For these DA arrangement studies, the widely used 2,1,3-benzothiadiazole (B) unit, already presented in chapter 3.1, is suitable. The B acceptor units are supposed to be coupled with (hexyl-)thiophenes as donor units since thiophene derivatives are widely used as donor in LBG materials. Therefore, suitable routes for the synthesis of the novel monomers shall be investigated. In order to obtain directly comparable DA materials, the syntheses of bifunctional AA/BB and AB type monomers shall be carried out. The copolymers will be polymerized via Suzuki polycondensation reactions.

One aim is to study the impact of different arrangements of D and A units in low molecular weight and oligomeric systems on the optical absorption. This shall be realized in a combined theoretical and experimental study. In order to obtain the lowest excitation energies, UV/Vis spectroscopy shall be performed and with the help of the theoretical computational methods a comparison study shall be carried out. For determining the molecular weight of oligomeric systems matrix-assisted laser desorption ionization-time of flight (MALDI-ToF) mass spectrometry shall be utilized.

Another aim is to examine the impact of random/alternating arrangement of different copolymers on the optical, electrical, thermal and charge transport properties. A variety of techniques shall be employed, among them cyclic voltammetry (CV) and UV/Vis spectroscopy. For the characterization of transport properties organic field effect transistors (OFETs) are the technique of choice.

Moreover, the influence of increasing donor strength in donor-acceptor-donor low molecular weight systems on optical and electrochemical properties shall be investigated. The inspiration for this study is the well performing DA copolymer P(NDI2OD-T2) (*cf.* chapter 3.1 Fig. 4a)). Hence, the well-known 1,4,5,8-naphthalenetetracarboxylic diimide (NDI) unit shall be utilized as an acceptor unit. For this, NDI as acceptor unit shall be used with different thiophenes (T) as donor units. In particular, the systematic increase of donor strength shall be achieved by attaching thiophene, 3-hexylthiophene as well as bithiophene substituents on the NDI core. Moreover, the charge carrier mobility of a selected donor-acceptor-donor compound shall be studied via space-charge limited current measurements.

These fundamental studies should give an insight into LBG systems and further guidelines regarding LBG design and development are to be provided.

References

- [1] T. S. van der Poll, J. A. Love, T.-Q. Nguyen and G. C. Bazan, *Advanced Materials* **2012**, *24*, 3646-3649.
- [2] P. Dutta, J. Kim, S. H. Eom, W.-H. Lee, I. N. Kang and S.-H. Lee, *ACS Applied Materials & Interfaces* **2012**, *4*, 6669-6675.
- [3] Y. Sun, G. C. Welch, W. L. Leong, C. J. Takacs, G. C. Bazan and A. J. Heeger, *Nat Mater* **2012**, *11*, 44-48.
- [4] H.-R. Tseng, H. Phan, C. Luo, M. Wang, L. A. Perez, S. N. Patel, L. Ying, E. J. Kramer, T.-Q. Nguyen, G. C. Bazan and A. J. Heeger, *Advanced Materials* **2014**, 10.1002/adma.201305084.
- [5] T. T. Steckler, X. Zhang, J. Hwang, R. Honeyager, S. Ohira, X.-H. Zhang, A. Grant, S. Ellinger, S. A. Odom, D. Sweat, D. B. Tanner, A. G. Rinzler, S. Barlow, J.-L. Brédas, B. Kippelen, S. R. Marder and J. R. Reynolds, *Journal of the American Chemical Society* **2009**, *131*, 2824-2826.
- [6] X.-H. Zhu, J. Peng, Y. Cao and J. Roncali, *Chemical Society Reviews* **2011**, *40*, 3509-3524.
- [7] P. M. Beaujuge, S. Ellinger and J. R. Reynolds, *Nat Mater* **2008**, *7*, 795-799.
- [8] G. E. Gunbas, A. Durmus and L. Toppare, *Advanced Materials* **2008**, *20*, 691-695; E. Oguzhan, H. Bilgili, F. Baycan Koyuncu, E. Ozdemir and S. Koyuncu, *Polymer* **2013**, *54*, 6283-6292; W. T. Neo, L. M. Loo, J. Song, X. Wang, C. M. Cho, H. S. On Chan, Y. Zong and J. Xu, *Polymer Chemistry* **2013**, *4*, 4663-4675; A. Balan, D. Baran and L. Toppare, *Polymer Chemistry* **2011**, *2*, 1029-1043.
- [9] P. M. Beaujuge, S. V. Vasilyeva, D. Y. Liu, S. Ellinger, T. D. McCarley and J. R. Reynolds, *Chemistry of Materials* **2012**, *24*, 255-268.
- [10] Y. Jin, F. Ye, M. Zeigler, C. Wu and D. T. Chiu, *ACS Nano* **2011**, *5*, 1468-1475; F. Ye, C. Wu, Y. Jin, Y.-H. Chan, X. Zhang and D. T. Chiu, *Journal of the American Chemical Society* **2011**, *133*, 8146-8149.
- [11] C. Wu, T. Schneider, M. Zeigler, J. Yu, P. G. Schiro, D. R. Burnham, J. D. McNeill and D. T. Chiu, *Journal of the American Chemical Society* **2010**, *132*, 15410-15417.
- [12] "The Nobel Prize in Physics 1921". *Nobelprize.org*. Nobel Media AB 2013. Web. 13 Feb 2014.
<http://www.nobelprize.org/nobel_prizes/physics/laureates/1921/>

- [13] A. Einstein, *Annalen der Physik* **1905**, 322, 132-148.
- [14] P. A. Tipler and R. A. Llewellyn, *Moderne Physik*, Oldenbourg Wissenschaftsverlag, **2010**, p. 1-963.
- [15] A. H. Wilson, *Proceedings of the Royal Society of London. Series A* **1931**, 133, 458-491.
- [16] F. G. Allen and G. W. Gobeli, *Physical Review* **1962**, 127, 150-158.
- [17] C. K. Chiang, C. R. Fincher, Y. W. Park, A. J. Heeger, H. Shirakawa, E. J. Louis, S. C. Gau and A. G. MacDiarmid, *Physical Review Letters* **1977**, 39, 1098-1101; H. Shirakawa, E. J. Louis, A. G. MacDiarmid, C. K. Chiang and A. J. Heeger, *Journal of the Chemical Society, Chemical Communications* **1977**, 578-580.
- [18] J.-L. Brédas, *Materials Horizons* **2014**, 1, 17-19.
- [19] C. Deibel, D. Mack, J. Gorenflot, A. Schöll, S. Krause, F. Reinert, D. Rauh and V. Dyakonov, *Physical Review B* **2010**, 81, 085202.
- [20] Z.-L. Guan, J. B. Kim, H. Wang, C. Jaye, D. A. Fischer, Y.-L. Loo and A. Kahn, *Organic Electronics* **2010**, 11, 1779-1785.
- [21] C. Kitamura, S. Tanaka and Y. Yamashita, *Chemistry of Materials* **1996**, 8, 570-578.
- [22] J. Roncali, *Macromolecular Rapid Communications* **2007**, 28, 1761-1775.
- [23] J. Roncali, *Chemical Reviews* **1997**, 97, 173-206.
- [24] J. Kuerti, P. R. Surjan and M. Kertesz, *Journal of the American Chemical Society* **1991**, 113, 9865-9867.
- [25] F. Wudl, M. Kobayashi and A. J. Heeger, *The Journal of Organic Chemistry* **1984**, 49, 3382-3384; G. Tourillon and F. Garnier, *Journal of Electroanalytical Chemistry and Interfacial Electrochemistry* **1982**, 135, 173-178; J. L. Brédas, A. J. Heeger and F. Wudl, *The Journal of Chemical Physics* **1986**, 85, 4673-4678; A. O. Patil, A. J. Heeger and F. Wudl, *Chemical Reviews* **1988**, 88, 183-200.
- [26] J. L. Brédas, *Journal of Chemical Physics* **1985**, 82, 3808-3011.
- [27] Y.-J. Cheng, S.-H. Yang and C.-S. Hsu, *Chemical Reviews* **2009**, 109, 5868-5923.
- [28] G. Hieber, M. Hanack, K. Wurst and J. Strähle, *Chemische Berichte* **1991**, 124, 1597-1605.
- [29] E. E. Havinga, W. Hovee and H. Wynberg, *Polymer Bulletin* **1992**, 29, 119-126.
- [30] E. E. Havinga, W. ten Hovee and H. Wynberg, *Synthetic Metals* **1993**, 55, 299-306.

- [31] H. J. Son, F. He, B. Carsten and L. Yu, *Journal of Materials Chemistry* **2011**, *21*, 18934-18945; C. Winder and N. S. Sariciftci, *Journal of Materials Chemistry* **2004**, *14*, 1077-1086.
- [32] H. Yan, Z. Chen, Y. Zheng, C. Newman, J. R. Quinn, F. Dotz, M. Kastler and A. Facchetti, *Nature* **2009**, *457*, 679-686.
- [33] R. R. Søndergaard, M. Hösel and F. C. Krebs, *Journal of Polymer Science Part B: Polymer Physics* **2012**, *51*, 16-34; E. Bundgaard, O. Hagemann, M. Manceau, M. Jørgensen and F. C. Krebs, *Macromolecules* **2010**, *43*, 8115-8120.
- [34] C. M. Amb, M. R. Craig, U. Koldemir, J. Subbiah, K. R. Choudhury, S. A. Gevorgyan, M. Jørgensen, F. C. Krebs, F. So and J. R. Reynolds, *ACS Applied Materials & Interfaces* **2012**, *4*, 1847-1853.
- [35] Z. He, C. Zhong, S. Su, M. Xu, H. Wu and Y. Cao, *Nat Photon* **2012**, *6*, 591-595.
- [36] Z. He, C. Zhong, X. Huang, W.-Y. Wong, H. Wu, L. Chen, S. Su and Y. Cao, *Advanced Materials* **2011**, *23*, 4636-4643.
- [37] C. M. Amb, P. M. Beaujuge and J. R. Reynolds, *Advanced Materials* **2012**, *22*, 724-728.
- [38] I. Kang, H.-J. Yun, D. S. Chung, S.-K. Kwon and Y.-H. Kim, *Journal of the American Chemical Society* **2013**, *135*, 14896-14899.
- [39] C. Cabanetos, A. El Labban, J. A. Bartelt, J. D. Douglas, W. R. Mateker, J. M. J. Fréchet, M. D. McGehee and P. M. Beaujuge, *Journal of the American Chemical Society* **2013**, *135*, 4656-4659.
- [40] Z. Cai, Y. Guo, S. Yang, Q. Peng, H. Luo, Z. Liu, G. Zhang, Y. Liu and D. Zhang, *Chemistry of Materials* **2013**, *25*, 471-478.
- [41] Y.-H. Chen, L.-Y. Lin, C.-W. Lu, F. Lin, Z.-Y. Huang, H.-W. Lin, P.-H. Wang, Y.-H. Liu, K.-T. Wong, J. Wen, D. J. Miller and S. B. Darling, *Journal of the American Chemical Society* **2012**, *134*, 13616-13623; M. T. Lloyd, J. E. Anthony and G. G. Malliaras, *Materials Today* **2007**, *10*, 34-41.
- [42] Y. Liu, Y. Yang, C.-C. Chen, Q. Chen, L. Dou, Z. Hong, G. Li and Y. Yang, *Advanced Materials* **2013**, *25*, 4657-4662.
- [43] S. Loser, C. J. Bruns, H. Miyauchi, R. P. Ortiz, A. Facchetti, S. I. Stupp and T. J. Marks, *Journal of the American Chemical Society* **2011**, *133*, 8142-8145.
- [44] S. Wang, M. Wang, X. Zhang, X. Yang, Q. Huang, X. Qiao, H. Zhang, Q. Wu, Y. Xiong, J. Gao and H. Li, *Chemical Communications* **2014**, *50*, 985-987.
- [45] B. A. D. Neto, A. A. M. Lapis, E. N. da Silva Júnior and J. Dupont, *European Journal of Organic Chemistry* **2013**, *2013*, 228-255.

- [46] J.-M. Raimundo, P. Blanchard, H. Brisset, S. Akoudad and J. Roncali, *Chemical Communications* **2000**, 939-940.
- [47] S. Mathew, A. Yella, P. Gao, R. Humphry-Baker, B. F. E. Curchod, N. Ashari-Astani, I. Tavernelli, U. Rothlisberger, M. K. Nazeeruddin and M. Grätzel, *Nat Chem* **2014**, *6*, 242-247.
- [48] X. Zhao and X. Zhan, *Chemical Society Reviews* **2011**, *40*, 3728-3743.
- [49] J.-K. Lee, M. C. Gwinner, R. Berger, C. Newby, R. Zentel, R. H. Friend, H. Sirringhaus and C. K. Ober, *Journal of the American Chemical Society* **2011**, *133*, 9949-9951.
- [50] F. Cicoira and C. Santato, *Organic Electronics* Wiley-VCH, **2013**, p. 464.
- [51] M. C. Gwinner, D. Kabra, M. Roberts, T. J. K. Brenner, B. H. Wallikewitz, C. R. McNeill, R. H. Friend and H. Sirringhaus, *Advanced Materials* **2012**, *24*, 2728-2734.
- [52] N. Banerji, E. Gagnon, P.-Y. Morgantini, S. Valouch, A. R. Mohebbi, J.-H. Seo, M. Leclerc and A. J. Heeger, *The Journal of Physical Chemistry C* **2012**, *116*, 11456-11469; S. H. Park, A. Roy, S. Beaupré, S. Cho, N. Coates, J. S. Moon, D. Moses, M. Leclerc, K. Lee and A. J. Heeger, *Nat Photon* **2009**, *3*, 297-302; X. Lu, H. Hlaing, D. S. Germack, J. Peet, W. H. Jo, D. Andrienko, K. Kremer and B. M. Ocko, *Nat Commun* **2012**, *3*, 795; T.-Y. Chu, S. Alem, S.-W. Tsang, S.-C. Tse, S. Wakim, J. Lu, G. Dennler, D. Waller, R. Gaudiana and Y. Tao, *Applied Physics Letters* **2011**, *98*, -; H.-J. Jhuo, P.-N. Yeh, S.-H. Liao, Y.-L. Li, Y.-S. Cheng and S.-A. Chen, *Journal of the Chinese Chemical Society* **2014**, *61*, 115-126.
- [53] S. V. Bhosale, C. H. Jani and S. J. Langford, *Chemical Society Reviews* **2008**, *37*, 331-342; M. Sommer, *Journal of Materials Chemistry C* **2014**, *2*, 3088-3098; N. Sakai, J. Mareda, E. Vauthey and S. Matile, *Chemical Communications* **2010**, *46*, 4225-4237.
- [54] B. Robotham, K. A. Lastman, S. J. Langford and K. P. Ghiggino, *Journal of Photochemistry and Photobiology A: Chemistry* **2013**, *251*, 167-174.
- [55] S. Langford, J. , M. Latter, J. and C. Woodward, P. , *Photochemistry and Photobiology* **2006**, *82*, 1530-1540; N. P. Redmore, I. V. Rubtsov and M. J. Therien, *Journal of the American Chemical Society* **2003**, *125*, 8769-8778; S. Wallin, C. Monnereau, E. Blart, J.-R. Gankou, F. Odobel and L. Hammarström, *The Journal of Physical Chemistry A* **2010**, *114*, 1709-1721.
- [56] L. Favereau, J. Warnan, Y. Pellegrin, E. Blart, M. Boujtita, D. Jacquemin and F. Odobel, *Chemical Communications* **2013**, *49*, 8018-8020.

- [57] L. E. Polander, S. P. Tiwari, L. Pandey, B. M. Seifried, Q. Zhang, S. Barlow, C. Risko, J.-L. Brédas, B. Kippelen and S. R. Marder, *Chemistry of Materials* **2011**, *23*, 3408-3410.
- [58] G. Ren, E. Ahmed and S. A. Jenekhe, *Advanced Energy Materials* **2011**, *1*, 946-953; E. Ahmed, G. Ren, F. S. Kim, E. C. Hollenbeck and S. A. Jenekhe, *Chemistry of Materials* **2011**, *23*, 4563-4577.
- [59] X. Guo, F. S. Kim, M. J. Seger, S. A. Jenekhe and M. D. Watson, *Chemistry of Materials* **2012**, *24*, 1434-1442.
- [60] T. Earmme, Y.-J. Hwang, N. M. Murari, S. Subramaniyan and S. A. Jenekhe, *Journal of the American Chemical Society* **2013**, *135*, 14960-14963; Y.-J. Hwang, N. M. Murari and S. A. Jenekhe, *Polymer Chemistry* **2013**, *4*, 3187-3195.
- [61] Y.-J. Hwang, G. Ren, N. M. Murari and S. A. Jenekhe, *Macromolecules* **2012**, *45*, 9056-9062.
- [62] M. Yuan, M. M. Durban, P. D. Kazarinoff, D. F. Zeigler, A. H. Rice, Y. Segawa and C. K. Luscombe, *Journal of Polymer Science Part A: Polymer Chemistry* **2013**, *51*, 4061-4069.
- [63] Y. Kim, J. Hong, J. H. Oh and C. Yang, *Chemistry of Materials* **2013**, *25*, 3251-3259.
- [64] R. Steyrlleuthner, M. Schubert, F. Jaiser, J. C. Blakesley, Z. Chen, A. Facchetti and D. Neher, *Advanced Materials* **2010**, *22*, 2799-2803.
- [65] E. Zhou, J. Cong, K. Hashimoto and K. Tajima, *Advanced Materials* **2013**, *25*, 6991-6996.
- [66] M. García-Melchor, A. A. C. Braga, A. Lledós, G. Ujaque and F. Maseras, *Accounts of Chemical Research* **2013**, *46*, 2626-2634.
- [67] K. C. Nicolaou, P. G. Bulger and D. Sarlah, *Angewandte Chemie International Edition* **2005**, *44*, 4442-4489.
- [68] J. Sołoducho, K. Olech, A. Świst, D. Zając and J. Cabaj., *Advances in Chemical Engineering and Science* **2013**, *3*, 19-32.
- [69] J. Sakamoto and D. A. Schlüter in *Synthesis of Polymers: New Structures and Methods, Vol. 1* Eds.: D. A. Schlüter, C. Hawker and J. Sakamoto, Wiley-VCH Weinheim, **2012**, pp. 627-675.
- [70] A. J. J. Lennox and G. C. Lloyd-Jones, *Chemical Society Reviews* **2014**, *43*, 412-443.

- [71] A. Suzuki, *Journal of Organometallic Chemistry* **1999**, *576*, 147-168; R. Martin and S. L. Buchwald, *Accounts of Chemical Research* **2008**, *41*, 1461-1473; J. Hassan, M. Sevignon, C. Gozzi, E. Schulz and M. Lemaire, *Chemical Reviews* **2002**, *102*, 1359-1470; N. Miyaura and A. Suzuki, *Chemical Reviews* **1995**, *95*, 2457-2483.
- [72] J. Tsuji, *Palladium reagents and catalysts: new perspectives for the 21st century*, **2004**, p.
- [73] F. Bellina, A. Carpita and R. Rossi, *Synthesis* **2004**, *2004*, 2419-2440; A. F. Littke, C. Dai and G. C. Fu, *Journal of the American Chemical Society* **2000**, *122*, 4020-4028.
- [74] S. D. Walker, T. E. Barder, J. R. Martinelli and S. L. Buchwald, *Angewandte Chemie International Edition* **2004**, *43*, 1871-1876.
- [75] A. Balanta, C. Godard and C. Claver, *Chemical Society Reviews* **2011**, *40*, 4973-4985.
- [76] M. T. Reetz, R. Breinbauer and K. Wanninger, *Tetrahedron Letters* **1996**, *37*, 4499-4502.
- [77] G. Lu, R. Franzén, Q. Zhang and Y. Xu, *Tetrahedron Letters* **2005**, *46*, 4255-4259.
- [78] C. Liu, A. Repoley and B. Zhou, *Journal of Polymer Science Part A: Polymer Chemistry* **2008**, *46*, 7268-7272.
- [79] M. Rehahn, A.-D. Schlüter, G. Wegner and W. J. Feast, *Polymer* **1989**, *30*, 1060-1062.
- [80] J. Sakamoto, M. Rehahn, G. Wegner and A. D. Schlüter, *Macromolecular Rapid Communications* **2009**, *30*, 653-687.
- [81] M. D. Lechner, K. Gehrke and E. H. Nordmeier in *Makromolekulare Chemie, Vol. 4* Birkhäuser Verlag, Basel **2010**, pp. 48-170.
- [82] W. H. Carothers, *Transactions of the Faraday Society* **1936**, *32*, 39-49.
- [83] J. P. Parrish, Y. C. Jung, R. J. Floyd and K. W. Jung, *Tetrahedron Letters* **2002**, *43*, 7899-7902; Y. Nishihara, H. Onodera and K. Osakada, *Chemical Communications* **2004**, 192-193.
- [84] C. Adamo, C. Amatore, I. Ciofini, A. Jutand and H. Lakmini, *Journal of the American Chemical Society* **2006**, *128*, 6829-6836.
- [85] H. G. Kuivila, J. F. Reuwer Jr and J. A. Mangravite, *Canadian Journal of Chemistry* **1963**, *41*, 3081-3090; M. Jayakannan, J. L. J. van Dongen and R. A. J. Janssen, *Macromolecules* **2001**, *34*, 5386-5393.

- [86] L. o. Ghosez, C. c. Franc, F. d. r. Denonne, C. Cuisinier and R. Touillaux, *Canadian Journal of Chemistry* **2001**, *79*, 1827-1839; O. Navarro, H. Kaur, P. Mahjoor and S. P. Nolan, *The Journal of Organic Chemistry* **2004**, *69*, 3173-3180.
- [87] P. He, S. J. Haswell and P. D. I. Fletcher, *Lab on a Chip* **2004**, *4*, 38-41; H. Seyler, D. J. Jones, A. B. Holmes and W. W. H. Wong, *Chemical Communications* **2012**, *48*, 1598-1600.
- [88] M. Verswyvel, C. Hoebbers, J. De Winter, P. Gerbaux and G. Koeckelberghs, *Journal of Polymer Science Part A: Polymer Chemistry* **2013**, *51*, 5067-5074.
- [89] C. S. Fischer, M. C. Baier and S. Mecking, *Journal of the American Chemical Society* **2013**, *135*, 1148-1154.
- [90] A. Yokoyama, H. Suzuki, Y. Kubota, K. Ohuchi, H. Higashimura and T. Yokozawa, *Journal of the American Chemical Society* **2007**, *129*, 7236-7237.
- [91] H.-H. Zhang, C.-H. Xing and Q.-S. Hu, *Journal of the American Chemical Society* **2012**, *134*, 13156-13159.
- [92] E. Elmalem, A. Kiriy and W. T. S. Huck, *Macromolecules* **2011**, *44*, 9057-9061; E. Elmalem, F. Biedermann, K. Johnson, R. H. Friend and W. T. S. Huck, *Journal of the American Chemical Society* **2012**, *134*, 17769-17777.
- [93] S. Tiwari and N. C. Greenham, *Optical and Quantum Electronics* **2009**, *41*, 69-89.
- [94] F. Laquai, G. Wegner and H. Bässler, *Philosophical Transactions of the Royal Society A: Mathematical, Physical and Engineering Sciences* **2007**, *365*, 1473-1487.
- [95] R. Noriega and A. Salleo in *Charge Transport Theories in Organic Semiconductors, Vol. Wiley-VCH*, **2012**, pp. 67-104.
- [96] H. Bässler, *physica status solidi (b)* **1993**, *175*, 15-56.
- [97] A. Miller and E. Abrahams, *Physical Review* **1960**, *120*, 745-755.
- [98] R. M. Metzger, H. Bässler and A. Köhler in *Charge Transport in Organic Semiconductors, Vol. 312 Springer Berlin Heidelberg*, **2012**, pp. 1-65.
- [99] I. I. Fishchuk, A. Kadashchuk, S. T. Hoffmann, S. Athanasopoulos, J. Genoe, H. Bässler and A. Köhler, *Physical Review B* **2013**, *88*, 125202.
- [100] W. F. Pasveer, J. Cottaar, C. Tanase, R. Coehoorn, P. A. Bobbert, P. W. M. Blom, D. M. de Leeuw and M. A. J. Michels, *Physical Review Letters* **2005**, *94*, 206601.

- [101] R. Coehoorn and P. A. Bobbert, *physica status solidi (a)* **2012**, *209*, 2354-2377; I. I. Fishchuk, A. K. Kadashchuk, J. Genoe, M. Ullah, H. Sitter, T. B. Singh, N. S. Sariciftci and H. Bässler, *Physical Review B* **2010**, *81*, 045202.
- [102] X. Zhang, H. Bronstein, A. J. Kronemeijer, J. Smith, Y. Kim, R. J. Kline, L. J. Richter, T. D. Anthopoulos, H. Sirringhaus, K. Song, M. Heeney, W. Zhang, I. McCulloch and D. M. DeLongchamp, *Nat Commun* **2013**, *4*: 2238; H. Bronstein, Z. Chen, R. S. Ashraf, W. Zhang, J. Du, J. R. Durrant, P. Shakya Tuladhar, K. Song, S. E. Watkins, Y. Geerts, M. M. Wienk, R. A. J. Janssen, T. Anthopoulos, H. Sirringhaus, M. Heeney and I. McCulloch, *Journal of the American Chemical Society* **2011**, *133*, 3272-3275; J. Li, Y. Zhao, H. S. Tan, Y. Guo, C.-A. Di, G. Yu, Y. Liu, M. Lin, S. H. Lim, Y. Zhou, H. Su and B. S. Ong, *Scientific Reports* **2012**, *2*: 754.
- [103] R. Noriega, A. Salleo and A. J. Spakowitz, *Proceedings of the National Academy of Sciences* **2013**, *110*, 16315-16320.
- [104] R. A. Street, *Science* **2013**, *341*, 1072-1073.
- [105] R. Noriega, J. Rivnay, K. Vandewal, F. P. V. Koch, N. Stingelin, P. Smith, M. F. Toney and A. Salleo, *Nat Mater* **2013**, *12*, 1038-1044.
- [106] C. R. Singh, G. Gupta, R. Lohwasser, S. Engmann, J. Balko, M. Thelakkat, T. Thurn-Albrecht and H. Hoppe, *Journal of Polymer Science Part B: Polymer Physics* **2013**, *51*, 943-951.
- [107] A. Luzio, L. Criante, V. D'Innocenzo and M. Caironi, *Scientific Reports* **2013**, *3*: 3425.
- [108] A. Kokil, K. Yang and J. Kumar, *Journal of Polymer Science Part B: Polymer Physics* **2012**, *50*, 1130-1144.
- [109] H. Bässler and A. Köhler in *Organic Light-Emitting Diodes (OLEDs), Materials, Devices and Applications, Vol. 1* (Ed. A. Buckley), Woodhead Publishing Sawston, **2013**, pp. 1-688.
- [110] P. N. Murgatroyd, *Journal of Physics D: Applied Physics* **1970**, *3*, 151.
- [111] Z. An, J. Yu, B. Domercq, S. C. Jones, S. Barlow, B. Kippelen and S. R. Marder, *Journal of Materials Chemistry* **2009**, *19*, 6688-6698.
- [112] G. Horowitz, *Journal of Materials Research* **2004**, *19*, 1946-1962; G. Horowitz in *Semiconducting Polymers: Chemistry, Physics and Engineering, Vol. 2* Eds.: G. Hadziannou and G. G. Malliaras, Wiley, Weinheim, **2007**, pp. 531-566; A. R. Brown, C. P. Jarrett, D. M. de Leeuw and M. Matters, *Synthetic Metals* **1997**, *88*, 37-55.

- [113] S. M. Sze and K. K. Ng, *Physics of Semiconductor Devices*, Wiley, Weinheim, **2007**, pp 1-815.
- [114] C. R. Newman, C. D. Frisbie, D. A. da Silva Filho, J.-L. Brédas, P. C. Ewbank and K. R. Mann, *Chemistry of Materials* **2004**, *16*, 4436-4451.
- [115] W. Shockley, *Proceedings of the IRE* **1952**, *40*, 1365-1376.
- [116] G. Horowitz, *Advanced Materials* **1998**, *10*, 365-377.

4. OVERVIEW OF THE THESIS

This thesis deals with the tailor-made synthesis and characterization of different donor (D) - acceptor (A) conjugated materials and fundamental investigation of their structure-property relationship. This includes the primary question of influences on optical, electrochemical and electronic properties due to a specific DA arrangement. In general, a successful strategy to extend the absorption to longer wavelengths for low band gap materials is the alternation of D and A units along a conjugated polymer chain.

The key for understanding of structure-property correlations of this class of materials is essential for developing new low band gap (LBG) materials for the application in optoelectronic devices. Thus, this thesis focuses on fundamental issues like the diverse arrangement of D and A units in conjugated materials, e.g. random or alternating, and their influence on optical, electrochemical and electronic properties.

The primary part of the work is the comparison of conjugated compounds which have either a random or an alternating arrangement of D and A units. Herein, the main priority lies on the tailor-made syntheses and characterization of materials with incorporated D and A units in a varying arrangement. This includes the synthesis, by a modular synthetic strategy, of random and alternating well-defined monodisperse low molecular weight compounds on the one hand and on the other hand, oligomers and copolymers. To make this possible, a few unique monomers were synthesized to obtain the specific target molecules. The synthetic strategy is based on the combination of bifunctional AB type and AA/BB type monomers. These were converted into conjugated oligomers and copolymers with a palladium catalyzed Suzuki coupling polycondensation. Thus, this systematic structural variation enables us to directly compare the alternating with the randomly arranged conjugated systems in a precise manner.

This thesis focuses on the optical, electrochemical and electronic properties of conjugated materials with varying DA arrangement. We examined different DA systems as illustrated in a brief schematic overview in Figure 1. We choose 2,1,3-benzothiadiazoles (B) and 1,4,5,8-naphthalenetetracarboxylic diimides (NDI) as important acceptor moieties and widely used thiophenes (T) as donor units. The different systems are well-defined low molecular weight BT molecules, their oligomers and copolymers and T-NDI-T systems. Key aspects were the comparison of random and alternating arrangement of the D and A units as well as the investigation of donor-acceptor-donor systems in which the donor strength is increased.

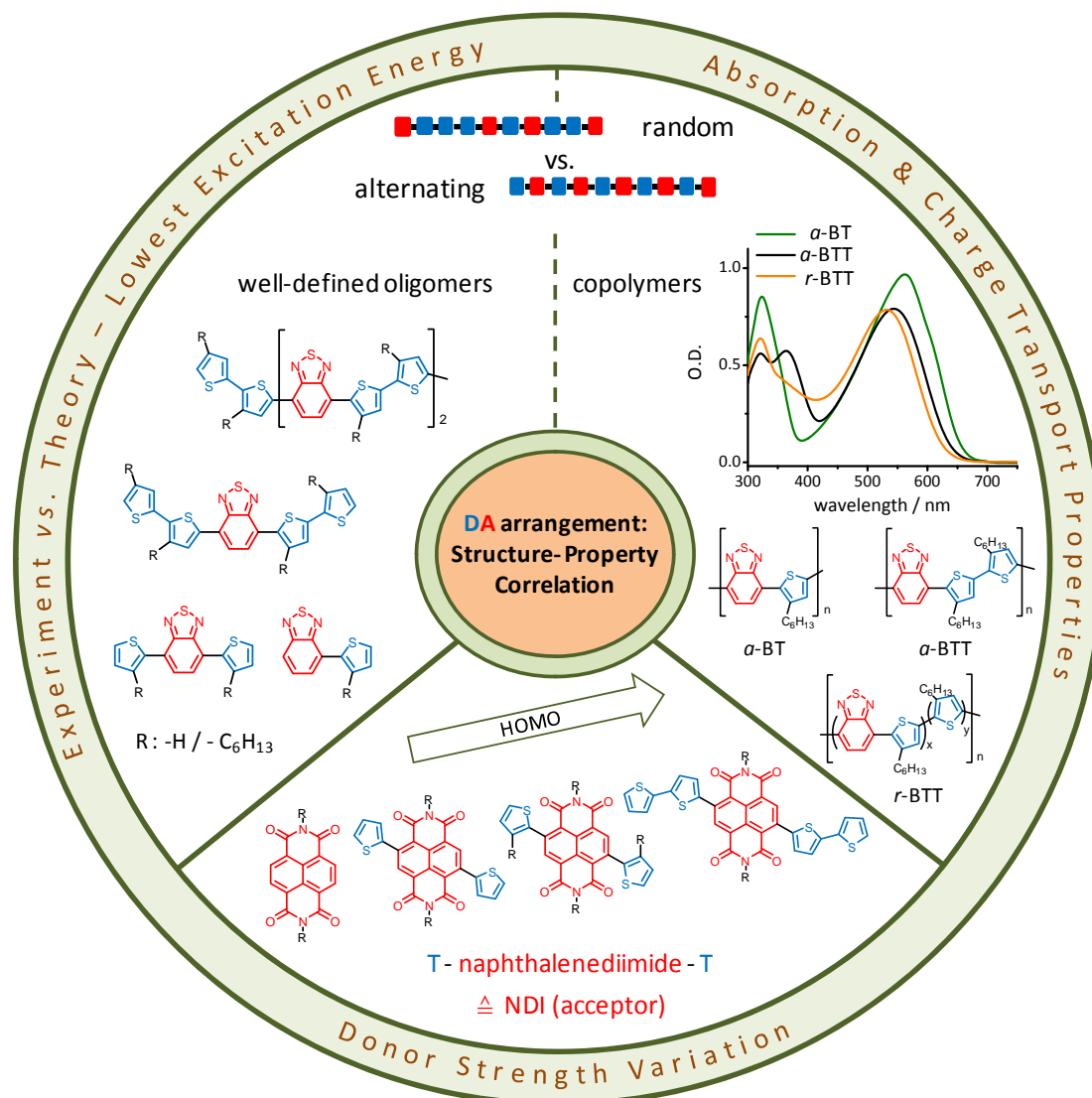


Figure 1: The fundamental structure-property relationship and its influence on important parameters such as absorption, charge transport, thermal properties and energy levels are investigated. We developed a modular concept using AB and AA/BB type monomers, consisting of 2,1,3-benzothiadiazole (B) as acceptor and thiophenes (T) as donor units, to examine conjugated materials with similar DA composition. We compared experiments with theory and investigated different molecular weights with diverse DA arrangements. Another relevant aspect is the impact of increasing donor strength on the absorption and energy levels in low molecular weight compounds consisting of naphthalenediimides (NDI) as acceptor and thiophenes (T) as donor units.

The first part of this thesis (chapter 5) deals with well-defined monodisperse low molecular weight systems and oligomers with a specific arrangement, alternating or random, which were investigated in a combined experimental and theoretical study.

In particular the energetic position of the first electronic transition was discussed due to its importance in LBG materials. In this manuscript alternating and corresponding random systems with thiophene (T) as donor unit and 2,1,3-benzothiadiazole (B) as acceptor unit are synthesized and experimental as well as theoretical data are critically compared against each other. The problem of discrepancies between experiment and theory is addressed and interestingly the results show no dependency of DA arrangement on the first excitation energies.

In the second part (chapter 6) we extended the question towards copolymers. We addressed our investigations also on the electrochemical and charge carrier properties. For this, a target random copolymer was compared with two appropriate alternating copolymers, all consisting of B as acceptor and hexylthiophene (T) as donor units. The systematic structural variation enables us to compare the copolymers in a precise manner. The goal was to evaluate the diversity between random and alternating arrangement in conjugated copolymers. With this comparative study we elucidated the interdependence of the DA arrangement in these copolymers and material properties.

The third part (chapter 7) includes the investigation of low molecular weight donor-acceptor-donor compounds. Herein the main question was how an increase of the number of donor units and thus the donor strength influences the optical and electrochemical properties. Therefore, a series of low molecular weight 1,4,5,8-naphthalenetetracarboxylic diimides (NDI) as acceptor were synthesized. By attaching different thiophene (T) donor units to the NDI core, we were able to tune the donor strength. The structure-property relationship was investigated by a systematic study of the optical and electrochemical properties. The results demonstrate that the increasing donor strength has considerable impact on the optical as well as electrochemical properties.

Tailored syntheses of AB type monomers

A challenging task in this work was the syntheses of the tailor-made AB type bifunctional monomers M1 and M2. The synthetic route is depicted in Figure 2. We synthesized the monomers in such a way, that the acceptor is bromo-substituted and the donor unit contains the boronic acid ester functionality, to enhance the oxidative addition in the Suzuki coupling reaction.

To obtain comparable DA molecules, first an asymmetric starting compound 3 consisting of D and A units is necessary. The drawbacks in synthesis of such

asymmetric compounds like over-reaction of the reagents to form symmetric products, by-products, and residual starting materials which lead to an inefficient synthesis route could be effectively overcome by a careful selection of the reaction conditions. High yields of 56 % for **3** were achieved by Suzuki coupling reaction of 4,7-dibromo-2,1,3-benzothiadiazole with 3-hexylthiophene-2-boronic acid pinacol ester **2** instead of an ineffective Kumada coupling reaction of 4,7-dibromo-2,1,3-benzothiadiazole with 2-bromo-3-hexylthiophene leading to a mixture of product and by-products.

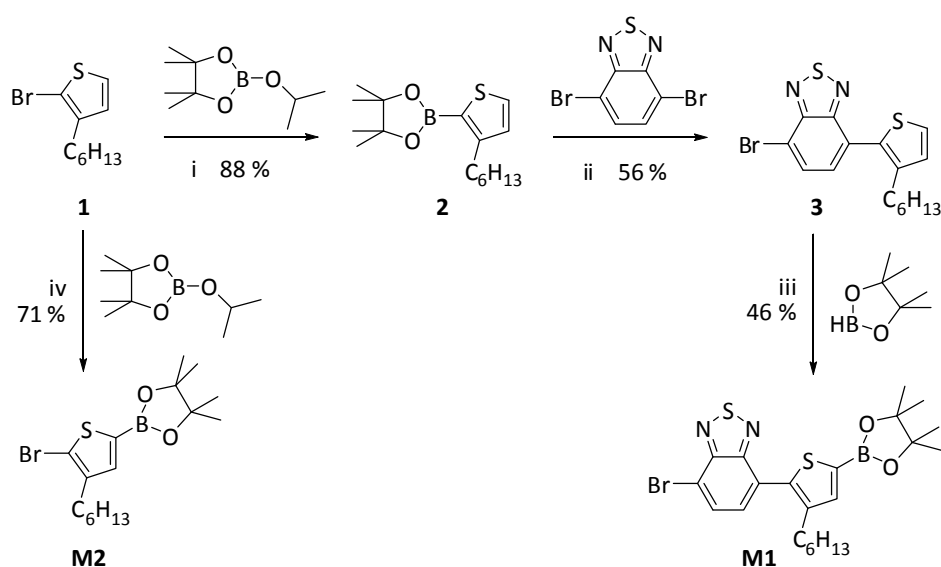


Figure 2: Synthesis of AB type monomers **M1** and **M2**. Reaction conditions: (i) $i\text{PrMgCl}$ in THF at rt; (ii) $\text{Pd}(\text{PPh}_3)_4$, aq. Na_2CO_3 in EtOH/toluene at reflux; (iii) $[\text{Ir}(\text{COD})\text{Cl}]_2/\text{dtbpy}$ in THF at reflux; (iv) $\text{TMPMgCl}\cdot\text{LiCl}$ in THF at rt.

Regarding the syntheses of the desired bifunctional monomers, conventional methods to introduce the boronic acid ester functionality are not applicable since the bromo functional group is present. Hence, we chose to lithiate the bromo-substituted compounds, quenching them with trimethylborate and generate the boronic acid ester by hydrolysis. Subsequent conversion into boronic acid pinacol ester was ineffective and led to relatively low yields.

Therefore, the conversion into the desired final monomer **M1** was successfully performed in relatively high yields of 46 % by Ir-catalyzed borylation of the asymmetric compound **3**. The AB type monomer **M2** was synthesized starting from compound **1** with the Knochel-Hauser base in high yields of 71 %. Hence, the conversion into the desired bifunctional monomers was successfully performed by

optimization of synthesis methods and by overcoming difficulties in the purification. These bifunctional AB type monomers are important for a tailor-made synthesis and characterization of direct comparable DA conjugated molecules which are presented in the next chapters.

In the following, a brief summary of the main results is presented for each manuscript. Further details concerning the synthesis, characterization and interpretation of the data can be found in the respective chapters (5-7).

Optical absorption in donor-acceptor polymers - alternating vs. random (Chapter 5)

This chapter focuses on the question of whether the alternating or random arrangement of D and A units of conjugated materials have an impact on the optical absorption of small molecular weight DA systems. In detail we discuss the energetic position of the first electronic transition, because of its importance in low bandgap materials. Herein, we calculate the excitations in oligomers with thiophene (T) as donor and 2,1,3-benzothiadiazole (B) as acceptor component. This was done by using time-dependent density functional theory (TDDFT) based on non-empirically tuned range separated hybrid functionals. Corresponding systems are synthesized and experimental and theoretical data are critically compared against each other.

We developed a synthesis strategy to obtain directly comparable alternating and random polymers. This was realized by a combination of bifunctional AB type and AA/BB type monomers. They were converted into conjugated oligomers and copolymers with palladium catalyzed Suzuki coupling polycondensation. We deliberately make use of this AB type and AA/BB type approach to obtain materials that are expected to have in total the same amount of donor (T) and acceptor (B) units. This results in conjugated random copolymers *r*-BTT ($n = 4; 15$) and alternating copolymers *a*-BTT ($n = 5; 10$) with varying molecular weights, where n is the number of repeat units.

The first question of concern is, is there any difference in optical gap for alternating and random arrangement. We compared experimental results (measured in solution) with the corresponding theoretically calculated systems (for single molecules in gas phase). The molecules in experiment have hexyl side chains on the thiophene units, whereas for simplicity the side chains are replaced by hydrogen in theory.

The experimental measured maxima of the lowest absorption peaks for the higher molecular weight oligomers of *a*-BTT and *r*-BTT show only small differences with a magnitude of 0.09 eV. Our data suggests that the nature of the D and A ordering has

only little influences on the gap. The theoretical findings are in line with the experimental results. The first excitation energies for alternating and random systems differ just with a magnitude of 0.05 eV. We conclude that the influence of the specific arrangement of donor and acceptor units on the optical gap is almost negligible. The noticeable interesting difference between experiment and theory are the absolute values of the excitation energies. We observe around 0.7 eV higher excitation energies for the experimental values than for the theoretically calculated ones. The higher excitation energies obtained in the experiment are larger than one would expect based on the accuracy of the experiment and calculations. As we can exclude that our TDDFT underestimates charge transfer excitation energies, the disagreement is regarded as physically significant.

To analyze the discrepancy between the experimental data and theoretical predictions we investigate the lowest excitation energies in dependence of the molecular weight (*cf.* Fig. 3). Therefore we additionally synthesized well-defined monodisperse low molecular weight compounds.

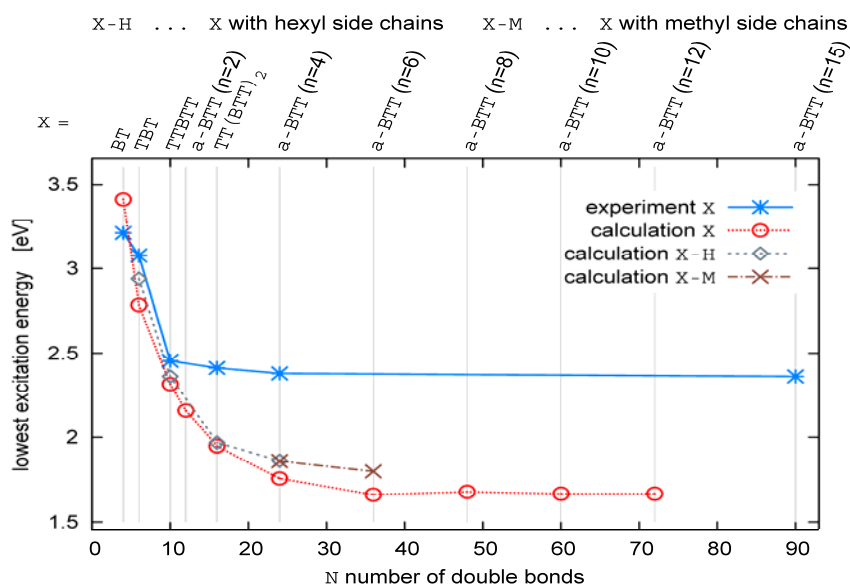


Figure 3: Lowest excitation energies as a function of the number of double bonds N . The experimental data points reflect the maxima of the UV/Vis spectra. The calculated data points are obtained from tuned BNL TDDFT linear response calculations. All systems in the experiment have hexyl side chains (C_6H_{13}) attached to the thiophene rings; for the calculations we show data points for systems with none, hexyl and methyl side chains. The number n of repeat units is given in brackets, where one n corresponds to 6 double bonds ($n = 6N$).

As result we observe a good agreement between experiment and theory for small systems. However, when the systems get larger, the difference between our experimental and calculated data increases. For further investigation of any influence of the side chains, we extend our theoretical calculations on systems with hexyl and methyl side chains. In fact the theoretical excitation energy changes by at most 0.15 eV towards the experimental value for hexyl or methyl side chains. That indicates that the influence of the side chains could explain part of the discrepancy, but not all of it.

We additionally discussed any solvent effects and conclude that the solvent plays only a little role, not only for the experiment but also for theory. Furthermore, the possibility that the experimental geometries are more distorted than the stretched geometries used in the calculation is discussed. However, utilizing a curved structure for theoretically calculations did not explain the discrepancy. But what really matters is a difference in the effective conjugation length. On the one hand the experimental excitation energies start to saturate at a number of double bonds of $N = 15$, whereas on the other hand in the theory the saturation is at $N = 35$. This is not unexpected due to different factors that are able to limit the effective conjugation length like interactions between different chains, kinks and torsions in the structure.

We conclude that the influence of the specific arrangement of donor and acceptor monomers on the optical gap is limited and that effects beyond the single molecule level truly limit the size of the experimentally observed optical gap.

Random vs. alternating donor-acceptor copolymers: A comparative study of absorption and field effect mobility (Chapter 6)

This chapter is a follow-up chapter of 5, where we compared random and alternating conjugated small molecular weight molecules in terms of their optical properties in a combined experimental and theoretical study. We demonstrated that the influence of the specific arrangement of donor and acceptor units on the optical gap is very small within these molecules. Encouraged from these results we extended our study to conjugated DA copolymers. These copolymers consist of hexylthiophene (T) as the donor and 2,1,3-benzothiadiazole (B) as the acceptor component. The copolymers were synthesized via Suzuki coupling polycondensation and were fully examined in respect to their thermal, optical, electrochemical, and charge carrier properties. Here also, the strategy was to synthesize a target random copolymer and compare it to appropriate alternating copolymers of structural similarity. We take

advantage of the bifunctional AB type monomers to obtain the randomly linked copolymer *r*-BTT. For comparison we synthesized on the one hand a strict alternating α -BTT copolymer where B units alternate with a bithiophene unit (TT) and on the other hand a strict alternating copolymer α -BT in which one B unit is coupled just with one thiophene unit (T). The copolymers show similar thermal stability ($T_{d-5\%} \geq 420$ °C) and similar glass transition temperatures of 72 °C and 60 °C for *r*-BTT and α -BTT, respectively. The copolymer α -BT shows the highest T_g of 122 °C.

The UV/Vis absorption spectra in solution indicate that the randomly linked copolymer *r*-BTT is very similar to the alternating copolymer α -BTT (*cf.* Fig. 4a)). In contrast, copolymer α -BT shows a considerable red-shift (31 nm) of the absorption maximum indicating a better intra-chain delocalization/planarization. The corresponding absorption in thin films is broadened for all copolymers (*cf.* Fig. 4b)). However, only the copolymers *r*-BTT and α -BTT reveal bathochromically shifted absorption, whereas the latter one shows the most red-shifted absorption and a significantly reduced optical gap (1.75 eV). This implies that copolymer α -BTT exhibits stronger inter-chain interactions leading to an energetically more delocalized π -electron system than the copolymers *r*-BTT or α -BT.

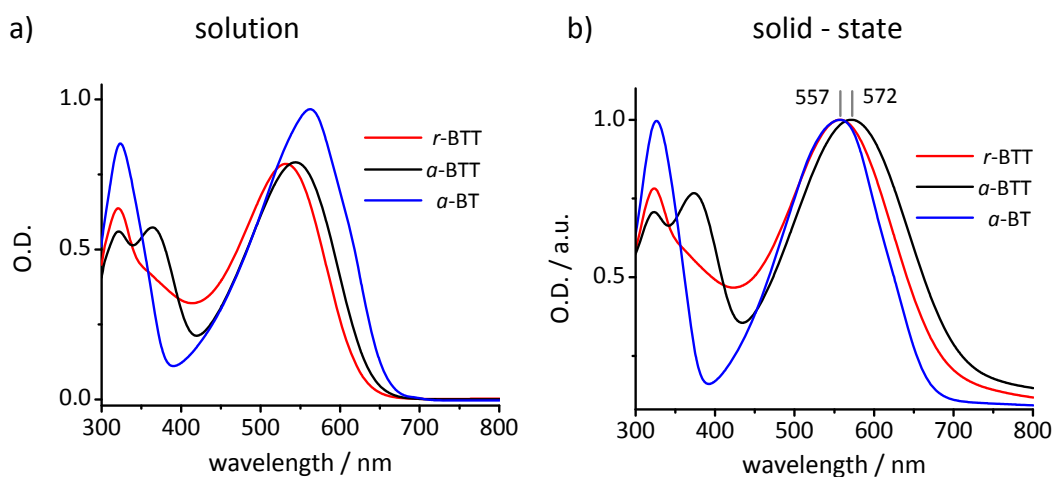


Figure 4: UV/Vis absorption spectra of the copolymers *r*-BTT, α -BTT, and α -BT **(a)** in *o*-Dichlorobenzene solution at a concentration of 0.02 mg mL^{-1} at room temperature and **(b)** in films doctor-bladed from chlorobenzene solution on glass slides.

The remarkable difference between the copolymers *r*-BTT and α -BTT can be found in the charge carrier properties. The copolymer α -BTT is superior in terms of its hole carrier mobility of $1.5 \times 10^{-3} \text{ cm}^2 \text{ V}^{-1} \text{ s}^{-1}$ which is two orders of magnitude higher than that of the random copolymer *r*-BTT ($3.0 \times 10^{-5} \text{ cm}^2 \text{ V}^{-1} \text{ s}^{-1}$). Further studies in a series of

well-defined molecular weight samples without change in the DA arrangement are required to elucidate any influences of molecular weight on the mobility.

The conclusion of this comparative study was that the copolymers *r*-BTT and *a*-BTT are similar concerning their thermal, electrochemical and optical properties, but differ in terms of their hole carrier mobility. This work clearly elucidates the interdependence of the DA arrangement in donor-acceptor copolymer and material properties.

Optical gap tuning in thiophene-substituted naphthalenediimides (Chapter 7)

Besides the structure-property relationship in low band gap copolymers with varying DA arrangement, we were also interested to understand the difference between donor-acceptor-donor and donor-donor-acceptor-donor-donor systems. A relevant question in chapter 7 is therefore, how the number of donor units influences the optical gap. We want to decrease the optical gap towards LBG materials to improve the visible light absorption over a broad wavelength range. The structure-property relationship for model compounds consisting of naphthalenediimides (NDI) as acceptor and diverse thiophenes (T) as donor units was elucidated by a systematic study of the optical and electrochemical properties. The aim of this study was to selectively lower the band gap energies of T-NDI-T systems by raising the HOMO energy level.

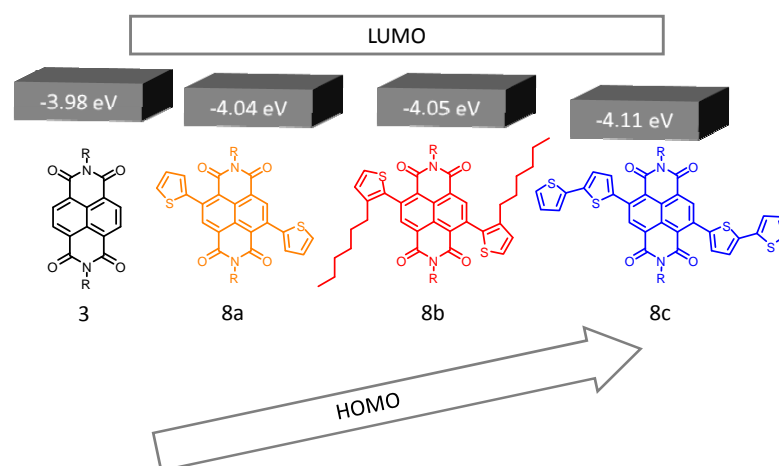


Figure 5: Energy level scheme of naphthalenediimides illustrating that the thiophene substituents lead to a considerably bathochromic shift of the absorption and influence the HOMO energy level. With increasing number of donor (T) units the HOMO level is increasing whereas the NDI acceptor (A) core is responsible for the LUMO energy level, which stays nearly constant.

Therefore, a series of low molecular weight NDIs extended with thiophene (T) donor units are synthesized from 2,6-dibromonaphthalene dianhydride by imidization and a subsequent Suzuki coupling reaction. In particular, we synthesized four soluble compounds, one of them without any donor substituent as reference compound (3) and three others with different types and numbers of thiophene donor substituents at the 2,6-positions of the NDIs. Based on a systematic variation of the donor units using single thiophene (8a), 3-hexylthiophene (8b) and bithiophene (8c) substituents, we were able to investigate the relationship between structure and the electronic, thermal and optical properties.

As can be seen in Figure 5 the electrochemical reduction and thus the LUMO energy levels are not significantly affected by the attached thiophene units. However, these donor substituents drastically reduce the optical gap from 3.16 eV to 1.81 eV followed by increasing of the HOMO energy level. Since the electron-withdrawing naphthalene diimide core is responsible for the reduction potential, the LUMO value remains almost constant and thus, we are able to decrease the optical gap selectively about 1.35 eV by raising the HOMO energy level.

Furthermore, we tested 8b with the SCLC method in order to elucidate the charge carrier mobility. The remarkable electron mobility of $2.3 \times 10^{-3} \text{ cm}^2 \text{ V}^{-1} \text{ s}^{-1}$ for 8b makes this class of donor-acceptor systems a highly suited electron acceptor material (n-type) for various applications like photovoltaic devices or field-effect transistors.

In conclusion the results clearly correlate the properties to the structure of the T-NDI-T systems.

Individual Contributions to Joint Publications

The individual contributions of the authors to each manuscript are specified in the following.

Chapter 5

This work is published in *Physical Chemistry Chemical Physics* (2013, 15, 20016 - 20025) with the title:

“Optical absorption in donor-acceptor polymers - alternating vs. random”

by Andreas Karolewski, **Anne Neubig**, Mukundan Thelakkat and Stephan Kümmel

I synthesized and characterized all compounds of this work, did the analysis and wrote the part “Synthesis and characterization” of the manuscript. I was involved in the scientific discussion and the manuscript correction. Andreas Karolewski did all calculations and wrote the first version of the manuscript except for the section “Synthesis and characterization”. He was involved in the scientific discussion and the manuscript correction. Mukundan Thelakkat and Stephan Kümmel supervised the project, were involved in the scientific discussion and corrected the manuscript.

Chapter 6

This work is published in *Polymer* (2014, 55, 2621 - 2627) with the title:

“Random vs. alternating donor-acceptor copolymers: A comparative study of absorption and field effect mobility”

by **Anne Neubig** and Mukundan Thelakkat.

I synthesized and characterized all compounds of this work, did the analysis and wrote the manuscript. Mukundan Thelakkat supervised the project, was involved in the scientific discussion and corrected the manuscript.

Chapter 7

This work is prepared as manuscript with the title:

“Optical gap tuning in thiophene-substituted naphthalenediimides”

by **Anne Neubig**, Mathis-Andreas Muth and Mukundan Thelakkat

I did the synthesis and characterization of compound 8b, performed the CV analysis and did UV/Vis film measurements of all compounds. I wrote the manuscript except for the part “charge carrier mobility measurements”. This section was written by Mathis-Andreas Muth who also did the SCLC measurements of compound 8b. The other samples arise from my diploma thesis.

Mukundan Thelakkat supervised the project, was involved in the scientific discussion and corrected the manuscript.

5. *OPTICAL ABSORPTION IN DONOR-ACCEPTOR POLYMERS - ALTERNATING VS. RANDOM*

*Andreas Karolewski^{‡a}, Anne Neubig^{‡b}, Mukundan Thelakkat^{*b} and
Stephan Kümmel^{*a}*

^aTheoretical Physics IV, University of Bayreuth, 95440 Bayreuth, Germany.
E-mail: Stephan.Kuemmel@uni-bayreuth.de

^bMacromolecular Chemistry I, University of Bayreuth, 95440 Bayreuth, Germany.
E-mail: Mukundan.Thelakkat@uni-bayreuth.de

‡ These authors contributed equally to this work.

Published in *Physical Chemistry Chemical Physics* **2013**, 15, 20016-20025.

Reproduced by permission of the PCCP Owner Societies.

Abstract

We investigate in a combined theoretical and experimental study the influence that the specific arrangement, e.g., alternating or random, of donor and acceptor units has on the optical absorption of extended molecules. Because of its important role in low gap polymers we discuss in particular the energetic position of the first electronic transition. We theoretically determine the excitations in extended oligomers with thiophene as the donor and 2,1,3-benzothiadiazole as the acceptor component by using time-dependent density functional theory based on non-empirically tuned range separated hybrid functionals. Corresponding systems are synthesized and theoretical and experimental data are critically compared to each other. We conclude that the influence of the specific arrangement of donor and acceptor monomers on the optical gap is limited and that effects beyond the single molecule level effectively limit the size of the experimentally observed optical gap.

1 Introduction

The search for low gap polymers is an important step in improving the efficiency of organic solar cells based on conjugated polymers.^[1-5] For systematically designing low gap polymers it is beneficial to understand the complex electronic processes that typically occur in these systems. The absorption of light that results in an excitation (“exciton formation”) is one important step in the sequence of processes that determine solar cell efficiency.^[6] There are different strategies for obtaining low gap polymers.^[4] Among the most important ones are increasing the conjugation length, e.g., by increasing the planarity of the polymer, and the combination of electron rich (donor) and electron poor (acceptor) monomers along the conjugated polymer backbone.^[7] In the latter case the reduction of the bond length alternation and the formation of partial intramolecular charge transfer (CT) excitations between the donor (D) and acceptor (A) moieties are considered to be responsible for the low gap.^[4,8]

In this article we focus on donor acceptor (DA) polymers and analyze how far the specific arrangement of D and A units within a polymer influences the optical absorption. Specifically we address the question of whether the optical gap and other absorption peaks differ considerably between a molecule with a random arrangement of D and A units and a molecule in which the same total number of D and A units is arranged in a strictly alternating way. The answer to this question is important for our fundamental understanding of DA systems and for developing future synthesis strategies. Usually low gap polymers based on D and A moieties are synthesized by arranging the D and A units in a strict alternating order. Whether this strict alternating order is necessary for lowering the gap is not studied. If this is not necessary and the D and A units can be arranged in any random order to obtain the same effect, then the synthetic strategy to obtain a variety of new low gap polymers can be more innovative involving different kinds of monomers in any random fashion. This also allows improving the solubility of such polymers. Therefore, the question of the importance of the ordering of the D and A units is discussed in this paper.

Our study is based on thiophene (T) as the D and 2,1,3-benzothiadiazole (B) as the A component. Both of these constituents are frequently used in the field of low gap oligomers and polymers for organic photovoltaic devices.^[9-15] We computationally analyze the low lying excitations of these systems in detail. In agreement with other studies of similar systems^[16] we find that they can be described as having, at best, “partial” CT character, and we compare the theoretical findings in detail to experiments.

The type of accurate, non-empirical calculations for systems of considerable size that we present here, are made possible by recent progress in the development of (Time Dependent) Density Functional Theory ((TD) DFT).^[17–24] Specifically, we employ a range separated hybrid (RSH) functional in which the range separation parameter is chosen according to a non-empirical, self-consistent procedure designed to yield a reliable description of excitations in multichromophoric systems.^[21,25,26] Using the correct functional class to account for the complexity of the excitations in DA polymers is a decisive prerequisite for the type of computational study that we present here.

Our manuscript is organized as follows. In Section 2 we give a brief overview of the studied systems, followed by an outline of the theoretical approach and the experimental synthesis in Section 3. We present the results of our calculations in Section 4, comparing different D–A arrangements and oligomer sizes in a single molecule approach and predicting the effective saturated conjugation length. In the same section we compare the theoretical findings to the corresponding experimental data. Occurring differences are analyzed in Section 5. The maximum achievable conjugation length emerges as the main factor limiting the optical gap.

2 Systems

Fig. 1 and 2 schematically depict the oligomers that we examine in this article. a-BTT and a-BTT-H show strictly alternating arrangements of thiophene (T) as a donor and 2,1,3-benzothiadiazole (B) as an acceptor (upper left and left in Fig. 1 and 2, respectively). The difference between these two systems is the presence of hexyl side chains (H) on the thiophene units in a-BTT-H. The systems r-BTT and r-BTT-H (upper right and right in Fig. 1 and 2, respectively) are molecules in which T and B units are combined to yield random arrangements of T and BT (Fig. 3) components. For a-BTT and r-BTT we did calculations with the number n of repeat units ranging from $n = 1$ to $n = 12$.

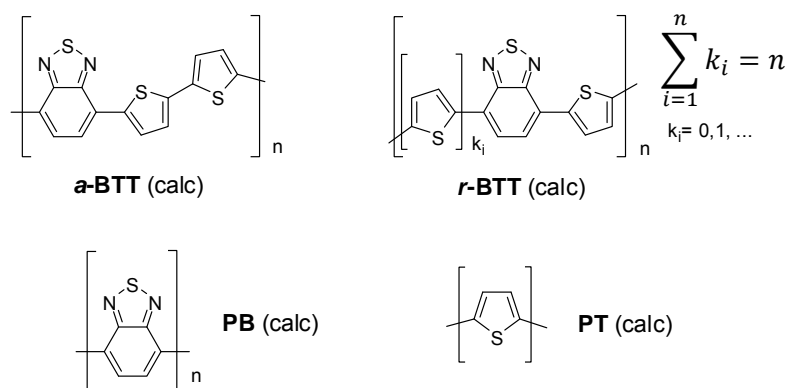


Figure 1: Schematic of the oligomeric systems examined in the calculations.

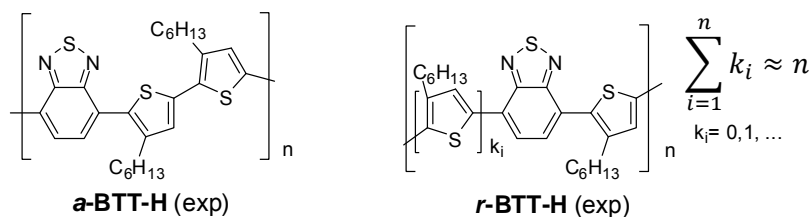


Figure 2: Schematic of the oligomeric systems examined in experiments. The chain length n can only be determined on average (\bar{n}) from gel permeation chromatography.

For illustration we show the optimized structures for the largest oligomeric calculated systems ($n = 12$) in Fig. 4. For reasons that become clear further below it is sufficient to study just one representative for r-BTT, i.e., one specific random arrangement, for each chain length. In our experiments we synthesized a-BTT-H with an

average number \bar{n} of repeat units of $\bar{n} = 4$ and $\bar{n} = 15$ and a polydispersity $M_w/M_n = 1.7$ and 1.6 , as well as r-BTT-H with $\bar{n} = 5$ and $\bar{n} = 10$ and $M_w/M_n = 1.5$ and 1.6 (see caption of Fig. 2) The only difference to the systems that we use in the calculations are the hexyl side chains. The influence of such side chains is discussed in detail in Section 5. It is important to note that in the calculations we always combined n B with $2n$ T. In this way we ensure that our results are only influenced by the DA arrangement (and not by different D and A ratios). In the synthesis, however, we were only able to obey this rule approximately in the case of r-BTT-H. For a deeper understanding of DA systems and the differences between calculations and experiment we furthermore investigated the donor-only oligomer PT, the acceptor-only oligomer PB as well as the donor-acceptor systems BT, TBT, TBT-H, TTBTT, TTBTT-H, TT(BTT)₂, and TT(BTT)₂-H as shown in Fig. 3 (monodisperse low molecular weight in experiment).

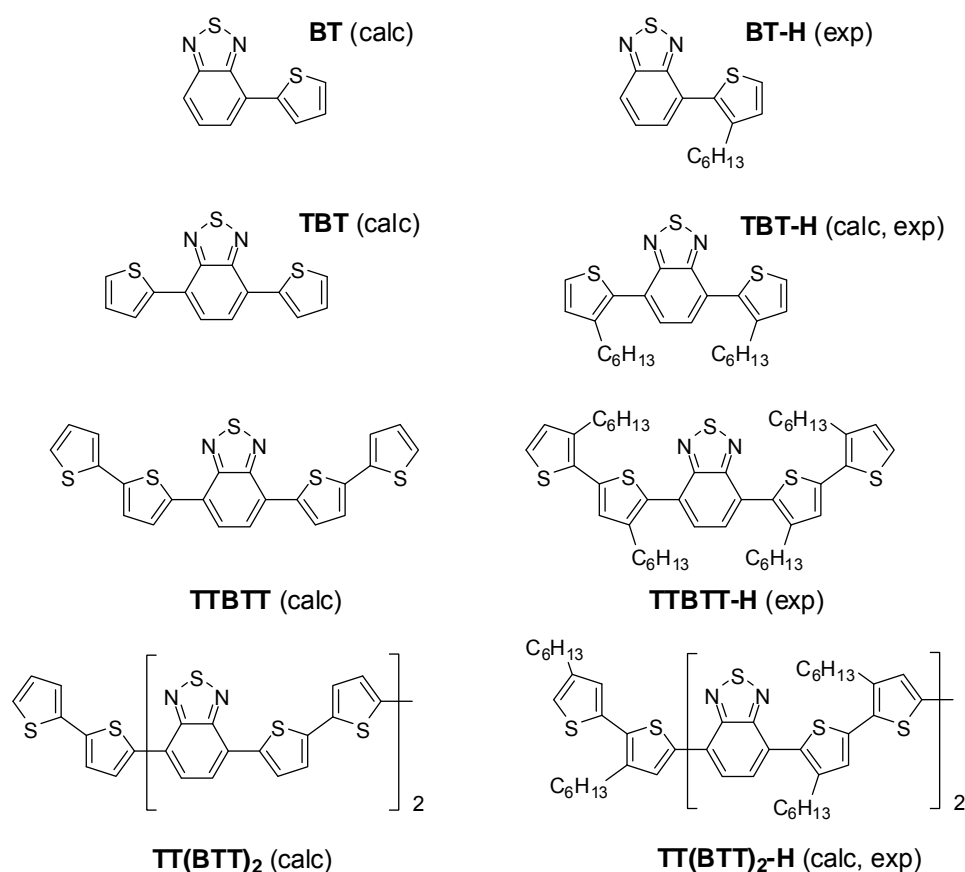


Figure 3: Schematic of the well defined monodisperse low molecular weight systems examined in experiments (labeled with exp) and calculations (labeled with calc).

3 Methodology and synthesis

3.1 Methodology (theory)

The largest systems that we examined in our calculations are conjugated molecular chains with up to 36 aromatic rings. Our method of choice for systems of such size is DFT^[27,28] or TDDFT,^[29,30] respectively, because of its favorable ratio of reasonable quality of results to moderate computational cost. With appropriately chosen functionals, it also allows for little or no empiricism.

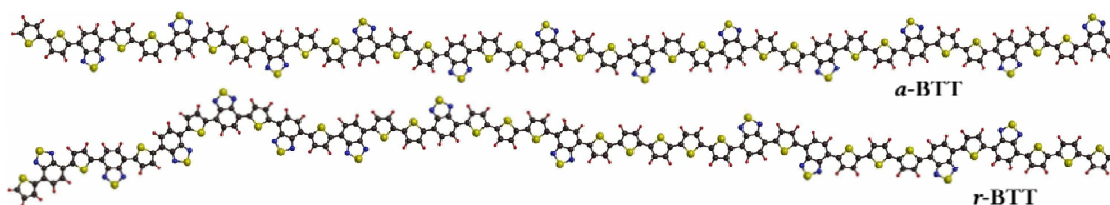


Figure 4: Optimized geometries of α -BTT and r -BTT for $n = 12$, corresponding to a length of 15 nm. The optimization method is described in Section 3.

We optimized the geometries of the systems in Fig. 1 and 3 using the B3LYP functional^[31] with the def2-SV(P) basis set and the Grimme dispersion correction^[32] in Turbomole.^[33,34] This choice is pragmatically motivated by previous experience showing that this approach yields reliable geometries for this type of system.

For the calculation of the excitation energies, which is the critical step in our study, we used linear response TDDFT with the Baer–Neuhauser–Livshits (BNL) RSH functional. It combines LDA-type short range exchange and long range Fock exchange with the Lee–Yang–Parr correlation functional.^[35–37] Since we are calculating optical excitation energies we choose the least square gap tuning condition^[26,38]

$$T_{LS}(\gamma) = \sqrt{\sum_{i=N}^{N+1} [\epsilon_{HOMO}^{\gamma}(i) + E^{\gamma}(i-1) - E^{\gamma}(i)]^2} = \min \quad (1)$$

to determine the range separation parameter γ , which corresponds to approximately twice the inverse of the separation length between short range and long range electronic exchange.^[39,40] $E^{\gamma}(i)$ is the γ -dependent total energy for a system with i electrons and $\epsilon_{HOMO}^{\gamma}(i)$ the eigenvalue of the highest occupied generalized Kohn–Sham

orbital. To account for the system specific magnitude of the highest occupied and lowest unoccupied orbitals we performed the tuning for each molecule separately. With the optimized γ we calculate the BNL excitation energies with the program package QChem^[41] and the 6-31G(d,p) basis set. We expect reliable results from this procedure because it has been shown, e.g. in ref. 16 and 25, that tuned RSH functionals can successfully be applied to DA systems that are similar to the ones studied here, and the resulting excitation energies are consistent with experimental absorption spectra.

In order to test the reliability of this approach we performed several control calculations. To check basis set limitations we optimized the geometries of BT, TBT, and TT(BTT)₂ also with the def2-TZVP basis set (in Turbomole) and performed the γ -tuning and the calculation of the BNL excitation energies with the 6-311G(d,p) basis set (in QChem). In comparison to the calculations with the basis sets mentioned in the previous paragraph, this lead to differences of less than 0.1 eV in the lowest excitation energy. As another test we checked how much using a different RSH functional alters the results. We used the ω PBE functional^[18] for the γ optimization as well as the TDDFT calculation on TT(BTT)₂. Compared to the BNL functional the lowest excitation energy changed by only about 0.02 eV. This is in line with other studies showing that differences between various RSH approaches appear in the ground state energy^[38] and not in optical and fundamental gaps.^[16,42] Finally, we tested how far environmental influences as described by the COSMO solvation model^[43] within Turbomole affect the B3LYP geometries and TDDFT excitation energies and found an overall effect of only 0.04 eV.^[44] These tests confirm the validity of our theoretical setup since all the discrepancies are within the limits of the predictive power of our method itself.

3.2 Synthesis and characterization

3.2.1 Monomer synthesis. The synthesis procedures of the monomers M1 and M2 are outlined in Fig. 5. The AB-type monomer M1 is not documented in the literature; the details of the synthesis are given in the ESI. M1 was obtained by the Ir-catalyzed (Ir(COD)Cl₂) borylation of an asymmetrically substituted compound 1 in the presence of 4,4'-di-tert-butyl bipyridine (dtbpy). The other AB-type monomer M2 is known in the literature but we synthesized it starting from 2-bromo-3-hexylthiophene 2 with the Knochel–Hauser-base (2,2,6,6-tetramethylpiperidinylmagnesium chloride lithium chloride: TMPMgCl·LiCl). Details are given in the ESI. M3 was synthesized by

bromination of 3,4'-dihexyl-2,2'-bithiophene with N-bromosuccinimide according to published procedures.^[45] M4 is commercially available.

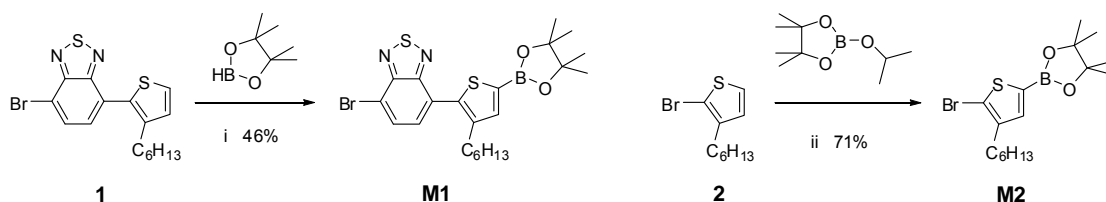


Figure 5: Synthesis of monomers M1 and M2. Reaction conditions: (i) $\text{Ir}(\text{COD})\text{Cl}_2/\text{dtbpy}$ in tetrahydrofuran at reflux; (ii) $\text{TMPMgCl}\cdot\text{LiCl}$ in tetrahydrofuran at room temperature.

3.2.2 Polymer synthesis. Following the synthetic route shown in Fig. 6, the AB-type monomers M1 and M2 were used to obtain the conjugated copolymers r-BTT-H ($\bar{n} = 4$; 15). Using monomers M3 and M4 the alternating copolymers a-BTT-H ($\bar{n} = 5$; 10) were obtained. All copolymers were synthesized via palladium catalyzed Suzuki coupling polycondensation. A variation of reaction conditions led to different molecular weights for r-BTT-H and a-BTT-H. For synthetic details and characterization see the ESI.

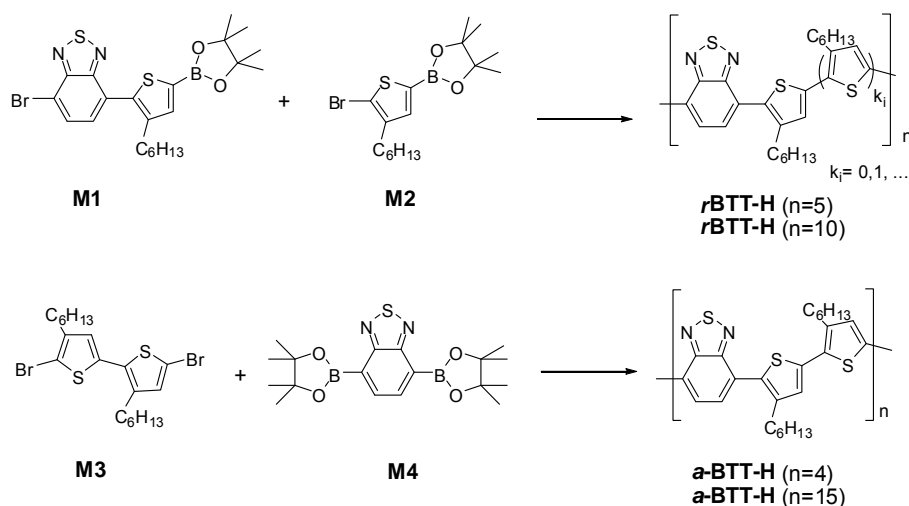


Figure 6: Synthesis of copolymers r-BTT-H and a-BTT-H.

All four conjugated copolymers are completely soluble in common organic solvents like toluene, tetrahydrofuran or methylene chloride. The number average molecular weights of these copolymers were determined using oligomeric gel permeation

chromatography (GPC). Polystyrene was used for calibration of molecular weights. The GPC traces of the copolymers are shown in Fig. S1 (ESI), the respective data are summarized in Table 1.

3.2.3 Oligomer synthesis. The well-defined oligomers TTBTT-H and TT(BTT)₂-H were obtained from polymer a-BTT-H ($\bar{n} = 4$) by preparative GPC after extraction with particular solvents. The crude polymer was extracted sequentially with methanol, ethanol, acetone and methylene chloride. The acetone fraction was used for preparative GPC. Narrow fractions were collected and measured on an analytical GPC setup. Molecular weight analysis of TTBTT-H and TT(BTT)₂-H was done by matrix assisted laser desorption ionization with time of flight detection (MALDI-ToF) mass spectrometry and GPC. The GPC traces and MALDI-ToF spectra of TTBTT-H and TT(BTT)₂-H are shown in the ESI.

Table 1. Number average molecular weights (M_n) determined with GPC, polydispersity index (M_w/M_n) and absorption maximum (E_{max}) of the synthesized compounds.

| | M_n [g mol^{-1}] (GPC) | M_w/M_n (GPC) | E_{max} [eV] |
|----------------------------|-------------------------------------|-----------------|----------------|
| TBT-H | | | 3.08 |
| TTBTT-H | 913 | 1.01 | 2.46 |
| TT(BTT) ₂ -H | 1443 | 1.04 | 2.41 |
| a-BTT-H ($\bar{n} = 4$) | 1841 | 1.74 | 2.38 |
| a-BTT-H ($\bar{n} = 15$) | 7201 | 1.64 | 2.36 |
| r-BTT-H ($\bar{n} = 5$) | 2490 | 1.46 | 2.49 |
| r-BTT-H ($\bar{n} = 10$) | 4478 | 1.59 | 2.45 |

4 Influence of the D and A arrangement on the gap

One of the key properties of a low gap system designed for the use in organic solar cells is the optical gap which is defined as the transition energy between the vibrational ground state (GS) of the electronic GS and the vibrational GS of the first excited electronic state. However, more accessible to theory is the vertical excitation energy that is close or identical to the absorption maximum E_{\max} (see Fig. 7). It is the energy difference of the GS and the first excited state with both states in the GS geometry. Hence, the vertical excitation energy is the optical gap (also called adiabatic excitation energy) plus a first or higher order vibrational energy. The energy that we obtain from a standard TDDFT calculation (E_{calc}) is the vertical excitation energy plus the vibrational zero point energy of the electronic GS. This zero point vibrational energy is below the accuracy of the calculation and the error of the experiment and can be neglected. Therefore E_{calc} and E_{\max} are comparable. The situation and mentioned energies are illustrated in Fig. 7. In the following, if we write lowest or first excitation energy we mean E_{calc} in a calculation and E_{\max} in an experiment.

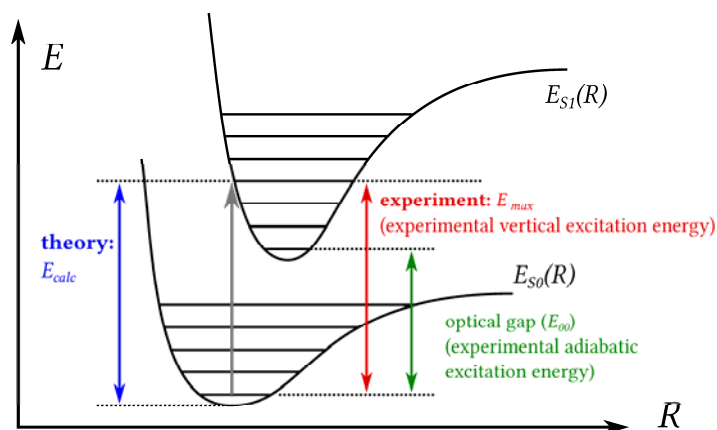


Figure 7: Schematic of the different excitation energy expressions discussed in this work. R is a generalized coordinate. $E_{S_0}(R)$ is the GS energy and $E_{S_1}(R)$ the first excited state energy as a function of this coordinate.

Our focus in this section lies on the differences between the lowest excitation energies of the DA arrangements a-BTT and r-BTT. These differences directly reveal how large the influence of the DA arrangement on the optical gap is. We calculated these energies for the oligomers $n = 1$ up to $n = 12$ with the RSH approach explained in Section 3, studying one representation of r-BTT for each repeat unit n . The resulting

energies E_{calc} are plotted in Fig. 8 as a function of the inverse number of double bonds N^{-1} along the molecular backbone. As discussed in earlier work^[25] we use an exponential fit to extrapolate to the saturation limit. For the monomer ($n = 1$) both systems are identical. Hence, both curves start at the same point. During the progression to larger N the excitation energies of a-BTT and r-BTT almost overlap each other and saturate at 1.63 and 1.67 eV, respectively. Note that all data points are close to the exponential fitting curves. This confirms that for the purposes of our study it is not necessary to consider different statistical arrangements for r-BTT.

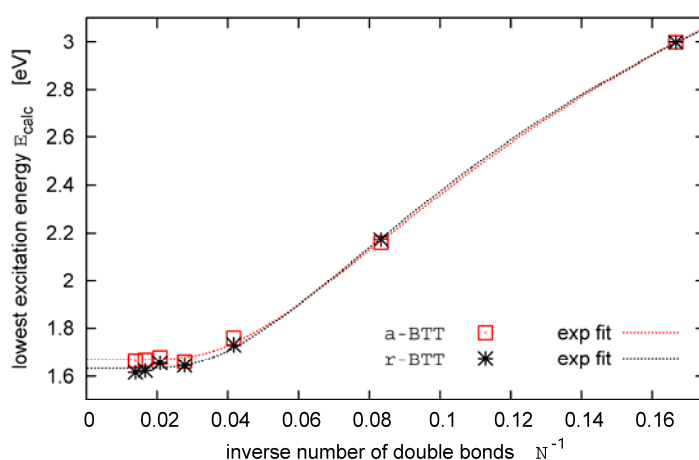


Figure 8: Lowest calculated vertical absorption energies (TDDFT with tuned BNL and 6-31G(d,p) basis) as a function of the inverse number of double bonds N^{-1} .

In addition to predicting the saturation energies we can draw two conclusions from this graph. The first one is the saturation length – the amount of repeat units at which the lowest excitation energy saturates. For both systems it lies between $n = 6$ and $n = 8$. The second conclusion concerns the influence of the relative ordering of D and A components on the first excitation energy. Comparing a-BTT with r-BTT we observe that the respective energy values are very close to each other. Thus, the relative order of D and A in the polymer chain has only a minor influence.

In order to further elucidate the question of how much the DA arrangement influences the first excitation energy we compare the above results to first excitation energies of oligomers that consist of only either D or A monomers. Fig. 9 shows these energies for T oligomers (PT, $n = 1$ to 32) and B oligomers (PB, $n = 1$ to 25) as a function of the inverse number of double bonds N^{-1} . Both systems coincidentally saturate at a vertical excitation energy of 2.15 eV, which is 0.5 eV above the respective

energies of a-BTT and r-BTT. We thus observe the well known effect that combining D and A units reduces the first excitation energy, but in our calculations the magnitude of this reduction is at most 0.5 eV.

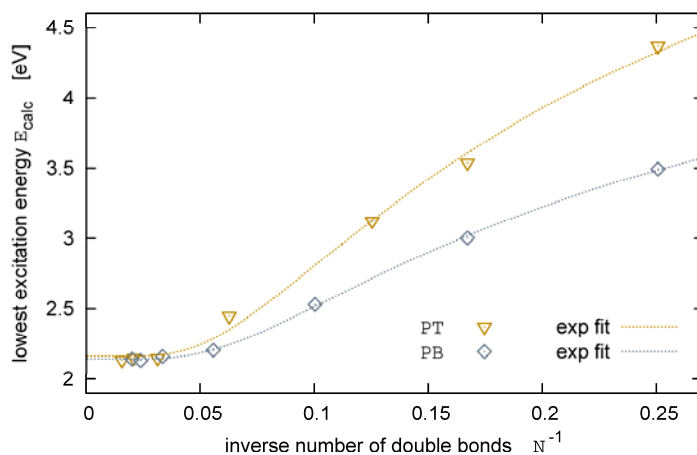


Figure 9: Lowest calculated vertical absorption energies of T and B oligomers as a function of the inverse number of double bonds N^{-1} .

Similar conclusions hold when the analysis is extended to not only take the first excitation energies into account, but also the corresponding oscillator strengths and higher excitations. To this end we show the optical spectra of a-BTT and r-BTT for $n = 6$ in Fig. 10. It shows that both systems have very dominant first excitations with oscillator strengths of similar magnitude. Comparing the spectra obtained for different chain lengths (not shown here) confirms that the oscillator strength and dominance increase with n . Besides the main peak the spectra of a-BTT and r-BTT do not show large differences at higher energies. Thus, the calculations show that the conclusions drawn previously for the first excitation energy are valid in a similar way for the overall optical spectrum: the rearrangement of D and A from a-BTT to r-BTT leads to only relatively small changes.

To gain further insight into the physics of these systems we analyze whether CT is important in the lowest excitations. CT excitations are defined as excitations where a transfer of electronic density from one part of a system to another part occurs during the excitation. Typically, CT excitations are prevalent in DA systems since they combine electron poor and electron rich components. In a figurative sense an electron leaves the donor, thus creating a hole, and is absorbed by the acceptor. It is not clear whether this picture holds in DA oligomers or polymers in which the D and A units are

distributed along the molecular backbone such that D and A parts are not necessarily adjacent to each other.

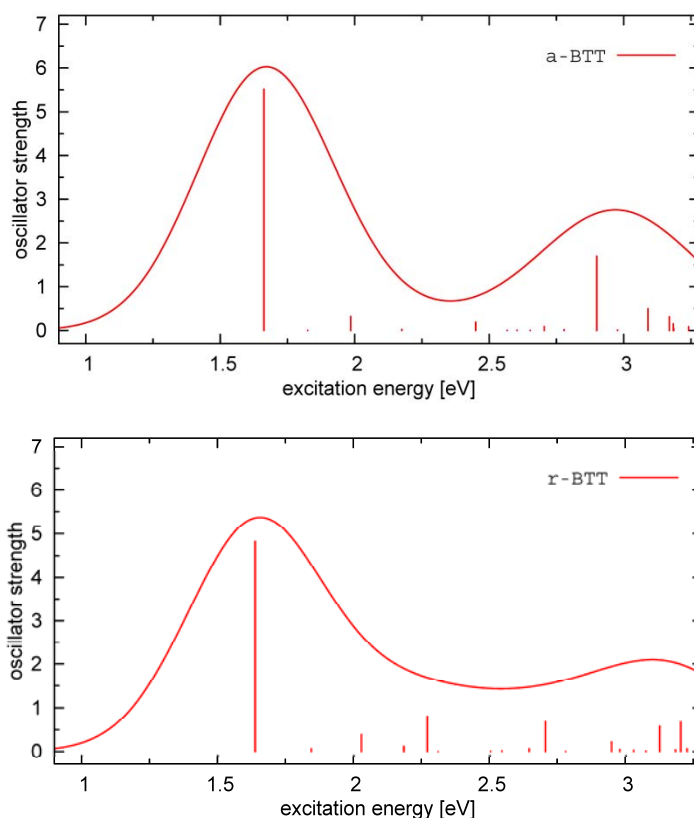


Figure 10: Calculated electronic excitation spectra of a-BTT and r-BTT with $n = 6$ repeat units (6 B and 12 T units). The calculated positions and oscillator strengths are represented by the bars. Linewidths as present in typical experiments are mimicked by a Gaussian broadening with 0.3 eV HWHM (half width half maximum).

In order to examine the CT character of a-BTT and r-BTT we calculated the most dominant natural transition orbital^[46] (NTO) holes and electrons of the first excitation for both systems with a chain length $n = 10$. Fig. 11 (top) shows the most dominant NTO pair for r-BTT accounting for 54 % of the excitation. The “hole orbital” and the corresponding “electron orbital” are localized on the same parts of the molecule and are nearly equal in extension. The only difference that we observe is that parts of the electron NTO are located on the sulfur and nitrogen atoms of the benzothiadiazole unit, whereas the hole NTO does not extend to these regions. This difference is so small that this excitation can be classified as having predominantly valence character and just a small CT component. An analysis of the less dominant NTO pairs (shown in

Fig. S4 of the ESI) shows that some of these have more CT character, but still overall the excitation appears as being of mixed valence-CT character at most, and not a hallmark CT one. Similar conclusions hold for a-BTT.

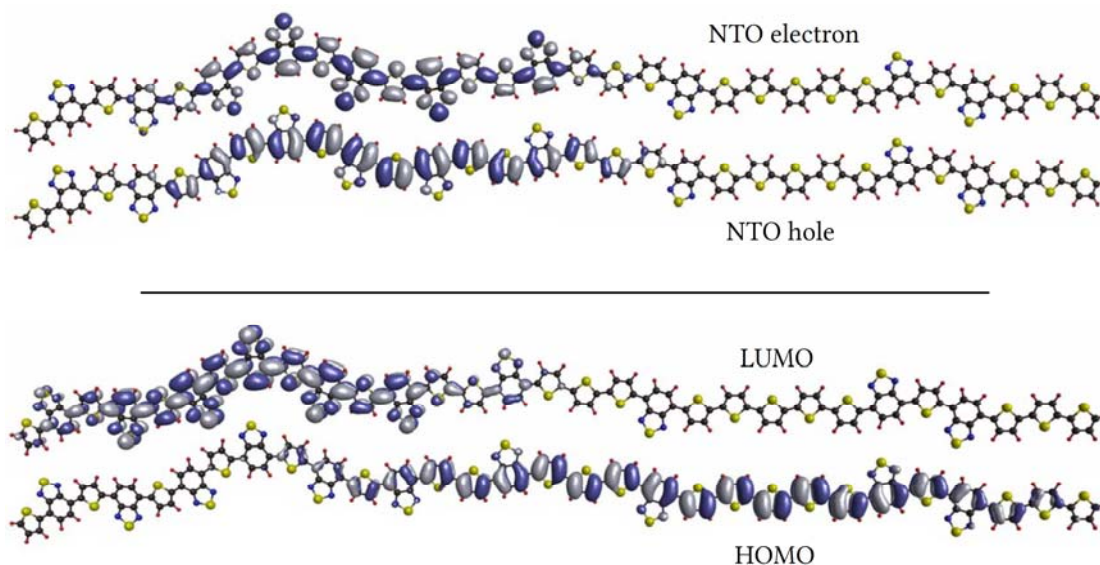


Figure 11: Most dominant NTO hole/electron of the first excitation (top) and HOMO–LUMO plot (bottom) for *r*-BTT with $n = 10$. The NTO pair contribution to the excitation is 54% and from the HOMO–LUMO pair 8%. The next three less dominant NTO pairs (accounting for 93% of the excitation) also show no significant CT. The isosurface value is 0.01.

In this context it is worthwhile to draw attention to a limitation of the frequently used technique of using HOMO and LUMO orbital plots for analyzing the CT character of an excitation. The present systems are hallmark examples where such a simplified view would lead to even qualitatively wrong conclusions, because many different generalized Kohn–Sham orbital pairs contribute to the lowest excitations. In the case of *r*-BTT an analysis of the HOMO and LUMO orbitals (Fig. 11 (bottom)) would lead to the conclusion that long-range CT is very dominant here. However, the HOMO–LUMO pair accounts for only 8% of the excitation, i.e., does not suffice to characterize its nature. The other orbital pairs with a significant contribution to the lowest excitation are shown in Fig. S5 of the ESI. Their structure does not allow for clearly assigning a certain character to the excitation.

In the second part of this section, we compare the theoretical results with measurements of a-BTT-H ($\bar{n} = 4,15$) and *r*-BTT-H ($\bar{n} = 5, 10$), corresponding to the calculated systems a-BTT and *r*-BTT. Fig. 12 shows the measured UV/Vis spectrum of a-BTT-H and *r*-BTT-H in chloroform solution and Table 2 compares the maxima of the

lowest absorption peaks to our calculated excitation energies. The measured and calculated values for the lowest excitation energy are a good approximation to the vertical excitation energy (cf. Section 4). The maxima of absorption for the longer oligomers of a-BTT-H and r-BTT-H are at 2.36 and 2.45 eV, respectively. The small difference with a magnitude of only 0.09 eV is in line with the theoretical finding that the nature of the arrangement of D and A has only a small influence on the optical gap. Regarding that the difference is not exactly the same – 0.05 eV versus 0.09 eV – one has to keep in mind possible small differences between the random arrangements in the calculation and the experiment: in the calculation r-BTT contains exactly twice as many thiophene rings as benzothiadiazole rings, whereas in experiments this ratio can only be achieved approximately.

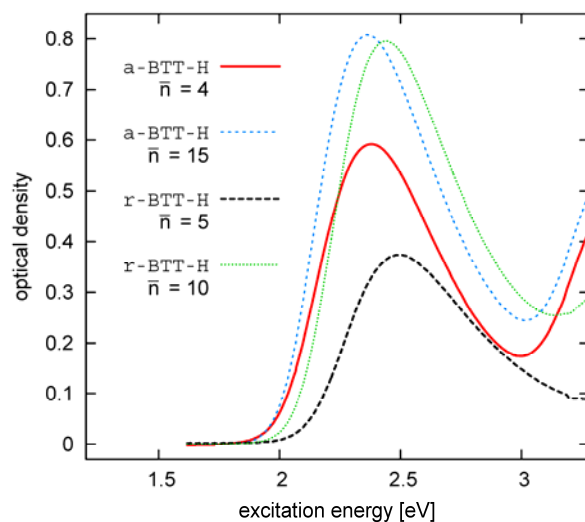


Figure 12: UV/Vis absorption spectra of a-BTT-H ($\bar{n} = 4, 15$) and r-BTT-H ($\bar{n} = 5, 10$) in chloroform solution (0.02 mg ml^{-1}) at room temperature.

Table 2. Lowest excitation energies: Comparison of alternating vs. random system in experiment and calculation, respectively. The calculations refer to $n = 12$ for both cases. The experiments refer to $\bar{n} = 15$ for a-BTT-H and $\bar{n} = 10$ for r-BTT-H. In both theory and experiment, the chosen numbers of repeat units lie in the saturated regime (compare Fig. 13 and Sec. 5).

| First excitation energy [eV] | | | |
|------------------------------|-------------|---------|-----------------------|
| | Alternating | Random | |
| | a-BTT | r-BTT | Δ (alt-random) |
| Calculation | 1.67 | 1.62 | 0.05 |
| First excitation energy [eV] | | | |
| | Alternating | Random | |
| | a-BTT-H | r-BTT-H | Δ (alt-random) |
| Experiment | 2.36 | 2.45 | -0.09 |

The most noticeable difference between experiment and theory is found for the absolute values of the excitation energies. The experimental excitation energies are approximately 0.7 eV larger than the theoretical ones, i.e., the difference is considerably larger than what one expects based on the accuracy of the experiments and calculations. We consider our experimental values as reliable since they are in accordance with measurements for similar systems.^[9-11,47,48] One may argue that it is a well known effect that TDDFT based on local, semilocal or hybrid functionals underestimates CT excitation energies^[25,49,50] and that this may explain the discrepancy. However, because of this reason we use the tuned RSH approach that remedies this problem and is known for very accurately predicting the lowest excitation energies of DA systems.^{§[16,21,25,26]} The discrepancy may thus be regarded as physically significant, and we elaborate on it in the following section.

§ B3LYP calculations would result in an even lower gap. For a-BTT one would obtain a saturated lowest excitation energy of 1.33 eV, 0.34 eV lower than our tuned BNL calculations.

5 Analysis of the differences between experiment and theory

In order to analyze the disagreement between the theoretical predictions and the experimental data we also synthesized DA systems with a smaller chain length and compared their lowest absorption energies to the corresponding calculated excitation energies. These additionally synthesized systems are BT, TBT-H, TTBTT-H, and TT(BTT)₂-H, as schematically represented in Fig. 3. The calculated systems are BT, TBT, TBT-H, TTBTT, TT(BTT)₂, and TT(BTT)₂-H, also shown in Fig. 3. We compare the measured and calculated lowest excitation energies in Fig. 13 along with results for the systems a-BTT and a-BTT-H as a function of the number of double bonds *N*. Additionally, we also show two data points for a-BTT with methyl side chains (indicated by “M” in the graph). In the left part of the graph (small systems) we have good agreement between theory and experiment. If the difference between theory and experiment were to be attributed solely to unreliability of the theoretical predictions, then the tuned RSH would have to be accurate for small systems but systematically fail for larger ones – a scenario that we do not consider likely, at least not in the size range studied here, given the previously published results obtained with the tuned RSH approach. We also note that the experimental values are in line with measurements of other, similar systems.^[8,52–55] Yet, as the systems get larger the difference between the experimental and the theoretical results increases.

In the experiment, the B units can have neighboring T units with hexyl chains pointing inwards, away, or in both directions. This can happen because during the synthesis the orientation of the bithiophene can change from one B to the next B unit (cf. Fig. 6). To examine the consequences that the different side-chain orientations can have we calculated the excitation energy for TBT with asymmetrically and symmetrically attached side chains. In the symmetric case the side chains point inwards and as a consequence lead to larger torsion angles between the thiophene and benzothiadiazole units. Furthermore, the chains are spatially closer and can therefore interact more. In line with this reasoning we observe in Fig. 14 that indeed in the symmetric case ((ii) in Fig. 14) the excitation energy changes by 0.15 eV whereas the changes are negligible for the asymmetric case ((i) in Fig. 14). Fig. 13 shows results that were obtained for different molecules with hexyl (H) and methyl (M) side chains attached as schematically shown in Fig. 2 (left side), i.e., one of the neighboring T rings has a side chain pointing towards the B unit and the other pointing away. We chose this configuration in the calculations because it occurs on average in the experiment

since the hexyl chains on the bithiophene units are asymmetrically attached (cf. Fig. 6). The lowest excitation shifts by at most 0.15 eV towards the experimental value. In summary these results indicate that the influence of the side chains may be able to explain part of the discrepancy between theory and experiment, but not all of it.

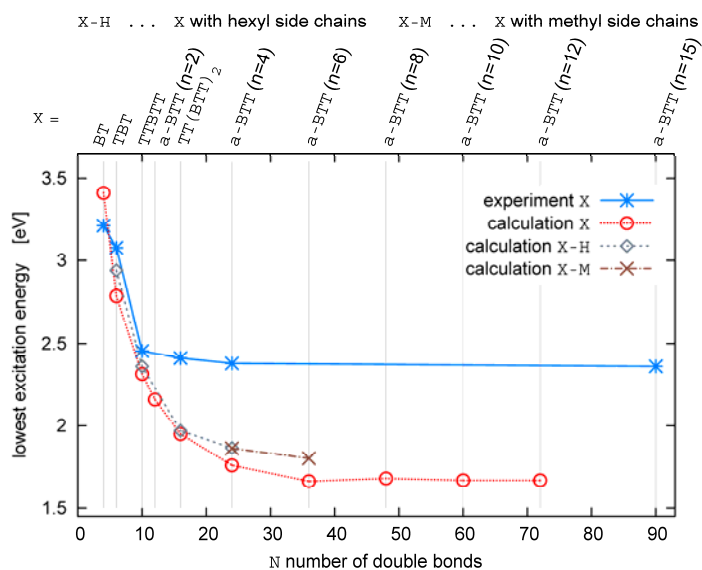


Figure 13: Lowest excitation energies as a function of the number of double bonds N . The experimental data points reflect the maxima of the UV/vis spectra. The calculated data points are obtained from tuned BNL TDDFT linear response calculations. The dotted lines are drawn as guides to the eye. All systems in the experiment have hexyl side chains (C_6H_{12}) attached to the thiophene rings as shown in Fig. 2 and 3; for the calculations we show data points for systems with hexyl and methyl side chains^[51] and compare them to systems without side chains.

One possibility which we so far did not take into account and which may play a role in explaining the discrepancy are interactions between the systems and the solvent that may change the experimental excitation energies. Therefore, we explored the influence of the solvent on some of the smaller systems. In the calculations, the solvent (as modeled by the solution model) has only little influence on the structure during geometry optimization. It also influences the excitation energies very little; the overall effect is less than 0.04 eV. Hence, solution models (cf. Section 3) cannot explain the large differences between experiment and theory. Also, the direct electronic effects of a solvent (e.g., screening) should influence small and large systems in a similar way. On the experimental side we explored the effects of using different

solvents. Besides chloroform we also measured the UV/vis spectrum of r-BTT-H with tetrahydrofuran and toluene. The observed shifts of the absorption maximum are less than 0.02 eV, i.e. very small. Thus, the discrepancies between experiments and calculations are not solvent dependent or at least similar for all tested solvents.

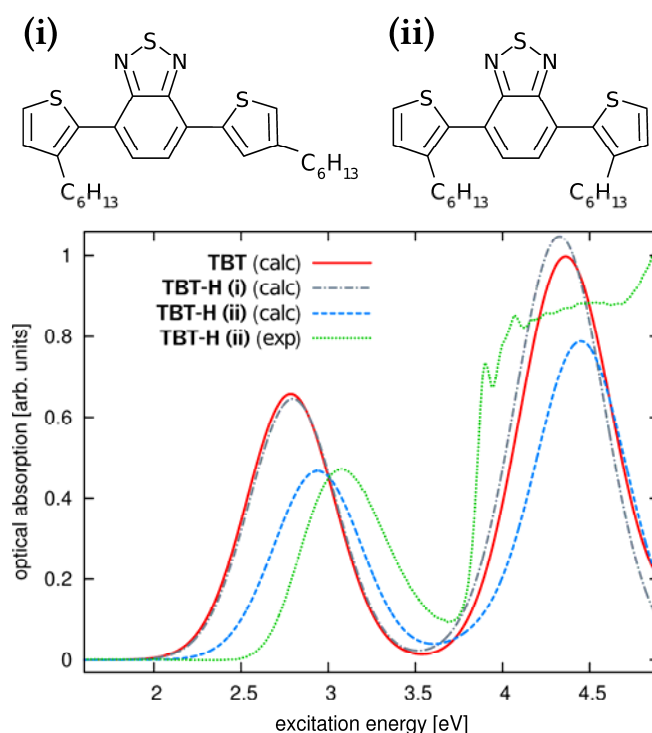


Figure 14: Comparison of the calculated spectra (calc) for TBT and TBT-H and the UV/Vis experimental spectrum (exp) for TBT-H in chloroform solution (0.02 mg ml^{-1}) at room temperature. For TBT-H we calculated a system with asymmetrically (i) and symmetrically (ii) attached hexyl side chains. Only case (ii) is examined in the experiment. As a guide to the eye the calculated peak positions are broadened with 0.3 eV HWHM and the measured optical density (experiment) is multiplied by a factor chosen to equalize the peak heights of the first peak of TBT-H (ii) in experiment and calculation.

Another possibility is that the experimental geometries are more distorted than the stretched geometries that we used in the calculations (cf. Fig. 4). Although changing the orientation of the T vs. the B unit has only a small local influence on the structure (different cases have been discussed, e.g., in ref. 56 and 57), it can change the global curvature of a chain, e.g., from a stretched to a curved geometry. For r-BTT we constructed such a curved structure by choosing the sulfur atom of thiophene to always point in the opposite direction of the sulfur atom in benzothiadiazole. The optimized geometry of this system is displayed in Fig. 15. Compared to the stretched

structure the excitation energy of this system changes by about 0.05 eV. This demonstrates that a globally curved structure can reach nearly as low a gap as a straight structure.

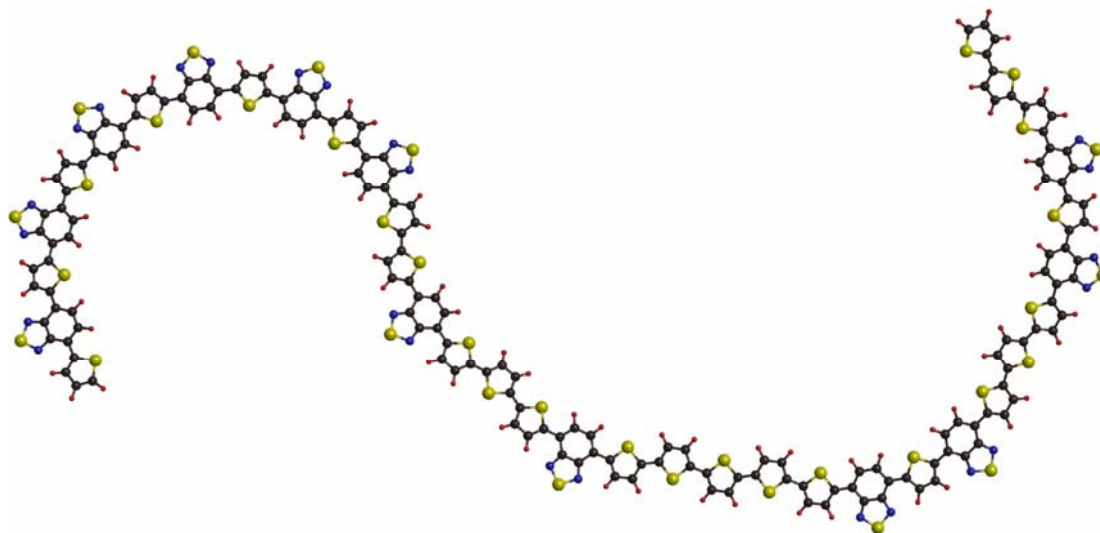


Figure 15: Example of a curved structure for *r*-BTT with $n = 12$. Fig. 4 shows an example of a stretched version of *r*-BTT.

Another reason that could explain the discrepancy between theory and experiment is a difference in the effective conjugation length. Fig. 13 shows a significant difference in how the experimental and theoretical curves saturate with increasing system size. The experimental excitation energies already start to saturate at a number of double bonds of $N \approx 15$, whereas in theory the saturation is at $N \approx 35$. This corresponds to a BTT repeat unit of $n \approx 3$ for the experiment and $n \approx 6$ for theory. This result might not be unexpected, however, its extent is worrisome and may well explain that the minimal achievable lowest excitation energy in the experiment is 0.7 eV above the calculated saturated energy. There are different factors that may lead to an effective limitation of the conjugation length in the experiments. Likely candidates are interactions between different chains and between chains and the solvent, which may lead to kinks and torsions in the structure and may thus break the electronic conjugation along the molecular backbone. The effect could be intensified by the hexyl chains that are attached to the structures in the experiment.

Thus, the results for all our systems, which cover both the well defined small molecule range as well as the oligomeric/polymeric range, can be summarized as follows. For the case of small molecules, there is full agreement between theory and

experiment. In the range of oligomers and polymers the theoretically found (first) excitation energies are by ca. 0.7 eV smaller than the ones found experimentally. However, the theoretical and the experimental results for the optical absorption agree with respect to the finding that different D and A arrangements lead to very similar excitation spectra. We extensively discussed the effects that can contribute to the 0.7 eV difference, and this brings us to our conclusion.

6 Conclusion

We studied theoretically and experimentally the influence that the relative ordering of D and A units has on the optical absorption of DA systems consisting of thiophene and benzothiadiazole. The lowest excitation energy changes only very little (<0.1 eV) in our TDDFT calculations based on a tuned RSH functional when going from the alternating to the randomly arranged DA system. This result was confirmed by our experimental study. Analysis of the NTOs showed that long-range CT is not dominant in the first optical excitation. Our calculations predicted the lowest possible excitation energy for a-BTT to be 1.67 eV with a saturation length of approximately 6 BTT repeat units. A comparison with measured excitation energies from a solution measurement reveals that the excitation already starts to saturate after 3 repeat units of BTT. Although the synthesized systems can have 15 repeat units or even more, they behave like oligomers with 3 BTT repeat units with respect to the optical properties. Thus, the maximum conjugation length in experiments is much lower than what appears to be theoretically achievable. Correspondingly, the minimum achievable optical gap is 2.36 eV, i.e., ca. 0.7 eV larger than the theoretical prediction. Effects that may cause this discrepancy between the experiment and the theoretical prediction were discussed and, in agreement with work on other DA systems,^[56,57] we conclude that future work may need to go beyond the single molecule level. Such work could provide further guidance in the design of oligomers or polymers that have the effective conjugation length that is necessary for a lower optical gap.

Acknowledgements

The authors acknowledge financial support from the German Research Foundation (GRK 1640) and the Bavarian State Ministry of Science, Research, and the Arts for the Collaborative Research Network "Solar Technologies go Hybrid".

References

- [1] J. Roncali, *Chemical Reviews* **1997**, 97, 173-206.
- [2] E. Bundgaard and F. C. Krebs, *Solar Energy Materials and Solar Cells*, **2007**, 91, 954–985.
- [3] R. Kroon, M. Lenes, J. C. Hummelen, P. W. M. Blom and B. de Boer, *Polymer Reviews*, **2008**, 48, 531–582.
- [4] Y.-J. Cheng, S.-H. Yang and C.-S. Hsu, *Chemical Reviews*, **2009**, 109, 5868–5923.
- [5] C. Risko, M. D. McGehee and J.-L. Brédas, *Chemical Science*, **2011**, 2, 1200–1218
- [6] J.-L. Brédas, J. E. Norton, J. Cornil and V. Coropceanu, *Accounts of Chemical Research*, **2009**, 42, 1691–1699.
- [7] E. E. Havinga, W. t. Hoeve and H. Wynberg, *Polymer Bulletin*, **1992**, 29, 119–126
- [8] C. Kitamura, S. Tanaka and Y. Yamashita, *Chemistry of Materials*, **1996**, 8, 570–578 .
- [9] M. Helgesen, S. A. Gevorgyan, F. C. Krebs and R. A. J. Janssen, *Chemistry of Materials*, **2009**, 21, 4669–4675 .
- [10] J.-Y. Lee, M.-H. Choi, H.-J. Song and D.-K. Moon, *Journal of Polymer Science Part A: Polymer Chemistry*, **2010**, 48, 4875–4883.
- [11] P. Sonar, E. L. Williams, S. P. Singh and A. Dodabalapur, *Journal of Materials Chemistry*, **2011**, 21, 10532-10541.
- [12] K.-H. Lee, H.-J. Lee, K. Kuramoto, Y. Tanaka, K. Morino, A. Sudo, T. Okauchi, A. Tsuge and T. Endo, *Journal of Polymer Science Part A: Polymer Chemistry*, **2011**, 49, 3543–3549.
- [13] S. Albrecht, S. Janietz, W. Schindler, J. Frisch, J. Kurpiers, J. Kniepert, S. Inal, P. Pingel, K. Fostiropoulos, N. Koch and D. Neher, *Journal of the American Chemical Society*, **2012**, 134, 14932–14944 .
- [14] W. Li, A. Furlan, K. H. Hendriks, M. M. Wienk and R. A. J. Janssen, *Journal of the American Chemical Society*, **2013**, 135, 5529–5532.
- [15] B. A. D. Neto, A. A. M. Lapis, E. N. da Silva Júnior and J. Dupont, *European Journal of Organic Chemistry*, **2013**, 228–255 .

- [16] L. Pandey, C. Doiron, J. S. Sears and J.-L. Brédas, *Physical Chemistry Chemical Physics*, **2012**, 14, 14243–14248.
- [17] H. Iikura, T. Tsuneda, T. Yanai and K. Hirao, *Journal of Chemical Physics*, **2001**, 115, 3540–3544
- [18] T. M. Henderson, B. G. Janesko and G. E. Scuseria, *Journal of Chemical Physics*, **2008**, 128, 194105 .
- [19] J.-D. Chai and M. Head-Gordon, *Journal of Chemical Physics*, **2008**, 128, 084106 .
- [20] M. A. Rohrdanz, K. M. Martins and J. M. Herbert, *Journal of Chemical Physics*, **2009**, 130, 054112 .
- [21] T. Stein, L. Kronik and R. Baer, *Journal of the American Chemical Society*, **2009**, 131, 2818–2820.
- [22] D. Hofmann, T. Körzdörfer and S. Kümmel, *Physical Review Letters*, **2012**, 108, 146401.
- [23] D. Hofmann and S. Kümmel, *Journal of Chemical Physics*, **2012**, 137, 064117.
- [24] I. Dabo, A. Ferretti, C.-H. Park, N. Poilvert, Y. Li, M. Cococcioni and N. Marzari, *Physical Chemistry Chemical Physics*, **2013**, 15, 685.
- [25] A. Karolewski, T. Stein, R. Baer and S. Kümmel, *Journal of Chemical Physics*, **2011**, 134, 151101.
- [26] L. Kronik, T. Stein, S. Refaely-Abramson and R. Baer, *Journal of Chemical Theory and Computation*, **2012**, 8, 1515–1531.
- [27] P. Hohenberg and W. Kohn, *Physical Reviews*, **1964**, 136, B864–B871.
- [28] W. Kohn and L. J. Sham, *Physical Reviews*, **1965**, 140, A1133–A1138.
- [29] E. Runge and E. K. U. Gross, *Physical Review Letters*, **1984**, 52, 997–1000.
- [30] M. E. Casida, in *Recent Advances in Computational Chemistry*, ed. D. P. Chong, World Scientific Publishing Co. Pte. Ltd., **1995**, pp. 155–192.
- [31]. P. J. Stephens, F. J. Devlin, C. F. Chabalowski and M. J. Frisch, *Journal of Physical Chemistry*, **1994**, 98, 11623–11627.
- [32] S. Grimme, *Journal of Computational Chemistry*, **2006**, 27, 1787–1799.
- [33] R. Ahlrichs, M. Bär, M. Häser, H. Horn and C. Kölmel, *Chemical Physics Letters*, **1989**, 162, 165–169.
- [34] Turbomole V6.0, **2009**.
- [35] C. Lee, W. Yang and R. G. Parr, *Physical Review B: Condensed Matter and Materials Physics*, **1988**, 37, 785–789.

- [36] R. Baer and D. Neuhauser, *Physical Review Letters*, **2005**, 94, 043002.
- [37] E. Livshits and R. Baer, *Physical Chemistry Chemical Physics*, **2007**, 9, 2932–2941.
- [38] A. Karolewski, L. Kronik and S. Kümmel, *Journal of Chemical Physics*, **2013**, 138, 204115.
- [39] A. Savin and H.-J. Flad, *International Journal of Quantum Chemistry*, **1995**, 56, 327–332.
- [40] T. Leininger, H. Stoll, H.-J. Werner and A. Savin, *Chemical Physics Letters*, **1997**, 275, 151–160.
- [41] Y. Shao, L. F. Molnar, Y. Jung, J. Kussmann, C. Ochsenfeld, S. T. Brown, A. T. B. Gilbert, L. V. Slipchenko, S. V. Levchenko, D. P. O'Neill, R. A. DiStasio Jr, R. C. Lochan, T. Wang, G. J. O. Beran, N. A. Besley, J. M. Herbert, C. Y. Lin, T. V. Voorhis, S. H. Chien, A. Sodt, R. P. Steele, V. A. Rassolov, P. E. Maslen, P. P. Korambath, R. D. Adamson, B. Austin, J. Baker, E. F. C. Byrd, H. Dachsel, R. J. Doerksen, A. Dreuw, B. D. Dunietz, A. D. Dutoi, T. R. Furlani, S. R. Gwaltney, A. Heyden, S. Hirata, C.-P. Hsu, G. Kedziora, R. Z. Khalliulin, P. Klunzinger, A. M. Lee, M. S. Lee, W. Liang, I. Lotan, N. Nair, B. Peters, E. I. Proynov, P. A. Pieniazek, Y. M. Rhee, J. Ritchie, E. Rosta, C. D. Sherrill, A. C. Simmonett, J. E. Subotnik, H. L. W. Iii, W. Zhang, A. T. Bell, A. K. Chakraborty, D. M. Chipman, F. J. Keil, A. Warshel, W. J. Hehre, H. F. S. Iii, J. Kong, A. I. Krylov, P. M. W. Gill and M. Head-Gordon, *Physical Chemistry Chemical Physics*, **2006**, 8, 3172–3191.
- [42] T. Körzdörfer, J. S. Sears, C. Sutton and J.-L. Brédas, *Journal of Chemical Physics*, **2011**, 135, 204107.
- [43] A. Klamt and G. Schüürmann, *Journal of the Chemical Society, Perkin Transactions 2*, **1993**, 799–805.
- [44] The relevance of indirect influences of solvation, e.g., on the RSH tuning approach, remains to be checked in future work.
- [45] H. Usta, C. Risko, Z. Wang, H. Huang, M. K. Deliomeroğlu, A. Zhukhovitskiy, A. Facchetti and T. J. Marks, *Journal of the American Chemical Society*, **2009**, 131, 5586–5608.
- [46] R. L. Martin, *Journal of Chemical Physics*, **2003**, 118, 4775–4777.
- [47] E. Bundgaard and F. C. Krebs, *Macromolecules*, **2006**, 39, 2823–2831.
- [48] A. A. El-Shehawy, N. I. Abdo, A. A. El-Barbary and J.-S. Lee, *European Journal of Organic Chemistry*, **2011**, 4841–4852.
- [49] D. Tozer, *Journal of Chemical Physics*, **2003**, 119, 12697.

- [50] S. Kümmel and L. Kronik, *Reviews of Modern Physics*, **2008**, 80, 3.
- [51] As explained in Section 3.1 we tuned the range separation γ according to eqn (1) for all calculations of this manuscript. However, for a-BTT ($n = 4,6$) we did not re-tune γ when we attached the hexyl and methyl side chains. Since the HOMO orbital does not change considerably by attaching side chains the effects of re-tuning of γ are expected to be small.
- [52] H. a. M. van Mullekom, J. a. J. M. Vekemans and E. W. Meijer, *Chemistry – A European Journal*, **1998**, 4, 1235–1243.
- [53] M. Jayakannan, P. A. van Hal and R. A. J. Janssen, *Journal of Polymer Science Part A: Polymer Chemistry*, **2002**, 40, 251–261.
- [54] P. Sonar, S. P. Singh, P. Leclère, M. Surin, R. Lazzaroni, T. T. Lin, A. Dodabalapur and A. Sellinger, *Journal of Materials Chemistry*, **2009**, 19, 3228–3237.
- [55] S. Ellinger, K. R. Graham, P. Shi, R. T. Farley, T. T. Steckler, R. N. Brookins, P. Taranekar, J. Mei, L. A. Padilha, T. R. Ensley, H. Hu, S. Webster, D. J. Hagan, E. W. Van Stryland, K. S. Schanze and J. R. Reynolds, *Chemistry of Materials*, **2011**, 23, 3805–3817.
- [56] M. C. Scharber, M. Koppe, J. Gao, F. Cordella, M. A. Loi, P. Denk, M. Morana, H.-J. Egelhaaf, K. Forberich, G. D. R. Gaudiana, D. Waller, Z. Zhu, X. Shi and C. J. Brabec, *Macromolecules*, **2010**, 22, 367.
- [57] L. Pandey, C. Risko, J. E. Norton and J.-L. Brédas, *Macromolecules*, **2012**, 45, 6405.

Electronic Supplementary Information

for the manuscript:

OPTICAL ABSORPTION IN DONOR-ACCEPTOR POLYMERS - ALTERNATING VS. RANDOM

*Andreas Karolewski^a, Anne Neubig^b, Mukundan Thelakkat^{*b} and Stephan Kümmel^{*a}*

^aTheoretical Physics IV, University of Bayreuth, 95440 Bayreuth, Germany.
E-mail: Stephan.Kuemmel@uni-bayreuth.de

^bMacromolecular Chemistry I, University of Bayreuth, 95440 Bayreuth, Germany.
E-mail: Mukundan.Thelakkat@uni-bayreuth.de

Table of Contents

| | |
|--|----|
| 1 Materials and Methods..... | 87 |
| 2 Gel Permeation Chromatography (GPC)..... | 88 |
| 3 Matrix-Assisted Laser Desorption Ionization – Time -of-Flight (MALDI-ToF) Mass Spectrometry | 89 |
| 4 Monomer Synthesis | 90 |
| 5 Polymer Synthesis | 92 |
| 6 Natural Transition Orbital Pairs of <i>r</i> -BTT | 96 |
| 7 Highest Occupied and Lowest Unoccupied Orbitals of <i>r</i> -BTT | 97 |
| 8 References | 98 |

1 Materials and Methods

All reactions were carried out in dry glassware and under inert atmosphere of purified argon using Schlenk techniques. All reagents and solvents were purchased from Aldrich, ABCR, Acros or TCI. They were used without further purification unless otherwise noted. 4,7-Dibromo-benzo[c][2,1,3]thiadiazole^[1] and 4,7-Bis(3-hexylthiophen-2yl)benzo[c][2,1,3]thiadiazole^[2] were synthesized according to modified literature procedures. Solvents used for precipitation were distilled under normal atmosphere.

¹H-NMR (300 MHz) spectra were recorded on a Bruker AC 300 spectrometer at room temperature. Chemical shifts for ¹H-NMR spectra are referenced relative to residual protons in the deuterated solvents (CDCl₃ δ=7.26 ppm; CD₂Cl₂ δ=5.33 ppm). Abbreviations used for splitting patterns are s (singlet), d (doublet), t (triplet), m (multiplet) and b (broad).

Mass spectroscopic data (MS) were obtained from a FINNIGAN MAT 8500 instrument.

UV/Vis spectra of solutions in CHCl₃ with a concentration of 0.02 mgmL⁻¹ were recorded on a Hitachi 3000 spectrophotometer.

Oligomeric gel permeation chromatography was carried out in THF as eluent at a flow rate of 0.5 mLmin⁻¹ at room temperature using a column setup comprising a guard column (Varian, 5 x 0.8 cm, particle size 3 μm) and two analytical columns (Varian, 30 x 0.8 cm, particle size 3 μm). Oligomers were monitored with UV (Waters model 486) at 254 nm and RI (Waters model 410) detectors. Polystyrene standards and *o*-Dichlorobenzene as an internal standard were used for calibration. Preparative gel permeation chromatography was carried out in THF as eluent and a flow rate of 5 mLmin⁻¹ at room temperature using a column setup comprising a guard column (SDV, 50 x 7.5 mm, particle size 10 μm) and four analytical columns (PLgel 10⁴ Å, 300 x 25 cm; PLgel 10³ Å, 300 x 25 cm; PLgel 100 Å, 600 x 25 cm; PLgel 100 Å, 300 x 25 cm; particle size 10 μm each).

Matrix-assisted laser desorption ionization with time of flight detection (MALDI-ToF) mass spectrometry measurements were performed on a Bruker Reflex III using *trans*-2-[3-(4-*tert*-Butylphenyl)-2-methyl-2-propenylidene]malonitrile (DCTB) as matrix material. The solutions of the analyte (1mg200mL⁻¹) and the matrix (1mg100mL⁻¹) in chloroform were mixed in the ratio 1:50 (v:v) and spotted onto the MALDI target plate prior to the measurement.

2 Gel Permeation Chromatography (GPC)

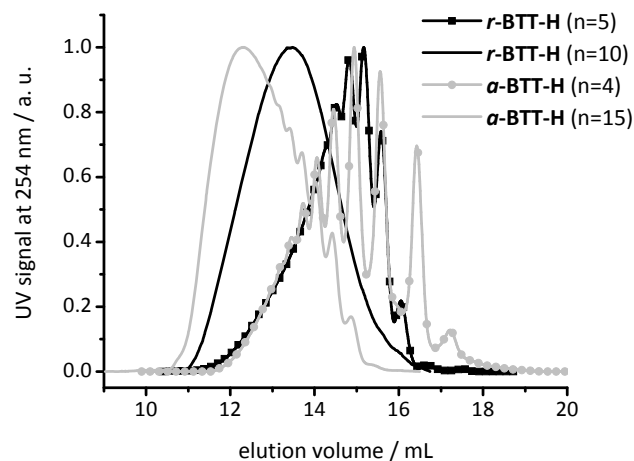


Figure S1: GPC traces of the systems $r\text{-BTT-H}$ (n=5), $r\text{-BTT-H}$ (n=10), $\alpha\text{-BTT-H}$ (n=4) and $\alpha\text{-BTT-H}$ (n=15). All curves are normalized to the maximum.

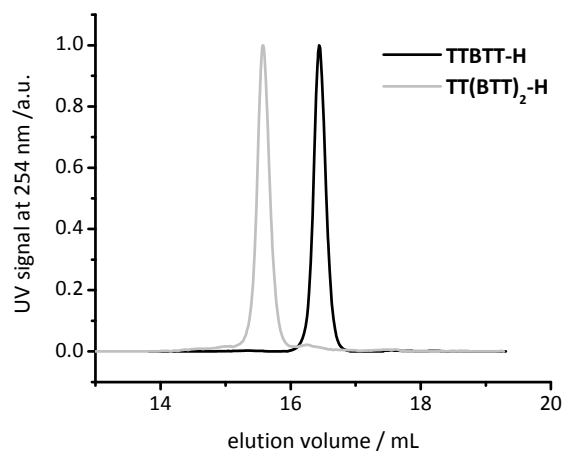


Figure S2: GPC traces of the fractionated TTBTt-H and $\text{TT(BTT)}_2\text{-H}$ oligomers. All curves are normalized to the maximum. The TTBTt-H fraction has a very low polydispersity index (PDI) of 1.01 analogous to monodisperse compounds and did not show any shoulders on either side. Similarly the $\text{TT(BTT)}_2\text{-H}$ fraction has a polydispersity index of 1.04. It is clearly shown that we separated the two well-defined low molecular weight systems from each other.

3 Matrix-Assisted Laser Desorption Ionization – Time of Flight (MALDI-ToF) Mass Spectrometry

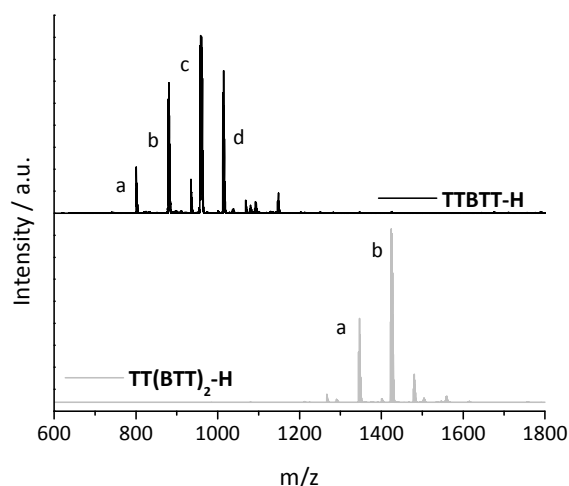
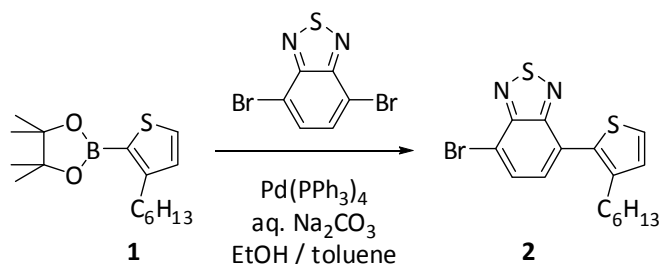


Figure S3: MALDI-ToF spectra of the **TTBTt-H** fraction (top) and **TT(BTt)₂-H** fraction (bottom). Each oligomer produces several peaks. This can be explained by the Suzuki-Miyaura polycondensation method which is used. The peaks correlate to the respective oligomer but with different end-groups which we all identified. For instance the four main peaks of the **TTBTt-H** can be clearly assigned as the **TTBTt-H** oligomer a) with H/H end-groups, b) with H/Br end-groups, c) Br/Br end-groups and d) with H/Br end-groups and one **B** unit. The two main peaks of the MALDI-ToF spectra of **TT(BTt)₂-H** can be correlated to the **TT(BTt)₂-H** oligomer a) with H/Br end-groups and b) with Br/Br end-groups. The corresponding mass-to-charge ratios are listed in Table S1. It is important to note that we clearly separated the two systems from each other in the sense that the species observed in the **TTBTt-H** spectrum are different from the species observed in the **TT(BTt)₂-H** spectrum.

Table S1: Mass-to-charge ratio (m/z) calculated and determined with MALDI-ToF mass spectrometry of the oligomers **TTBTt-H** and **TT(BTt)₂-H** with the respective end-groups.

| Sample | | m/z (MALDI) | m/z (calc) | End-groups |
|------------------------------|---|---------------|--------------|------------|
| TTBTt-H | a | 800.974 | 800.336 | H-/H- |
| | b | 878.646 | 878.247 | Br-/H- |
| | c | 956.456 | 956.157 | Br-/Br- |
| | d | 1012.484 | 1012.240 | H-/Br- |
| TT(BTt)₂-H | a | 1344.509 | 1344.404 | Br-/H- |
| | b | 1422.391 | 1422.314 | Br-/Br- |

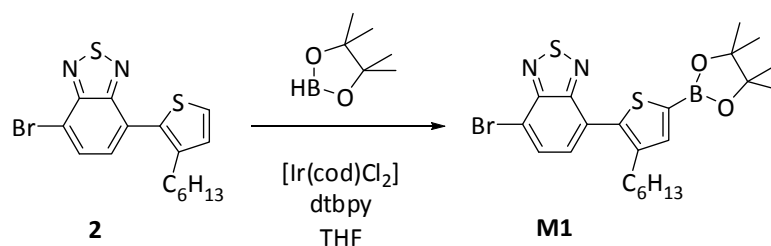
4 Monomer Synthesis

Synthesis of 4-Bromo-7-(3-hexylthiophen-2-yl) benzo [c] 2,1,3-thiadiazole (2)

To a 500mL three-necked round bottom flask were added 3-Hexylthiophene-2-boronic acid pinacol ester **1** (10 g, 34 mmol), 4,7-Dibromo-2,1,3-benzothiadiazole (15 g, 50mmol), 140 mL of toluene, 100 mL of EtOH and Na₂CO₃ (7.2g, 68 mmol) diluted in 100 mL water. The reaction mixture was degassed for 40 minutes and heated to reflux under stirring. Pd(PPh₃)₄ (393 mg, 0.34 mmol) was added and the mixture was refluxed for 16 h. After evaporating the solvent under reduced pressure, H₂O (200 mL) and methylene chloride (200 mL) were added. The aqueous layer was extracted with methylene chloride (80 mL) three times. The combined organic phases were washed with water (60 mL) three times, dried with Na₂SO₄ and filtrated. After the solvent was removed by rotary evaporation **2** was obtained by distillation under vacuum as yellow oil. Yield: 7.3 g (56 %).

¹H-NMR (300MHz, CDCl₃): δ ppm 7.90 (d, *J* 7.5Hz, 1H-BT-5H); 7.47 (d, *J* 7.55Hz, 1H-BT-6H); 7.43 (d, *J* 5.0Hz, 1H-Th-5H); 7.08 (d, *J* 5.0Hz, 1H-Th-4H); 2.58 (t, *J* 7.6Hz, 2H-α-H); 1.67-1.49 (m, 2H-β-H); 1.28-1.08 (m, 6H, -CH₂-); 0.81 (t, *J* 6.9Hz, 3H,-CH₃).

MS (EI) *m/z*: 382 (43) [M⁺] (calcd. 382.0).

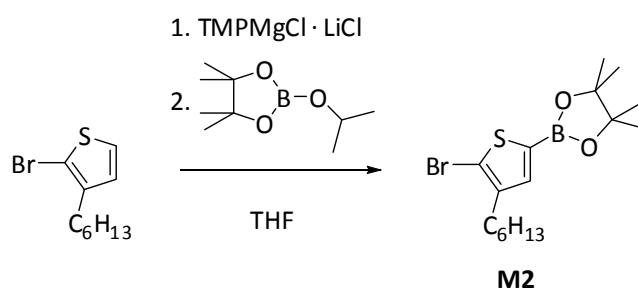
Synthesis of 4-Bromo-7-(5-boronic acid pinacolyl-3-hexylthiophen-2-yl) benzo-2,1,3-thiadiazole (M1)

To a 250 mL schlenk round bottom flask were added 4-Bromo-7-(3-hexylthiophen-2-yl) benzo [c] 2,1,3-thiadiazole **2** (3.3 g, 8.65 mmol) in 25 mL THF. Ir(COD)Cl₂ (57 mg, 0.086 mmol) and 4,4'-Di-tert-butyl bipyridine (23 mg, 0.086 mmol) were added and the mixture was degassed with argon for 20 min, which was followed by addition of 4,4'-5,5'-Tetramethyl-[1,3,2]dioxaborolane (2.437 g, 9.08 mmol) and an additional amount of THF (25 mL). After degassing for further 10 min the mixture was stirred and heated under reflux for 46 h. After having been allowed to cool to room temperature the reaction mixture was quenched with 200 mL ice water. THF was removed by rotary evaporation. The residue was extracted with ethyl acetate (120 mL) for three times. The combined organic layers were washed with brine (50 mL) for three times, dried with Na₂SO₄ and filtrated. After the solvent was removed the product **M1** was recrystallized from petrolether. Yield: 2.0 g (46 %).

¹H-NMR (300MHz, CDCl₃): δ ppm 7.90 (d, *J* 7.8Hz, 1H-*BT-5H*); 7.60 (s, 1H-*Th-4*); 7.46 (d, *J* 7.33Hz, 1H-*BT-6H*); 2.56 (t, *J* 7.8Hz, 2H-*α-H*); 1.66-1.48 (m, 2H-*β-H*); 1.36 (s, 12H, -CH₃); 1.27-1.08 (m, 6H, -CH₂-); 0.80 (t, *J* 6.7Hz, 3H, -CH₃).

MS (EI) *m/z*: 506 (70) [M⁺] (calcd. 506.1).

Synthesis of 5-Bromo-4-hexylthiophene-2-boronic acid pinacol ester (**M2**)



To a solution of 2-Bromo-3-hexylthiophene (10 g, 40.45 mmol) in 160 mL THF was added 2,2,6,6-Tetramethylpiperidinylmagnesium chloride lithium chloride solution (1M in THF/toluene) (14.71 g, 60.68 mmol) in one portion. The reaction mixture was stirred at room temperature for 24 h after which 2-Isopropoxy-4,4',5,5'-tetramethyl-1,3,2-dioxaborolane (15.05 g, 80.9 mmol) was added. The reaction mixture was allowed to stir at room temperature for further 4 h and was then quenched with 50 mL water. The organic solvents were removed under reduced pressure after which water was added and extracted with diethyl ether. The combined organic layers were washed with saturated NaCl-solution, dried with Na₂SO₄ and filtrated. After

evaporation of the solvent the crude product was distilled under vacuum to afford **M2** as yellowish oil. Yield: 10.72 g (71 %).

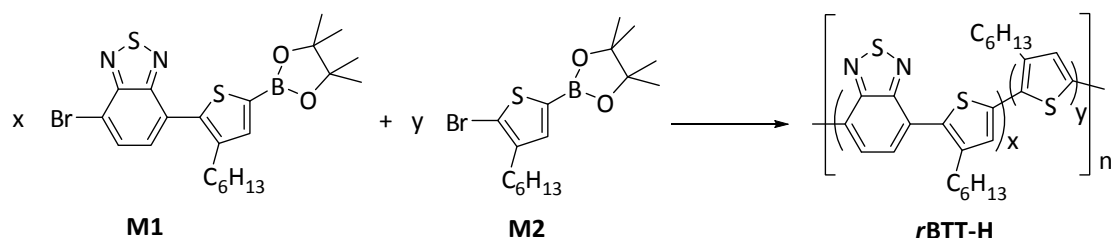
$^1\text{H-NMR}$ (300MHz, CDCl_3): δ ppm 7.31 (s, 1H-3H); 2.54 (t, J 7.7Hz, 2H- α -H); 1.70-1.47 (m, 2H- β -H); 1.42-1.18 (m, 18H, - CH_2 -, - CH_3); 0.88 (t, J 6.6Hz, 3H,- CH_3).

MS (EI) m/z : 374 (26) [M^+] (calcd. 374.1).

5 Polymer Synthesis

All polymers were synthesized via palladium catalyzed Suzuki coupling polycondensation. Monomers **M1** and **M2** were used to obtain the copolymers **r-BTT-H**. Using monomers **M3** and **M4** the alternating copolymers **a-BTT-H** were obtained. A variation of the reaction conditions led to different molecular weights for **r-BTT-H** ($n = 5$; 10) and **a-BTT-H** ($n = 4$; 15).

Synthesis of r-BTT-H



r-BTT-H ($n = 5$)

To a Schlenk tube monomer **M1** (190 mg, 0.375 mmol) and **M2** (140 mg, 0.375 mmol) were dissolved in THF (8 mL). An aqueous solution of Na_2CO_3 (1M, 2 mL) and two drops of Aliquat 336 were added to the solution and degassed with argon for 1 h. Afterwards $\text{Pd}(\text{PPh}_3)_4$ (8.7 mg, 0.0075 mmol) was added and the solution was degassed again for 10 min. The mixture was stirred under microwave conditions under reflux for 1 day. After cooling to room temperature the solvent was evaporated and the polymer was dissolved in chloroform and precipitated in methanol. Then it was dissolved in methylene chloride, extracted with water and again precipitated into methanol. The crude polymer was collected by filtration, dried and loaded into an extraction thimble to be washed with methanol, ethanol, acetone and methylene

chloride. The methylene chloride fraction was freeze dried from benzene to afford a dark solid. Yield: 19 %.

$^1\text{H-NMR}$ (300MHz, CD_2Cl_2): δ ppm 8.29-7.10 (b, 3.2H-*Ar-H*); 3.00-2.56 (m, 2H- α -*H*); 1.90-1.62 (m, 2H- β -*H*); 1.42-1.13 (m, 6H, - CH_2); 0.97-0.76 (m, 3H, - CH_3).

UV-Vis (CHCl_3 , nm): 497 nm (2.49 eV).

Oligomeric GPC: M_w : 3636 g mol^{-1} ; M_p : 1888 g mol^{-1} ; M_w/M_n : 1.46.

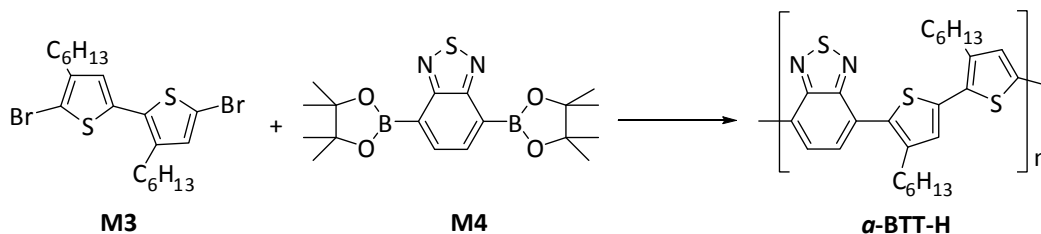
r-BTT-H (n = 10)

In a 20 mL high pressure microwave reactor tube, equipped with a sealed septum monomer **M1** (150 mg, 0.296 mmol) and **M2** (110 mg, 0.296 mmol) were dissolved in toluene (4 mL). Two drops of Aliquat 336, an aqueous solution of Na_2CO_3 (1M, 1 mL) and $\text{Pd}(\text{PPh}_3)_4$ (13.7 mg, 0.0118 mmol) were added to the solution. Then the tube was sealed and degassed with argon for 35 min. The reaction mixture was heated 7 days at 120 °C (oil bath temperature). The end-capping procedure was performed in 2 separate steps. After cooling to room temperature, a degassed solution of phenylboronic acid pinacol ester (60.34 mg, 0.296 mmol) in 1 mL toluene was added first, followed by heating for 5.5 h at 120 °C. After cooling to room temperature, degassed bromobenzene (92.29 mg, 0.591 mmol) was added, followed by heating for 15.5 h at 120 °C. After cooling to room temperature the polymer was dissolved in methylene chloride, extracted with water and precipitated into methanol. The crude polymer was collected by filtration, dried and loaded into an extraction thimble to be washed with methanol, ethanol, acetone, *n*-hexane and methylene chloride. The methylene chloride fraction was freeze dried from benzene to afford a dark solid. Yield: 15%.

$^1\text{H-NMR}$ (300MHz, CD_2Cl_2): δ ppm 8.22-6.94 (b, 2.5H-*Ar-H*); 3.07-2.37 (m, 2H- α -*H*); 1.89-1.59 (m, 2H- β -*H*); 1.49-1.10 (m, 6H, - CH_2); 0.97-0.75 (m, 3H, - CH_3).

UV-Vis (CHCl_3 , nm): 507 nm.

Oligomeric GPC: M_w : 7132 g mol^{-1} ; M_p : 5507 g mol^{-1} ; M_w/M_n : 1.59.

Synthesis of α -BTT-H **α -BTT-H (n = 4)**

To a Schlenk tube 2,1,3-Benzothiadiazole-4,7-bis(boronic acid pinacol ester) **M4** (385 mg, 0.94 mmol) and **M3** (461.0 mg, 0.94 mmol) were dissolved in THF (8 mL). An aqueous solution of Na_2CO_3 (1M, 4 mL), two drops of Aliquat 336 and $\text{Pd}(\text{PPh}_3)_4$ (54.1 mg, 0.00468 mmol) were added to the solution and degassed with argon for 30 min. The mixture was stirred under microwave conditions under reflux for 18 h. After cooling to room temperature the solvent was evaporated and the polymer was dissolved in methylene chloride, extracted with water and precipitated into methanol. The crude polymer was collected by filtration, dried and loaded into an extraction thimble to be washed with methanol, ethanol, acetone and methylene chloride. The methylene chloride fraction was freeze dried from benzene to afford a dark solid. Yield: 41 %.

$^1\text{H-NMR}$ (300MHz, CD_2Cl_2): δ ppm 8.09-6.91 (b, 2.6H-*Ar-H*); 3.14-2.33 (m, 2H- α -*H*); 1.89-1.57 (m, 2H- β -*H*); 1.51-1.13 (m, 6H, - CH_2); 1.04-0.77 (m, 3H, - CH_3).

UV-Vis (CHCl_3 , nm): 521 nm.

Oligomeric GPC: M_w : 3200 gmol^{-1} ; M_p : 2157 gmol^{-1} ; M_w/M_n : 1.74.

α -BTT-H (n = 15)

In a 20 mL high pressure microwave reactor tube, equipped with a sealed septum **M3** (261 mg, 0.53 mmol) and 2,1,3-Benzothiadiazole-4,7-bis(boronic acid pinacol ester) **M4** (204.9 mg, 0.53 mmol) were dissolved in toluene (7 mL). Two drops of Aliquat 336, an aqueous solution of Na₂CO₃ (1M, 1.75 mL) and Pd(PPh₃)₄ (12.2 mg, 0.011 mmol) were added to the solution. The tube was sealed and the mixture was degassed with argon for 45 min. The reaction was heated 2 days at 120 °C (oil bath temperature). The end-capping procedure was performed in 2 separate steps. After cooling to room temperature, a degassed solution of phenylboronic acid pinacol ester (108.2 mg, 0.53 mmol) in 3 mL toluene was added first, followed by heating for 5 h at 120 °C. After cooling to room temperature, degassed bromobenzene (166.4 mg, 1.06 mmol) was added, followed by heating for 12 h at 120 °C. After cooling to room temperature the polymer was dissolved in methylene chloride, extracted with water and precipitated into methanol. The crude polymer was collected by filtration, dried and loaded into an extraction thimble to be washed with methanol, ethanol, acetone and methylene chloride. The methylene chloride fraction was freeze dried from benzene to afford a dark solid. Yield: 32 %.

¹H-NMR (300MHz, CD₂Cl₂): δ ppm 8.55-6.85 (b, 5H-*Ar-H*); 2.99-2.49 (m, 4H- α -*H*); 1.88-1.57 (m, 4H- β -*H*); 1.50-1.13 (m, 6H, -*CH*₂); 1.04-0.75 (m, 3H, -*CH*₃).

UV-Vis (CHCl₃, nm): 525 nm.

Oligomeric GPC: M_w: 11800 gmol⁻¹; M_p: 12310 gmol⁻¹; M_w/M_n: 1.64.

6 Natural Transition Orbital Pairs of r-BTT

Fig. S4 shows the dominant natural transition orbital pairs for the lowest excitation of *r*-BTT with $n = 10$. Taking all these transitions into account confirms that the first excitation is of mixed valence-CT type.

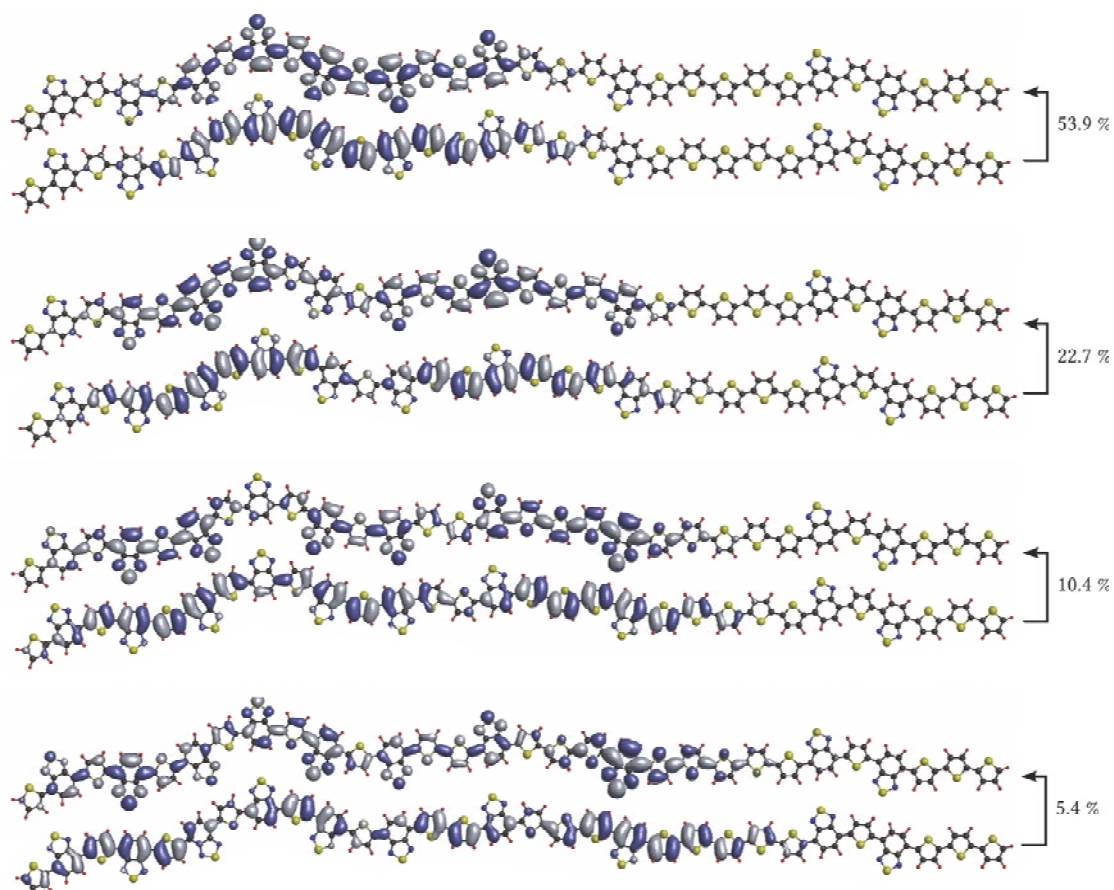


Figure S4: Most dominant natural transition orbital hole/electron pairs of the lowest excitation for *r*-BTT with $n=10$ from a BNL calculation with an optimized range separation parameter. The isosurface value is 0.01. The weight factors indicate the contribution to the lowest excitation for each pair.

7 Highest Occupied and Lowest Unoccupied Orbitals of r-BTT

Fig. S5 shows the four highest occupied orbitals and the four lowest unoccupied orbitals. Table S1 lists the corresponding orbital energies, obtained with the BNL functional and the optimized range separation parameter $\gamma = 0.121 \text{ a}_0^{-1}$.

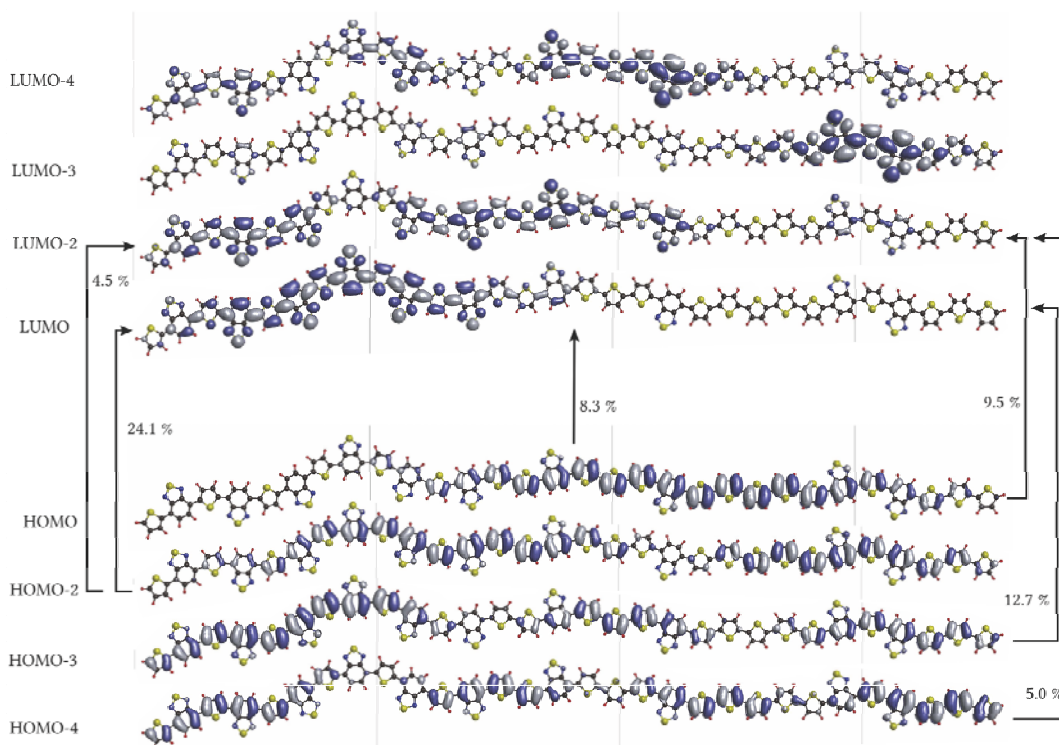


Figure S5: The four lowest unoccupied and highest occupied molecular orbitals for **r-BTT** with $n=10$ from a BNL calculation with an optimized range separation parameter. The isosurface value is 0.01. The weight factors indicate the most dominant contributions to the lowest excitation.

Table S1: Frontier orbital energies of **r-BTT** ($n=10$).

| orbital | eigenvalue [eV] |
|---------|-----------------|
| LUMO+3 | -1.820 |
| LUMO+2 | -1.917 |
| LUMO+1 | -1.948 |
| LUMO | -2.091 |
| HOMO | -5.414 |
| HOMO-1 | -5.512 |
| HOMO-2 | -5.616 |
| HOMO-3 | -5.727 |

8 References

- [1] B. A. DaSilveira Neto; A. S. A. Lopes; G. Ebeling; R.S. Gonçalves; V. E. U. Costa; F. H. Quina; J. Dupont, *Tetrahedron*, **2005**, 61, (46), 10975-10982.
- [2] J.-J. Kim; H. Choi; J.-W. Lee; M.-S. Kang; K. Song; S. O. Kang; J. Ko, *Journal of Materials Chemistry*, **2008**, 18, (43), 5223-5229.

6. *RANDOM VS. ALTERNATING DONOR-ACCEPTOR
COPOLYMERS: A COMPARATIVE STUDY OF
ABSORPTION AND FIELD EFFECT MOBILITY*

*Anne Neubig and Mukundan Thelakkat**

Macromolecular Chemistry I, University of Bayreuth, 95440 Bayreuth, Germany.
E-mail: Mukundan.Thelakkat@uni-bayreuth.de

Published in *Polymer* **2014**, 55, (11), 2621-2627.

Reprinted with permission from Elsevier.

Abstract

*The influence of the arrangement of donor and acceptor units in a conjugated copolymer chain on the absorption and field effect mobilities was studied. We synthesized a target random copolymer and compared it with two structurally relevant alternating copolymers, all consisting of 2,1,3-Benzothiadiazole (**BT**) as acceptor and 3-Hexylthiophene (**Th**) as donor units. Especially, bifunctional AB-type monomers were developed to obtain the desired randomly linked copolymer **r-BT-2Th**. We chose AA/BB-type monomers as well to obtain relevant alternating copolymers **a-BT-2Th** and **a-BT-1Th**. The systematic structural variation enables us to compare the copolymers in a precise manner. In dilute solutions **r-BT-2Th** and **a-BT-2Th** resemble closely in absorption spectra and have similar oxidation potentials regardless of random or alternating arrangement of donor and acceptor. In thin films, **a-BT-2Th** shows the lowest optical gap and depicts the highest field effect hole mobility of $1.5 \times 10^{-3} \text{ cm}^2 \text{ V}^{-1} \text{ s}^{-1}$.*

Keywords: Field effect mobility / Benzothiadiazole / Donor-acceptor copolymers

1 Introduction

In the last few years, syntheses of π -conjugated copolymers have been attracting huge interest for the use in polymer solar cells due to their promising optical and electronic properties.^[1-6] Using π -conjugated donor materials in combination with fullerene derivatives as acceptor, outstanding power conversion efficiencies of over 9 % have been already reached in single-junction and tandem cells.^[7] By developing new materials and device architectures, the operational mechanism of organic photovoltaics is more and more investigated, yet it remains not fully understood.^[8] To enable a rational macromolecular design with general validity for conjugated polymers, correlation of design strategy and the resulting properties has to be established. Not only a high mobility and intermolecular interaction, leading to π -electron delocalization, but also structural geometry parameters such as dihedral angle has to be taken into consideration.^[4, 9]

One general successful strategy to extend the absorption to longer wavelengths is the strict alternation of electron-rich (donor, D) and electron-deficient (acceptor, A) units in a conjugated polymer chain.^[1] But it is not verified if this strict alternation of D and A units is a basic necessity to tune the absorption. According to the principle of orbital overlap leading to bandgap reduction, only the proximity of the D and A units is required.^[10] Additionally, synthesizing the π -conjugated polymers in a random fashion would for example help to improve the solubility and processability for high molecular weight polymers. But the combination of different types of monomers in an arbitrary fashion may have an impact on the absorption, as well as on charge transport properties.

We recently showed in a combined theoretical and experimental study that the specific arrangement of D and A units in well-defined low molecular weight systems has no influence on the optical absorption.^[11] This raises the question whether the influence of D and A arrangement has consequences in polymer properties as well. Consequently, the following relevant questions have to be answered: Is there a difference in absorption between random and alternating copolymers? Does the sequential build-up of monomers influence the charge transport? In this contribution we address precisely these questions and compare a random copolymer with two relevant alternating copolymers. We deliberately use a combination of AB-type monomers to obtain a randomly linked copolymer, whereas conventional alternating copolymers were also obtained by AA/BB-type Suzuki polycondensation. With the use of AB-type monomers, each monomer can react with itself and the other comonomer.

Due to this synthesis strategy, it is possible to obtain directly comparable random and alternating copolymers.

We considered conjugated copolymers that incorporate 2,1,3-Benzothiadiazole units (BT) which are receiving intensive interest in recent years.^[12-17] 2,1,3-Benzothiadiazole derivatives exhibit a relatively high reduction potential as well as good air and thermal stability due to their fused-aromatic ring structure.^[18, 19] The BT moiety in D/A conjugated copolymers is one of the most studied electron-deficient units. It is usually directly coupled with electron-rich comonomers or with two thiophenes as spacer between the BT and electron-rich units.^[2, 20] In BT-thiophene based random copolymers, small amounts of incorporated BT units lead towards broadening of the absorption.^[21] The same tendency in optical properties has been observed on incorporating an additional acceptor unit.^[22]

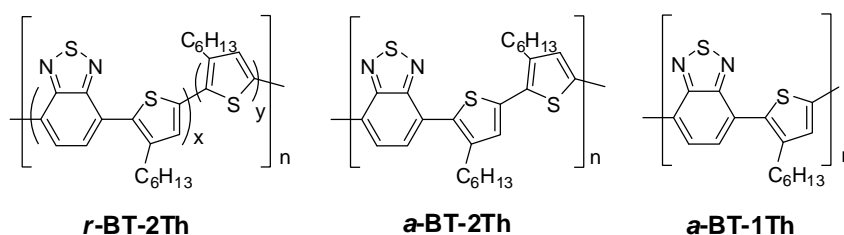


Figure 1: Random and alternating BT-Th based donor-acceptor conjugated copolymers

In particular we synthesized three copolymers consisting of 2,1,3-Benzothiadiazole (as acceptor) and 3-Hexylthiophene (as donor) units via Suzuki-Miyaura polycondensation (see Fig. 1). We synthesized the random copolymer **r-BT-2Th**, where BT-1Th units (M1) are randomly linked with an additional thiophene unit (M2) (*cf.* Scheme 1). To obtain comparable alternating copolymers, one must consider the fact that the BT-1Th unit can react with itself and with the additional thiophene unit. This results in a randomly linked copolymer where BT units are coupled with a varying number of thiophene units in between. Therefore, we synthesized on the one hand a strict alternating **a-BT-2Th** copolymer, where BT units alternate with a bithiophene unit and on the other hand a strict alternating copolymer **a-BT-1Th** where BT units alternate with just one thiophene unit. We want to investigate any possible differences or influences of a random order of donor-acceptor units versus a strictly alternating arrangement, with respect to the optical as well as field effect mobilities. Therefore, we studied the thermal, optical and charge transport properties of these polymers and compared them under one another.

2 Experimental section

2.1 Materials and methods

All reactions were carried out in dry glassware and under inert atmosphere of purified argon using Schlenk techniques. The reagents and solvents were purchased from Aldrich, ABCR, Acros or TCI. All reagents were used without further purification unless otherwise noted. Solvents used for precipitation and column chromatography were distilled under normal atmosphere. 4-[(Trimethylsilyl)ethynyl]phenylboronic acid pinacol ester was synthesized similar to a published procedure.^[23] ¹H-NMR (300 MHz) spectra were recorded on a Bruker AC 300 spectrometer at room temperature. Chemical shifts for ¹H-NMR spectra are referenced relative to residual protons in the deuterated solvents (CDCl₃ δ = 7.26 ppm, CD₂Cl₂ δ = 5.33 ppm, C₂Cl₄D₂ δ = 5.91 ppm). Abbreviations used for splitting patterns are s (singlet), d (doublet), t (triplet), m (multiplet) and b (broad). Mass spectroscopic data (MS) were obtained from a FINNIGAN MAT 8500 instrument. Differential scanning calorimetry experiments were conducted at a heating rate of 40 Kmin⁻¹ under a nitrogen atmosphere with a Perkin–Elmer Diamond DSC, calibrated with indium. Thermogravimetry measurements were conducted on a Mettler Toledo TGA/SDTA 851 under a nitrogen atmosphere at a heating rate of 10 Kmin⁻¹. Temperature decomposition (T_{d-5%}) correlates to the respective temperature at 5 % weight loss. UV/Vis spectra of solutions in *o*-Dichlorobenzene with a concentration of 0.02 mgmL⁻¹ and of films were recorded on a JASCO V-670 spectrophotometer at room temperature. Size exclusion chromatography (SEC) measurements were carried out in THF with two Varian Mixed-Columns (300 x 7.5 mm) at room temperature and a flow rate of 0.5 mLmin⁻¹ using UV (Waters model 486) with 254 nm detector wavelength for ***o*-BT-2Th**. Polystyrene standards and *o*-Dichlorobenzene as an internal standard were used for calibration. SEC measurements were carried out in 1,2,4-Trichlorobenzene with three PLgel Olexis-Columns (300 x 7.5 mm) at 150 °C using RI detector for ***r*-BT-2Th** and ***o*-BT-1Th**. Cyclic voltammetry measurements were carried out under moisture and oxygen free conditions using a standard three-electrode assembly connected to a potentiostat (model 263A, EG&G Princeton Applied Research) at a scanning rate of 50 mV s⁻¹. A Pt milli-electrode was used as working electrode. A platinum wire in the respective solvent plus conducting salt (tetra-*n*-butylammoniumhexafluorophosphate, 0.1M) was used as a counter electrode. The quasi-reference electrode consisted of an Ag-wire in a AgNO₃/acetonitrile solution (0.1 M). Each measurement was calibrated with the internal standard

ferrocene/ferrocenium. For **r-BT-2Th** and **α -BT-2Th** methylene chloride and for **α -BT-1Th** a mixture of *o*-Dichlorobenzene/acetonitrile (10/1; v/v) was used as solvent with 0.1 M conducting salt. The HOMO energy levels were calculated using the empirical relation: $E_{\text{HOMO}} = [-e(E^{1/2}(\text{x vs. Ag/AgNO}_3) - E^{1/2}(\text{Fc/Fc}^+ \text{ vs. Ag/AgNO}_3))] - 5.16$ eV for **r-BT-2Th** and **α -BT-2Th** and $E_{\text{HOMO}} = [-e(E^{1/2}(\text{x vs. Ag/AgNO}_3) - E^{1/2}(\text{Fc/Fc}^+ \text{ vs. Ag/AgNO}_3))] - 5.25$ eV for **α -BT-1Th**. The oxidation potentials of 5.16 eV and 5.25 eV for ferrocene/ferrocenium oxidation versus zero vacuum level are obtained from solvent dependent redox potentials.^[24]

2.2 Synthesis of polymers

2.2.1 Synthesis of *r*-BT-2Th

In a 20 mL high pressure microwave reactor tube, equipped with a sealed septum **M1** (227 mg, 0.448 mmol) and monomer **M2** (167 mg, 0.448 mmol) were dissolved in tetrahydrofuran (6 mL) and an aqueous solution of K₂PO₄ (2 M, 1.05 mL) were added to the solution and degassed with Argon for 5 min. Afterwards Pd₂(dba)₃ (16.4 mg, 0.0179 mmol) and [(*t*-Bu)₃PH]BF₄ (10.4 mg, 0.0358 mmol) were added, then the tube was sealed and degassed with Argon for 15 min. The reaction was heated 39 h at 80 °C (oil bath temperature). The end-capping procedure was performed in 2 separate steps. After cooling to room temperature, a degassed solution of 4-[(Trimethylsilyl)ethynyl]phenylboronic acid pinacol ester (268 mg, 0.895 mmol) in 3 mL tetrahydrofuran was added first, followed by heating for 27 h at 80 °C. After cooling to room temperature, degassed bromobenzene (281 mg, 1.79 mmol) was added, followed by heating for 41 h at 80 °C. After cooling to room temperature the polymer was dissolved in chlorobenzene, extracted with water and precipitated into methanol. The crude polymer was collected by filtration, dried and loaded into an extraction thimble to be washed with methanol, acetone, *n*-hexane and methylene chloride. The methylene chloride fraction was freeze dried from benzene to afford a dark solid. Yield: 130 mg (31 %).

¹H-NMR (300 MHz, CHCl₃): δ ppm 8.29–7.51 (m, 1.7H-*ArH*); 7.21–6.91 (m, 0.5H-*ArH*); 3.06–2.51 (m, 2H- α -H); 1.92–1.58 (m, 2H- β -H); 1.51–1.11 (m, 6H, -CH₂-); 1.03–0.72 (m, 3H, -CH₃).

UV/Vis (*o*DCB, nm): 532 nm.

SEC: M_w: 21970 g mol⁻¹; M_p: 18833 g mol⁻¹; M_w/M_n: 2.03.

2.2.2 Synthesis of α -BT-2Th

In a 20 mL high pressure microwave reactor tube, equipped with a sealed septum 2,1,3-Benzothiadiazole-4,7-bis(boronic acid pinacol ester) **M3** (204.9 mg, 0.53 mmol) and compound **M4** (261 mg, 0.53 mmol) were dissolved in toluene (7 mL). Two drops of Aliquat 336, an aqueous solution of Na₂CO₃ (1 M, 1.75 mL) and Pd(PPh₃)₄ (12.2 mg, 0.011 mmol) were added to the solution. Then the tube was sealed and degassed with Argon for 25 min. The reaction was heated 6 days at 120 °C (oil bath temperature). The end-capping procedure was performed in 2 separate steps. After cooling to room temperature, a degassed solution of phenylboronic acid pinacol ester (108.16 mg, 0.53 mmol) in 3 mL toluene was added first, followed by heating for 5 h at 120 °C. After cooling to room temperature, degassed bromobenzene (166.43 mg, 1.06 mmol) was added, followed by heating for 17 h at 120 °C. After cooling to room temperature the polymer was dissolved in chlorobenzene, extracted with water and precipitated into methanol. The crude polymer was collected by filtration, dried and loaded into an extraction thimble to be washed with methanol, ethanol, acetone and methylene chloride. The methylene chloride fraction was freeze dried from benzene to afford a dark solid. Yield: 173 mg (35 %).

¹H-NMR (300MHz, CD₂Cl₂): δ ppm 8.19–6.88 (b, 2.6H-*ArH*); 3.03–2.52 (m, 2H- α -H); 1.89–1.58(m, 2H- β -H); 1.52–1.13(m, 6H, -CH₂-); 1.05–0.71(m, 3H,-CH₃).
UV/Vis (*o*DCB, nm): 544 nm.

SEC: M_w: 10780 gmol⁻¹; M_p: 11110 gmol⁻¹; M_w/M_n: 1.66.

2.2.3 Synthesis of α -BT-1Th

In a 20 mL high pressure microwave reactor tube, equipped with a sealed septum **M1** (300 mg, 0.591 mmol) was dissolved in tetrahydrofuran (4 mL) and an aqueous solution of K₂PO₄ (2 M, 0.7 mL) were added to the solution and degassed with Argon for 5 min. Afterwards Pd₂(dba)₃ (10.8 mg, 0.0118 mmol) and [(*t*-Bu)₃PH]BF₄ (6.8 mg, 0.0236 mmol) were added, then the tube was sealed and degassed with Argon for 15 min. The reaction was heated 24 h at 80 °C (oil bath temperature). The end-capping procedure was performed in 2 separate steps. After cooling to room temperature, a degassed solution of 4-[(Trimethylsilyl)ethynyl]phenylboronic acid pinacol ester (177.5 mg, 0.591 mmol) in 2 mL tetrahydrofuran was added first, followed by heating for 27 h at 80 °C. After cooling to room temperature, degassed bromobenzene (185.6 mg, 1.18 mmol) was added, followed by heating for 36 h at 80 °C. After cooling to room temperature the polymer was dissolved in chlorobenzene and precipitated into methanol. The crude polymer was collected by filtration, washed several times

with methanol and methylene chloride, dried and dissolved with chlorobenzene after which it was precipitated into a mixture of tetrahydrofuran/methanol (1/2; v/v). The polymer was freeze dried from benzene to afford a dark solid. Yield: 100 mg (56 %). $^1\text{H-NMR}$ (300MHz, $\text{C}_2\text{Cl}_4\text{D}_2$): δ ppm 8.18–6.96 (b, 3.5H-*ArH*); 3.04–2.35 (m, 2H- α -*H*); 1.85–1.55 (m, 2H- β -*H*); 1.41–1.06 (m, 6H, - CH_2 -); 0.91–0.67 (m, 3H, - CH_3). UV/Vis (*o*DCB, nm): 563 nm. SEC: M_w : 22198 g mol^{-1} ; M_p : 16631 g mol^{-1} ; M_w/M_n : 1.72.

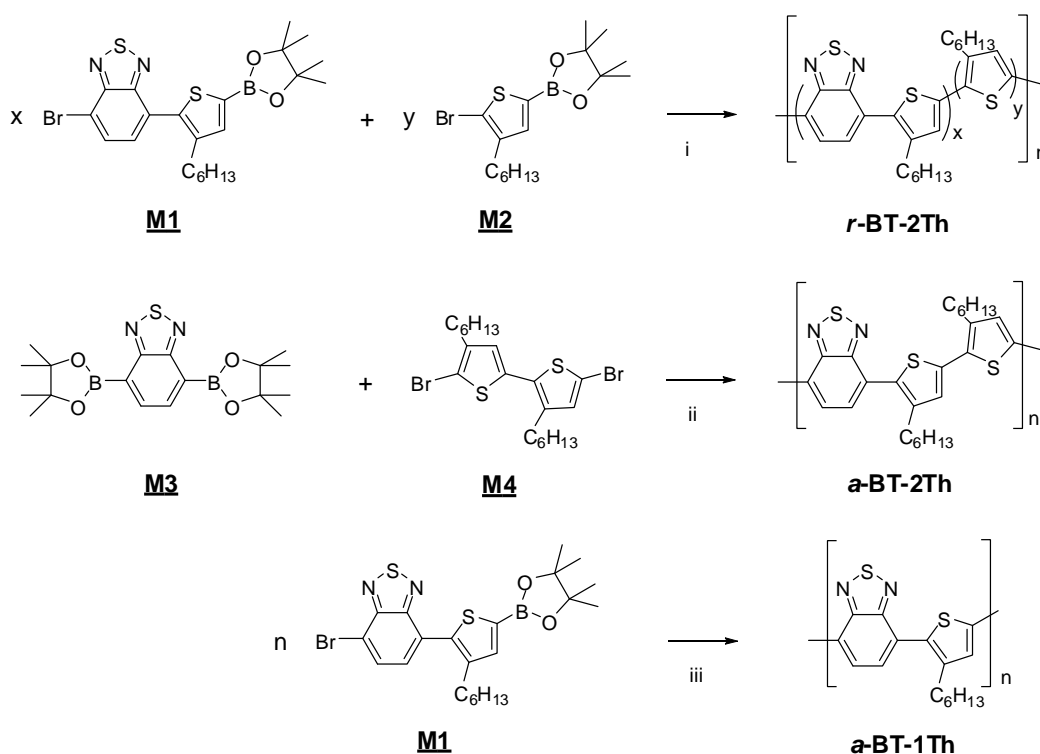
2.3 OFET Device Fabrication and Measurement

As transistor devices we used heavily *n*-doped silicon wafers as a bottom gate contact on which a 230 nm thermally grown SiO_2 layer is deposited as the gate dielectric which has a capacitance of approximately $1.5 \times 10^{-8} \text{ As/Vcm}^2$. The source and drain contacts were lithographically patterned Au interdigitating electrodes with a fixed channel width (10 μm). Prior to deposition of the semiconducting material the substrates were cleaned with acetone, H_2O and a mixture of $\text{H}_2\text{O}_2/\text{H}_2\text{SO}_4$ (1/3; v/v) and again rinsed with H_2O . After this treatment the devices were cleaned by sonication subsequently in H_2O , acetone and isopropanol (15 min each), followed by rinsing with *n*-hexane and drying under a flow of argon. The SiO_2 substrates were pretreated by plasma etching in a plasma chamber (Plasma Technology) for 10 min at 0.2 mbar. They were then exposed to hexamethyldisilazane (HMDS) vapor for 4 h in order to silanize the substrates. After HMDS exposure, the substrates were rinsed again with *n*-hexane and dried. The polymers were doctor-bladed from a 1 wt% (w/v) solution of ***r*-BT-2Th** or ***a*-BT-2Th** in chlorobenzene and from a 0.66 wt% (w/v) *o*-Dichlorobenzene solution of ***a*-BT-1Th**. This procedure and all subsequent device characterization steps were carried out in a glove box in inert gas ($\text{O}_2 < 13 \text{ ppm}$). The transistors were characterized using a HP4155A semiconductor parameter analyzer.

3 Results and discussion

3.1 Synthesis and characterization

The synthesis procedure of polymers is outlined in Scheme 1. The monomers were prepared according to published procedure.^[11] Following the synthetic route in Scheme 1, the randomly linked copolymer **r-BT-2Th** was synthesized from the asymmetrical AB-type BT-1Th monomer **M1** and another AB-type comonomer of thiophene (**M2**).



Scheme 1: Synthesis of copolymers **r-BT-2Th**, **a-BT-2Th** and **a-BT-1Th**. Reaction conditions: (i) = (iii) aq. K_2PO_4 (2M), $Pd(dba)_3$ / $[(t-Bu)_3PH]BF_4$ in THF at $80^\circ C$; (ii) aq. Na_2CO_3 (1M), $Pd(PPh_3)_4$ in toluene at $120^\circ C$.

Owing to this synthetic route utilizing AB-type monomers, the incorporation of a comonomer into the conjugated main chain is expected to be random. AA/BB-type monomers of BT (**M3**) and bithiophene (**M4**) were used to obtain the conjugated copolymer **a-BT-2Th** in which a BT unit alternates with a bithiophene unit. The alternating **a-BT-1Th** copolymer was synthesized utilizing the asymmetrical AB-type

monomer **M1** alone. All three conjugated copolymers were synthesized via palladium catalyzed Suzuki coupling polycondensation. The random and alternating copolymers were end-capped in order to eliminate any unwanted influence of reactive end groups. Details for the end-capping procedure can be found in the experimental section.

The electron-deficient BT unit has only limited positions for incorporating solubilizing substituents. Therefore, we chose hexyl side chains on the electron-rich thiophene units to assure sufficient solubility of the resulting copolymers. Whereas the resulting copolymer ***α*-BT-2Th** was completely soluble in common organic solvents like toluene, THF or chloroform, the higher molecular weight copolymers, ***r*-BT-2Th** and ***α*-BT-1Th** showed poor solubility in these solvents but good solubility in *o*-Dichlorobenzene. Due to this, measurements of the copolymers were done in *o*-Dichlorobenzene solution.

The number average molecular weights of these copolymers were determined using size exclusion chromatography (SEC) method. The SEC traces of the copolymers are shown in Figure 2, the respective data are summarized in Table 1. The SEC traces were measured on an analytical SEC setup with THF as the eluant for ***α*-BT-2Th** and using high-temperature SEC in 1,2,4-Tri-chlorobenzene as eluant for ***r*-BT-2Th** as well as ***α*-BT-1Th**. Polydispersity indices (M_w/M_n) of 2.03 for ***r*-BT-2Th**, 1.66 for ***α*-BT-2Th** and 1.72 for ***α*-BT-1Th** were obtained. Due to the broad PDI values, the corresponding peak molecular weights (M_p) are also given. The M_p s were found to be 18,833 g mol^{-1} for ***r*-BT-2Th**, 11,110 g mol^{-1} for ***α*-BT-2Th** and 16,631 g mol^{-1} for ***α*-BT-1Th**.

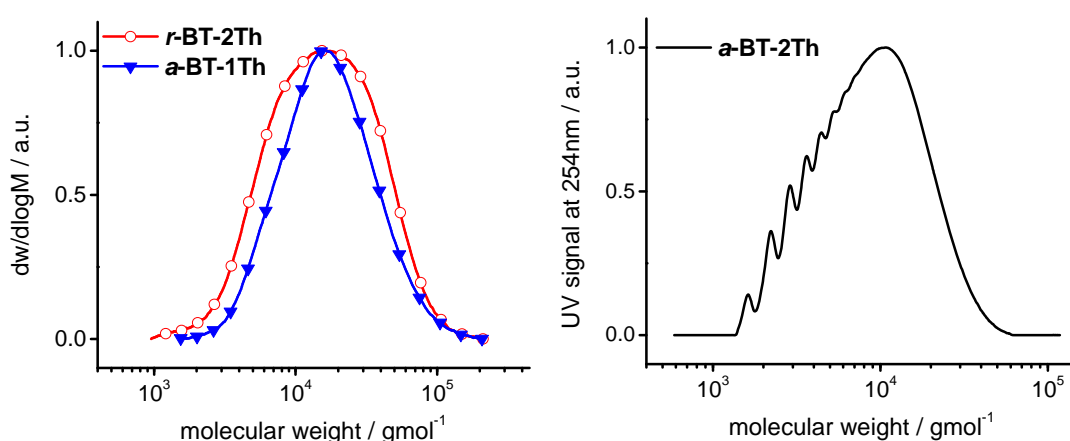


Figure 2: SEC traces of copolymers ***r*-BT-2Th**, ***α*-BT-1Th** and ***α*-BT-2Th**. (Eluant: THF for ***α*-BT-2Th** and 1,2,4-Trichlorobenzene for ***r*-BT-2Th** and ***α*-BT-1Th**. Polystyrene standards were used for calibration.)

Table 1: Number average molecular weight (M_n), peak molecular weight (M_p), polydispersity index (M_w/M_n) and thermal properties of copolymers ***r*-BT-2Th**, ***α*-BT-2Th** and ***α*-BT-1Th**.

| Sample | M_n / gmol^{-1} | M_p / gmol^{-1} | M_w / M_n | $T_{d-5\%} / ^\circ\text{C}$ | $T_g / ^\circ\text{C}$ |
|------------------|--------------------------|--------------------------|-------------|------------------------------|------------------------|
| <i>r</i> -BT-2Th | 10,802 | 18,833 | 2.03 | 427 | 72 |
| <i>α</i> -BT-2Th | 6481 | 11,110 | 1.66 | 428 | 60 |
| <i>α</i> -BT-1Th | 12,881 | 16,631 | 1.72 | 420 | 122 |

3.2 Thermal properties

The thermal decomposition of the copolymers was studied by thermogravimetric analysis (TGA) at a heating rate of $10\text{ }^\circ\text{Cmin}^{-1}$ under nitrogen purging. The TGA thermograms are shown in Figure 3A, the respective data are summarized in Table 1. All copolymers have a high thermal stability with 5 % weight loss temperature ($T_{d-5\%}$) $\geq 420^\circ\text{C}$. In particular $T_{d-5\%}$ was observed at 427, 428 and 420°C for ***r*-BT-2Th**, ***α*-BT-2Th** and ***α*-BT-1Th**, respectively.

The thermal transition behavior of all copolymers was investigated by differential scanning calorimetry (DSC). The DSC thermograms of the copolymers for the second heating and first cooling at a temperature rate of $40\text{ }^\circ\text{Cmin}^{-1}$ are shown in Figure 3B, the respective data are shown in Table 1. They exhibit glass transitions (T_g) which occur at temperatures of 72, 60 and $122\text{ }^\circ\text{C}$, for ***r*-BT-2Th**, ***α*-BT-2Th-2** and ***α*-BT-1Th** respectively. The glass transitions are in accordance to previous reports on similar conjugated copolymers.^[25] The noticeably quite high T_g for ***α*-BT-1Th** may be explained by the structural differences arising from less flexibility in comparison to the other copolymers. For all copolymers we do not observe any melting points within the temperature limits used in these measurements.

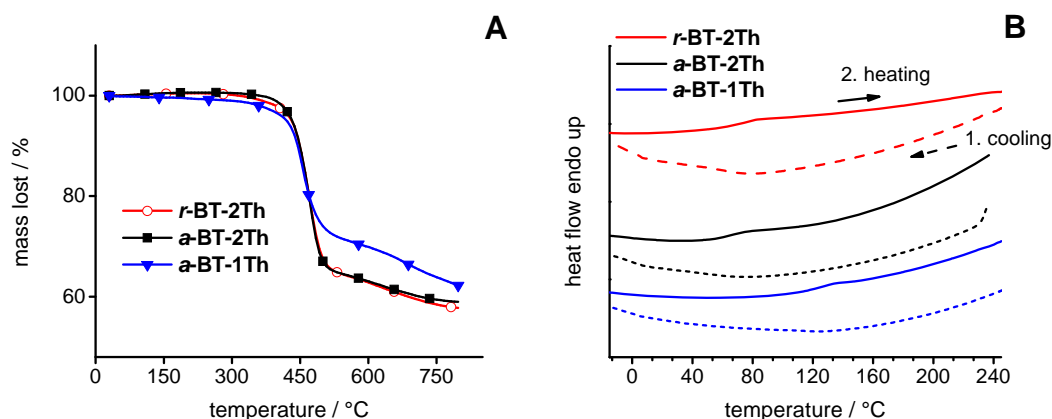


Figure 3: A) TGA thermograms of the copolymers, *r*-BT-2Th, *a*-BT-2Th and *a*-BT-1Th at the heating rate of 10 °Cmin⁻¹ under nitrogen purging. B) DSC thermograms of the copolymers at the heating rate of 40 °Cmin⁻¹ under nitrogen purging. The second heating and first cooling curve is shown for each copolymer.

3.3 Optical properties

The UV-Vis absorption of copolymers *r*-BT-2Th, *a*-BT-2Th and *a*-BT-1Th are measured in *o*-Dichlorobenzene solution, each at a concentration of 0.02 mgmL⁻¹. Thin film absorption spectra are measured at room temperature on glass slides. The corresponding spectra are depicted in Figure 4. The wavelengths of peak maxima of the UV/Vis spectra (λ_{abs}) in solution and thin film as well as the optical bandgaps (E_{opt}) are listed in Table 2. The E_{opt} values were calculated from the absorption edge of the absorption spectra ($E_{\text{opt}}=1240/\lambda$).

First we investigated the optical properties in very dilute solution to study intra-chain delocalization. From Table 2 and Figure 4A) it can be seen that there is no considerable difference in the absorption maxima on comparing the random copolymer *r*-BT-2Th with the alternating copolymer *a*-BT-2Th in solution. The maximum wavelengths of absorption are at 532 and 544 nm, and the E_{opt} values are 1.98 and 1.94 eV, respectively. Thus the optical properties of the random copolymer *r*-BT-2Th and the alternating copolymer *a*-BT-2Th are very similar. These absorption peak values are in the range of those observed for alternating donor-acceptor copolymers using BT and Th units.^[25, 26] This is also in agreement with our previous studies on well-defined low molecular weight D/A systems.^[11]

We earlier reported that the arrangement of the D and A units in a conjugated chain has only little influence on the lowest excitation energies due to a saturation of the

excitation energy. But small differences can be observed in the low-wavelength region (300-400 nm) of the absorption spectra in solution. These features are assigned to $\pi-\pi^*$ transitions of the donor units.^[25] Copolymer **r-BT-2Th** and copolymer **a-BT-2Th** have absorption peaks at around 322 nm, whereas **a-BT-2Th** exhibits an additional absorption peak at 364 nm.

On the other hand, polymer **a-BT-1Th** behaves differently in the long wavelength region. It shows a considerable red-shift of the absorption maximum (563 nm) compared to the random copolymer **r-BT-2Th** indicating a better intra-chain delocalization/planarization in **a-BT-1Th**. The inter-chain interactions influence the charge transport in conjugated polymers considerably.

In order to understand such effects, we studied optical properties of these polymers in thin films. All copolymers depict a broader absorption than the corresponding absorption in solution. The features in the low-wavelength region of the thin films do not differ remarkably from the appropriate ones in solution. As illustrated in Figure 4B), compared to the respective solution spectra, the thin film absorption spectra are red-shifted for **r-BT-2Th** ($\Delta\lambda = 25$ nm) and for **a-BT-2Th** ($\Delta\lambda = 28$ nm), whereas **a-BT-1Th** shows no bathochromic shift. As a result copolymer **a-BT-2Th** displays the most red-shifted absorption and depicts a significantly reduced optical bandgap (1.75 eV) in solid state compared to that in dilute solution (1.94 eV). This implies that copolymer **a-BT-2Th** exhibits stronger inter-chain interactions leading to an energetically more delocalized π -electron system than the copolymers **r-BT-2Th** or **a-BT-1Th**.

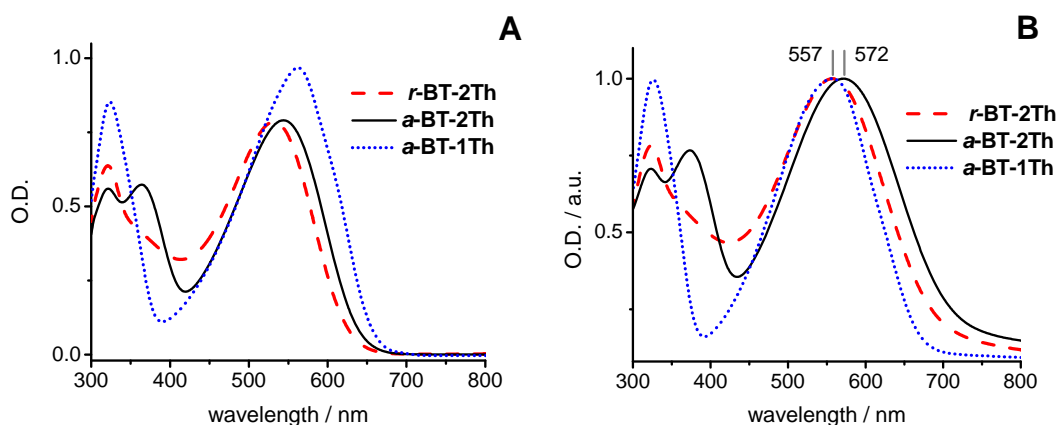


Figure 4: UV/Vis absorption spectra of the copolymers **r-BT-2Th**, **a-BT-2Th** and **a-BT-1Th** A) in *o*-Dichlorobenzene solution at a concentration of 0.02 mg mL^{-1} at room temperature and B) in thin films doctor-bladed from chlorobenzene solution on glass slides.

Table 2: Optical absorption (in solution and thin film) and electrochemical properties of copolymers *r*-BT-2Th, *a*-BT-2Th and *a*-BT-1Th.

| Sample | Solution | | Film | | HOMO / eV ^c |
|------------------|---|------------------------------------|---|------------------------------------|------------------------|
| | Absorption λ_{\max} / nm ^a | E _{opt} / eV ^b | Absorption λ_{\max} / nm ^a | E _{opt} / eV ^b | |
| <i>r</i> -BT-2Th | 532 | 1.98 | 557 | 1.80 | -5.81 |
| <i>a</i> -BT-2Th | 544 | 1.94 | 572 | 1.75 | -5.80 |
| <i>a</i> -BT-1Th | 563 | 1.88 | 557 | 1.86 | -5.26 |

^aWavelengths of peak maxima in UV/Vis spectra.

^bOptical bandgap estimated from the absorption edge of absorption in solution/thin film.

^cHOMO values calculated from half wave potentials of cyclic voltammetry measurements by calibrating vs. ferrocene and by taking into consideration the solvent effects.

3.4 Electrochemical properties

The electrochemical properties of the copolymers were investigated by cyclic voltammetry measurements in solution. The corresponding data are given in Table 2 and the cyclic voltammograms are shown in Figure 5. As expected, the copolymers exhibit a chemically reversible oxidation. Making use of the half-wave potentials, we calculated the HOMO energy levels by calibrating the measurements vs. ferrocene and by taking into consideration the solvent effect on oxidation potentials.^[24] The HOMO energy levels of *r*-BT-2Th (-5.81 eV) and *a*-BT-2Th (-5.80 eV) do not differ at all. This reveals that the copolymers consisting of BT and 2Th units have similar oxidation potentials in solution regardless of the arrangement in a random or alternating fashion. This is also in accordance with the observed optical bandgaps of 1.94 and 1.98 eV in solution. This additionally indicates that the oxidizability, which is a function of delocalization of π -electrons in a chain (in dilute solutions) for both polymers are very similar. The copolymer *a*-BT-1Th displays a quite different behavior concerning the electrochemical oxidation properties. It exhibits a higher HOMO (-5.26 eV) energy level, which is also in agreement with a lower optical bandgap of 1.88 eV observed in solution. This implies that the *a*-BT-1Th, lacking one thiophene unit, shifts the electrochemical properties to easier oxidation, meaning that the copolymer has an energetically more delocalized π -electron system in chain. This could arise from less steric interactions between the aromatic rings as a result of an extended wave function delocalization in dilute solution.^[27]

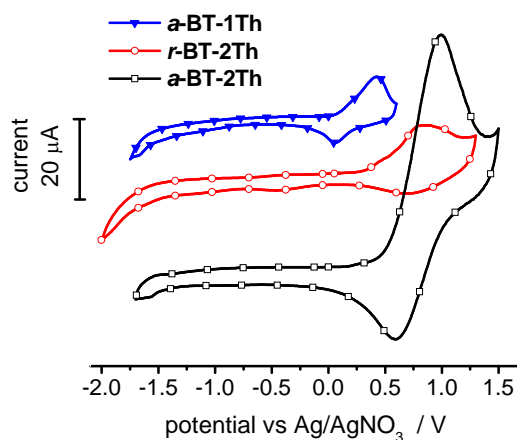


Figure 5: Cyclic voltammograms for the copolymers **a-BT-1Th**, **r-BT-2Th** and **a-BT-2Th** with ferrocene as internal standard (0.1M TBAF₆P, 50 mVs⁻¹; room temperature).

3.5 Charge transport properties

The next question of importance is: is there any influence of the arrangement of D and A units on the charge carrier mobility. For charge carrier transport, both inter-chain and intra-chain delocalization plays a role. In films, close contacts between chains favors inter-chain electronic coupling.^[28] The multiscale nature of charge transport processes depend very strongly on electronic coupling between the units.^[29] Organic field-effect transistors (OFETs) (Table 3) with bottom contacts and a bottom gate were used to investigate the hole transport properties of the different D/A copolymers. They were fabricated by doctor-blading the polymer solution onto hexamethyldisilazane-treated substrates. For the detailed procedure see experimental section. The channel between gold source and drain electrode was 20 μm long and 10 mm in width.

The charge carrier mobilities μ can be calculated from the transfer characteristics using the slope in the linear range of square root of drain-source current $I_{ds}^{1/2}$ versus gate voltage U_g plot with the following equation for the saturation regime: $I_{ds} = W/2L \mu_{sat} C_i (U_g - U_{th})^2$, where W is the channel width, L is the channel length, C_i is the dielectric capacitance and U_{th} is the threshold voltage. The output and transfer characteristics for devices **r-BT-2Th**, **a-BT-2Th** and **a-BT-1Th** are shown in Figure 6. The respective data are given in Table 4.

The devices show typical semiconductor features, such as a diode-like current increase with current saturation at high gate voltage in output curves (Fig.6 top row). All

devices exhibit p-channel performance. We monitor a more or less pronounced hysteresis in the devices. Such hysteresis phenomena are frequently mentioned in the literature.^[30] These electrical bistabilities originate for example from effects close to the channel such as trapping of charge carriers or charge injection from the semiconductor into the dielectric.

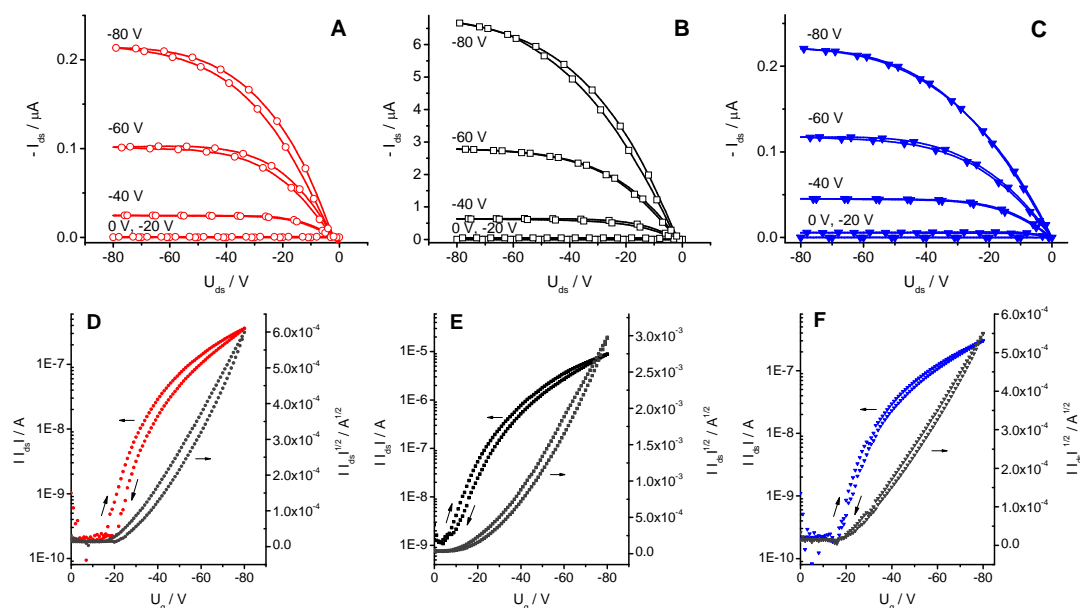


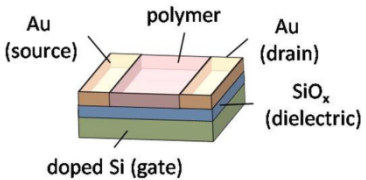
Figure 6: A/D = *r*-BT-2Th; B/E = *α*-BT-2Th; C/F = *α*-BT-1Th. Top row: output characteristics; bottom row: transfer characteristics of the polymer-transistors with a channel length of 20 μm and $U_{ds} = -80$ V.

The random copolymer *r*-BT-2Th exhibits a threshold voltage of -28 V and an on-off ratio of 10^3 . This is comparable to the alternating copolymer *α*-BT-2Th, which exhibits a threshold voltage of -26 V and an on-off ratio of 10^3 at large source-drain bias ($U_{ds} = -80$ V). But the alternating polymer *α*-BT-2Th is superior in terms of its hole carrier mobility of $1.5 \times 10^{-3} \text{ cm}^2\text{V}^{-1}\text{s}^{-1}$ which is two orders of magnitude higher than that of the random copolymer *r*-BT-2Th ($3.0 \times 10^{-5} \text{ cm}^2\text{V}^{-1}\text{s}^{-1}$). This may be explained by the observed absorption behavior of *α*-BT-2Th in thin films. Copolymer *α*-BT-2Th exhibited the lowest energy gap in thin film absorption properties, which shows the most red-shifted absorption spectra in contrary to the solution spectra. This can be attributed to stronger inter-chain interactions in copolymer *α*-BT-2Th leading to an energetically more delocalized π -electron system than in the copolymers *r*-BT-2Th or *α*-BT-1Th. The alternating copolymer *α*-BT-1Th is more similar to copolymer *r*-BT-2Th regarding its on-off ratio (10^3), its threshold voltage (-34 V) and its hole carrier mobility (5.4×10^{-5}

$\text{cm}^2\text{V}^{-1}\text{s}^{-1}$). We annealed the different devices but we do not detect any improvement in charge carrier mobilities.

These initial studies indicate that there is no difference in hole transport mobility between the random copolymer **r-BT-2Th** and the alternating copolymer **α -BT-1Th**, whereas hole transport mobility of copolymer **α -BT-2Th** differs by almost two orders of magnitude.

Table 3: Hole carrier mobility of polymers **r-BT-2Th**, **α -BT-2Th** and **α -BT-1Th** from OFET measurements. Results are mean values of at least three transistors. Schematic of a bottom gate bottom contact OFET device architecture.

| sample | r-BT-2Th | α-BT-2Th | α-BT-1Th |  |
|--|----------------------|-----------------------------------|-----------------------------------|---|
| hole carrier mobility, $\mu_h / \text{cm}^2\text{V}^{-1}\text{s}^{-1}$ | 3.0×10^{-5} | 1.5×10^{-3} | 5.4×10^{-5} | |

4 Conclusion

In conclusion, we have designed and synthesized a random copolymer and two relevant comparable alternating copolymers, with a varying arrangement of donor (thiophene) and acceptor (2,1,3-Benzothiadiazole) units in the polymer chain. We investigated these D/A copolymers to gain an understanding of the optical and charge transport properties as a function of the D/A arrangement. The D/A arrangement does not play any role in deciding the optical bandgap in comparable systems (*r*-BT-2Th vs. *α*-BT-2Th) in dilute solutions. But for *α*-BT-1Th, we observed a smaller bandgap and a higher HOMO energy level in solution. However, in thin films copolymer *α*-BT-2Th exhibits the smallest optical bandgap due to possibilities of an energetically more delocalized π -electron system. The randomly linked copolymer *r*-BT-2Th behaves very similar to *α*-BT-1Th regarding the field effect charge transport. The best hole transport mobility of $1.5 \times 10^{-3} \text{ cm}^2\text{V}^{-1}\text{s}^{-1}$ was measured for the alternating copolymer *α*-BT-2Th, which correlates with the smallest optical gap in solid state. This comparative study clearly elucidates the interdependence of the D/A arrangement in donor-acceptor copolymers and their material properties. It can be concluded that the multi-scale charge transport in solid state depends on inter-chain delocalization/coupling.

Acknowledgment

We gratefully acknowledge financial support from the German Research Foundation (SFB 840) and the Bavarian State Ministry of Science, Research, and the Arts for the collaborative Research Network "Solar Technologies go Hybrid". A.N. thanks the German Research Foundation (GRK 1640) for funding participations in conferences and workshops.

References

- [1] J. Roncali, *Chemical Reviews* **1997**, *97*, 173-206.
- [2] P.-L. T. Boudreault, A. Najari and M. Leclerc, *Chemistry of Materials* **2011**, *23*, 456-469.
- [3] H. J. Son, F. He, B. Carsten and L. Yu, *Journal of Materials Chemistry* **2011**, *21*, 18934-18945.
- [4] C. L. Chochos and S. A. Choulis, *Progress in Polymer Science* **2011**, *36*, 1326-1414.
- [5] E. Bundgaard and F. C. Krebs, *Solar Energy Materials and Solar Cells* **2007**, *91*, 954-985.
- [6] Z.-G. Zhang and J. Wang, *Journal of Materials Chemistry* **2012**, *22*, 4178-4187.
- [7] M. A. Green, K. Emery, Y. Hishikawa, W. Warta and E. D. Dunlop, *Progress in Photovoltaics: Research and Applications* **2013**, *21*, 827-837.
- [8] R. A. J. Janssen and J. Nelson, *Advanced Materials* **2012**, *25*, 1847-1858.
- [9] B. Balan, C. Vijayakumar, A. Saeki, Y. Koizumi and S. Seki, *Macromolecules* **2012**, *45*, 2709-2719.
- [10] Y.-J. Cheng, S.-H. Yang and C.-S. Hsu, *Chemical Reviews* **2009**, *109*, 5868-5923.
- [11] A. Karolewski, A. Neubig, M. Thelakkat and S. Kümmel, *Physical Chemistry Chemical Physics* **2013**, *15*, 20016-20025.
- [12] B. A. D. Neto, A. A. M. Lapis, E. N. da Silva Júnior and J. Dupont, *European Journal of Organic Chemistry* **2013**, *2013*, 228-255.
- [13] M. S. Miranda, M. A. R. Matos, V. M. F. Morais and J. F. Liebman, *The Journal of Chemical Thermodynamics* **2012**, *50*, 30-36.
- [14] M. C. Scharber, D. Mühlbacher, M. Koppe, P. Denk, C. Waldauf, A. J. Heeger and C. J. Brabec, *Advanced Materials* **2006**, *18*, 789-794.
- [15] S. H. Park, A. Roy, S. Beaupré, S. Cho, N. Coates, J. S. Moon, D. Moses, M. Leclerc, K. Lee and A. J. Heeger, *Nat Photon* **2009**, *3*, 297-302.
- [16] N. Blouin, A. Michaud and M. Leclerc, *Advanced Materials* **2007**, *19*, 2295-2300.
- [17] P. Anant, H. Mangold, N. T. Lucas, F. Laquai and J. Jacob, *Polymer* **2011**, *52*, 4442-4450.

- [18] Y. Morisaki, T. Ishida, H. Tanaka and Y. Chujo, *Journal of Polymer Science Part A: Polymer Chemistry* **2004**, *42*, 5891-5899.
- [19] B. A. DaSilveira Neto, A. S. A. Lopes, G. Ebeling, R. S. Gonçalves, V. E. U. Costa, F. H. Quina and J. Dupont, *Tetrahedron* **2005**, *61*, 10975-10982.
- [20] D. Mühlbacher, M. Scharber, M. Morana, Z. Zhu, D. Waller, R. Gaudiana and C. Brabec, *Advanced Materials* **2006**, *18*, 2884-2889.
- [21] B. Burkhart, P. P. Khlyabich, T. Cakir Canak, T. W. LaJoie and B. C. Thompson, *Macromolecules* **2011**, *44*, 1242-1246.
- [22] B. Burkhart, P. P. Khlyabich and B. C. Thompson, *Macromolecular Chemistry and Physics* **2013**, *214*, 681-690.
- [23] D. L. Browne, M. Baumann, B. H. Harji, I. R. Baxendale and S. V. Ley, *Organic Letters* **2011**, *13*, 3312-3315.
- [24] K. Gräf, M. A. Rahim, S. Das and M. Thelakkat, *Dyes and Pigments* **2013**, *99*, 1101-1106.
- [25] A. A. El-Shehawy, N. I. Abdo, A. A. El-Barbary and J.-S. Lee, *European Journal of Organic Chemistry* **2011**, *2011*, 4841-4852.
- [26] M. Jayakannan, P. A. van Hal and R. A. J. Janssen, *Journal of Polymer Science Part A: Polymer Chemistry* **2002**, *40*, 251-261.
- [27] L. Pandey, C. Risko, J. E. Norton and J.-L. Brédas, *Macromolecules* **2012**, *45*, 6405-6414.
- [28] D. Beljonne, G. Pourtois, C. Silva, E. Hennebicq, L. M. Herz, R. H. Friend, G. D. Scholes, S. Setayesh, K. Müllen and J. L. Brédas, *Proceedings of the National Academy of Sciences* **2002**, *99*, 10982-10987.
- [29] R. Noriega, A. Salleo and A. J. Spakowitz, *Proceedings of the National Academy of Sciences* **2013**, *110*, 16315-16320.
- [30] M. Egginger, S. Bauer, R. Schwödiauer, H. Neugebauer and N. Sariciftci, *Monatshefte für Chemie - Chemical Monthly* **2009**, *140*, 735-750.

7. *OPTICAL GAP TUNING IN THIOPHENE-SUBSTITUTED NAPHTHALENEDIIMIDES*

*Anne Neubig, Mathis-Andreas Muth and Mukundan Thelakkat**

Macromolecular Chemistry I, University of Bayreuth, 95440 Bayreuth, Germany.
E-mail: Mukundan.Thelakkat@uni-bayreuth.de

Prepared as manuscript.

Abstract

A series of low molecular weight naphthalenediimides carrying different thiophene donor units are synthesized from 2,6-dibromonaphthalene dianhydride by imidization and a subsequent Suzuki coupling reaction. The structure-property relationship for these donor-acceptor model compounds was elucidated by a systematic study of the optical and electrochemical properties. The thiophene substituents in the core positions enhance the absorption and influence the HOMO levels towards low band gap energy materials. With an increasing number of thiophene groups the optical gap can be selectively lowered to 1.81 eV by keeping the LUMO energy level constant at around 4 eV and raising the HOMO energy level. Owing to the strong absorption in the visible range, suitable HOMO/LUMO levels and remarkable electron mobility of $2.3 \times 10^{-3} \text{ cm}^2\text{V}^{-1}\text{s}^{-1}$, this class of donor-acceptor system is highly suited as potential electron acceptor material for various applications.

Keywords: absorption / semiconductors / low band gap / donor-acceptor / naphthalenediimide

Introduction

In recent years, various low band gap polymers have been synthesized for solar cell applications.^[1, 2] To achieve high performance in these devices, tuning a set of physical properties is essential. For example high solubility, low energy gap and high charge carrier mobility can be attained by modifying the molecular structure. Thus, low band gap materials are designed to absorb a large part of the solar spectrum, especially in the near-infrared region. A strategy to realize this involves the alternation of electron-rich and electron deficient moieties along the polymer chain.

A systematic study of factors influencing the position of the HOMO/LUMO energy levels in alternate donor-acceptor molecules is very important for the design of tailored low band gap materials.^[2-4] Naphthalenediimides or naphthalene-1,4,5,8-tetracarboxylic-*N,N'*-dialkyldiimide (NDIs) constitute a class of electron-deficient (acceptor) molecules having interesting physical and electronic properties as well as high electron transport mobility in organic field-effect transistors (OFETs). Polymers based on NDI acceptor units are known compounds for the use as electron acceptor (n-type) material.^[5] For example, Stille cross-coupling with thiophene donor units at 2,6-positions of the NDI leads to polymers carrying alternating NDI and thiophene units with high electron mobilities up to 0.85 cm²/Vs in OFETs.^[6] Furthermore, different core-substituted naphthalenediimide polymers are studied.^[7] A fundamental understanding of the structure-property relationship is a prerequisite for the molecular design for various application needs.

For ideal n-type materials in organic photovoltaic devices, HOMO (highest occupied molecular orbital) – LUMO (lowest unoccupied molecular orbital) energy levels are to be tuned to maximize the open circuit voltage and light harvesting. The band gap energy can be reduced in different ways - either by raising the HOMO or lowering the LUMO level of the active material or by bringing the two levels closer together simultaneously. It is known that the open-circuit voltage (V_{oc}) is linearly dependent on the difference of the HOMO level of a p-type material and the LUMO level of an n-type material.^[3, 8] For this reason, the reduction of the band gap in acceptor materials should be done by lifting up the HOMO level and keeping the LUMO level high. Moreover the LUMO level of the n-type material has to be lower (~ 0.3 eV) than the level of the corresponding p-type material to ensure efficient charge separation.

In this work we planned to synthesize highly soluble novel low molecular weight NDI-compounds carrying different donor units. We studied the optical and electrochemical properties in order to understand the factors influencing a lowering of the band gap energy. The final aim of this work is to selectively lower the band gap

energies of NDIs by raising the HOMO energy level.

To investigate the effect of donor substituents at the 2,6-core positions of an NDI moiety on the electronic and optical properties, different thiophene groups are introduced in the core positions (NDIs **8a**, **8b**, **8c**) and are compared with an unsubstituted NDI **3**. Cyclic voltammetry (CV), thermogravimetric analysis (TGA), differential scanning calorimetry (DSC) and UV-visible (UV/Vis) spectroscopy are performed to investigate the relationship between the donor-acceptor structure and the electronic, thermal and optical properties. In order to estimate the charge carrier mobility, in particular the electron mobility of the acceptor materials, we tested one selected T-NDI-T (**8b**) in a diode configuration by fitting the space-charge limited currents (SCLC) according to Mott-Gurney law. The chemical structures of the synthesized compounds **3**, **8a**, **8b** and **8c** are outlined in Figure 1.

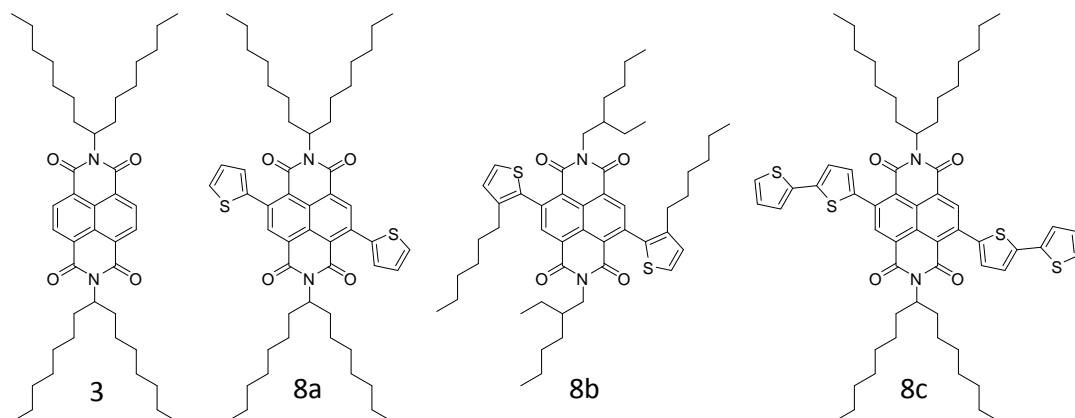
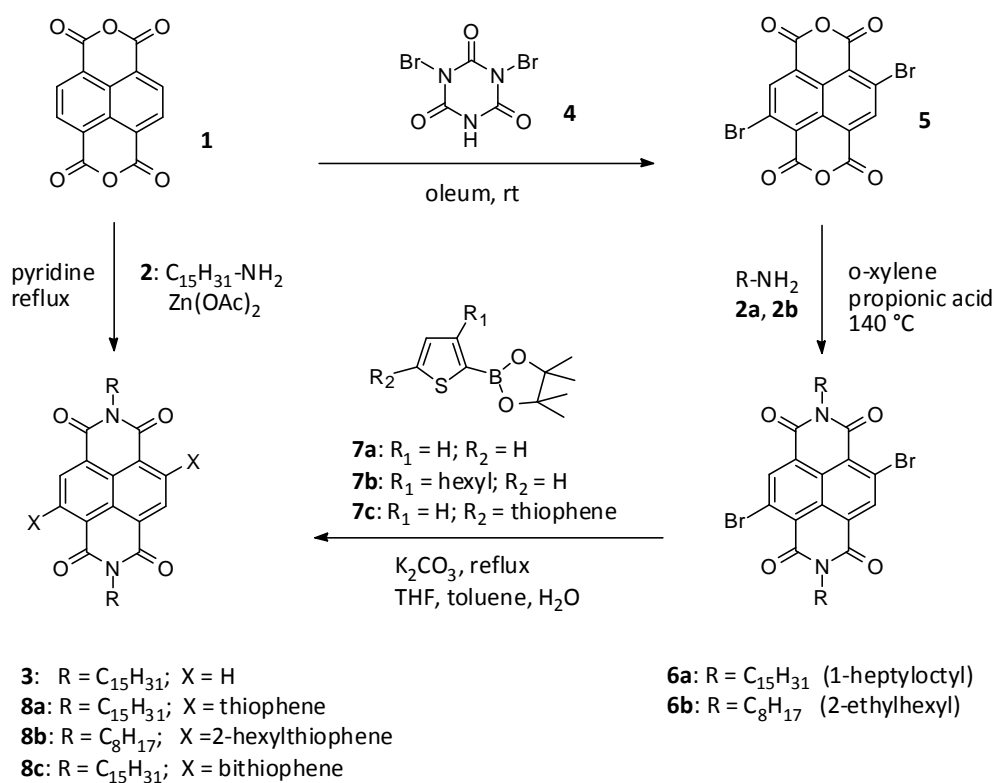


Figure 1: The structures of synthesized low molecular weight compounds **3**, **8a**, **8b** and **8c**.

Results and Discussion

Synthesis

The synthetic route is depicted in Scheme 1. The unsubstituted NDI **3** was directly obtained in high yields by imidization of commercially available naphthalene dianhydride **1** (NDA) with 1-heptyloctylamine **2a**. The preparation of the other derivatives **8a-c** is based on the common precursor 2,6-dibromonaphthalene-1,4,5,8-tetracarboxylic acid dianhydride **5**.^[9, 10] It has been reported that NDA can be brominated at its 2,6-positions with 1 equiv dibromoisocyanuric acid (DBI) **4** in fuming sulfuric acid, which is known as one of the most powerful brominating agents.^[10, 11] The bromination with dibromoisocyanuric acid could be performed in high yields according to literature methods.^[10] We obtained a mixture of products with varying levels of bromination. To enrich the mixture in the 2,6-dibromo NDA **5**, we used 2.5 equiv of DBI. Due to the low solubility in common solvents a separation of the 2,6-dibromo NDA is very challenging. This is not necessary because purification after the following imidization step is much easier.



Scheme 1: Synthetic route to compounds **3**, **8a**, **8b** and **8c**.

The published methods for the imidization reaction of the dibromo compound involve refluxing with the amines in acetic acid or in a mixture of *o*-xylene and propionic acid.^[9, 12] However, these procedures did not result in good yields for 1-heptyloctylamine **2a**. This is because preferably the well-known nucleophilic aromatic substitution occurs as a side reaction.^[10] But using 2-ethylhexylamine **2b** instead of 1-heptyloctylamine **2a** resulted in successful synthesis of NDI **6b**. 2-Ethylhexylamine is commercially available, while 1-heptyloctylamine **2** was prepared in one step from 8-pentadecanone through reductive amination by Borch method.^[13] This is described in detail in the experimental section.

Using Suzuki coupling techniques we converted both the brominated NDIs **6a,b** into soluble thiophene carrying NDIs **8a-c**.^[14] The pinacol boronic esters, which are stable towards water and oxygen were prepared and utilized for the Suzuki reaction.^[15] We used commercially available borylation reagents **7b** and **7c**, whereas **7a** was prepared in accordance with known methods.^[16] To ensure the solubility of the ethylhexyl-substituted NDI **8b**, we introduced alkyl-substituted thiophenes in the core positions. On the other hand, unsubstituted thiophenes are used with the longer heptyloctyl sidechains to get soluble derivatives **8a** and **8c**. The Suzuki reaction in the presence of a catalytic amount of Pd(Ph₃)₄ and K₂CO₃ as a base give the bis-coupled soluble products **8a-c**. All the coupling reactions take place at high yields (up to 81 %). Thus **8a**, **8b** and **8c** carrying thiophene, 3-hexylthiophene and bithiophene units respectively at 2,6-positions of NDI were obtained. The detailed characterization using various spectroscopy methods and mass spectrometry are given in the experimental section.

Optical Properties

UV/Vis absorption spectra of the derivatives **3**, **8a-c** were measured in chloroform solution at room temperature at concentrations of about 10⁻⁴-10⁻⁵ M. Figure 2a) demonstrates that **3**, **8a** and **8b** were found to display similar absorption pattern below 400 nm. The absorption spectra in solution show the characteristic fingerprint spectra of NDIs with vibronic bands of the S₀-S₁ transition at 342 nm, 360 nm, and 382 nm. However introducing bithiophene substituents on the core positions affects the vibronic pattern of the S₀ to S₁ transition considerably. **8c** shows different relative intensities for the corresponding vibronic transitions than **8a** and **8b**. More striking is the influence of thiophene substituents on the NDI core, which led to significant changes of the absorption spectrum at > 400 nm compared to the unsubstituted NDI **3**. Adding thiophene units (**8a-c**) at 2,6-positions leads to new broad absorption bands

in the green-red region > 400 nm. Furthermore, in this region **8a** and **8b** exhibit similar absorption spectra with maximum wavelength of absorption being 475 nm (**8a**) and 483 nm (**8b**). This indicates that the alkyl substituent on the donor unit has only a weak influence on electronic transition. By using bithiophene substituents in **8c** instead, the charge transfer band is significantly red shifted (~ 90 nm) to a maximum of 564 nm and the intensity is considerably higher than those of compounds **8a** and **8b**. This pronounced shift is caused by the strong donor character of the bithiophene unit and due to a more extended π -conjugation in **8c**. Additionally, the extinction coefficients increase with extended conjugation (*cf.* Fig. 2a)). This additional absorption band > 400 nm in **8a-c** is associated with an internal charge transfer (CT) transition from the electron-rich thiophene units to the electron-deficient NDI moiety. This assignment is in agreement with earlier works on naphthalenediimides.^[10, 17] A relevant question here is the influence of the strength of the donor (in terms of the number of thiophene donor units per NDI unit) in decreasing the energy gap towards low band gap materials in this class of compounds. Theoretical calculations were carried out for CT electronic transitions in such T-NDI-T systems for increasing number of thiophene units by Kümmel et al.^[18] They could observe a gradual decrease of band gap energy with increasing number of thiophene units and a saturation of energy gap with 4 thiophene units. Unlike the higher homologues perylenediimides, these compounds do not exhibit any fluorescence and virtually no emission could be observed for NDIs **3**, **8a-c**.^[19]

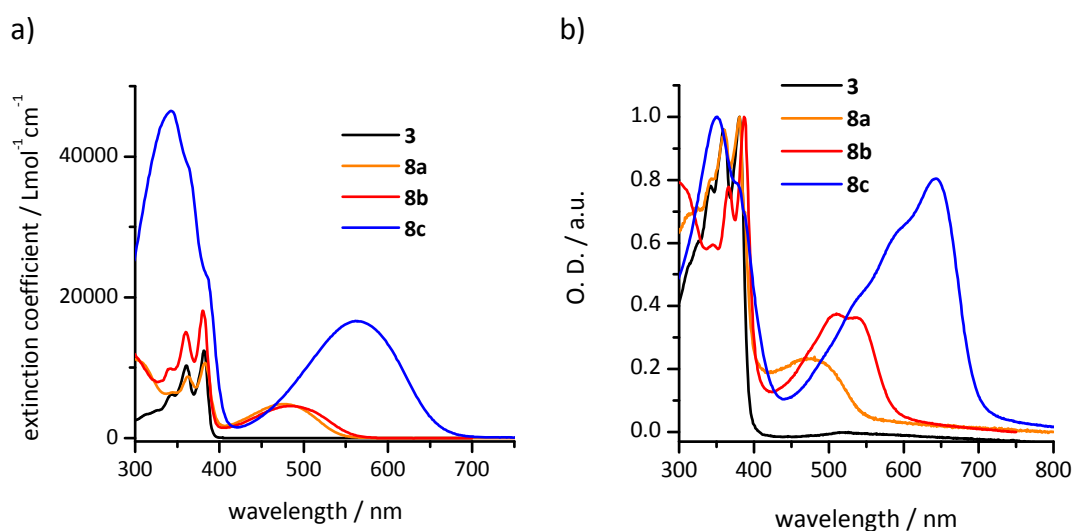


Figure 2: (a) Electronic absorption spectra of the NDI **3**, and T-NDI-T **8a**, **8b** and **8c** recorded in chloroform at concentrations of 2.5×10^{-5} M for **8c**, 5×10^{-5} M for **8b** and 1×10^{-4} M for **3** and **8a**. (b) Solid state electronic absorption spectra of the **3**, **8a**, **8b** and **8c**.

In thin films obtained from chloroform solution by spin-coating, the maxima of the short wavelength absorption < 400 nm are similar to those in solution (*cf.* Fig. 2b). Thus the absorption spectra in films display the same vibronic pattern of the S_0 to S_1 transition as in solution below 400 nm. But for the CT-absorption, these compounds exhibit different bathochromic shifts which reflect different levels of molecular planarization and π - π interactions in the solid state. Interestingly only films of **8b** and **8c** resulted in bathochromic shifts in the longer wavelength region with maxima at 510 nm (**8b**) and 642 nm (**8c**). Moreover these samples exhibit a more structured absorption profile, with additional weakly defined shoulders at 537 (**8b**), 539 and 592 nm (**8c**).

Redox Properties

Cyclic voltammetry (CV) measurements were carried out in solution using standard three-electrode cell geometry. An Ag/Ag⁺ electrode was used as the reference electrode in combination with a Pt milli-electrode as working electrode. Cyclic voltammograms are shown in Figure 3. The electrochemical properties of **3**, **8a-c** are summarized in Table 1. All the compounds exhibited two distinct reversible reduction peaks. No oxidation could be observed in the accessible measurement region of our system. The LUMO energy levels were calculated using the empirical relation: $E_{\text{LUMO}}(x) = [-e(E^{1/2}(x \text{ vs. Ag/AgNO}_3) - E^{1/2}(\text{Fc/Fc}^+ \text{ vs. Ag/AgNO}_3))] - 5.16 \text{ eV}$. The oxidation potentials of 5.16 eV for ferrocene/ferrocenium oxidation versus zero vacuum level are obtained from solvent dependent redox potentials.^[20]

In Figure 3 the peaks of the ferrocene-ferrocenium redox couple are also shown for illustration in the measurement for compound **8b**. Furthermore, the optical band gap energies were determined from the long wavelength absorption edge of the spectra in solution.

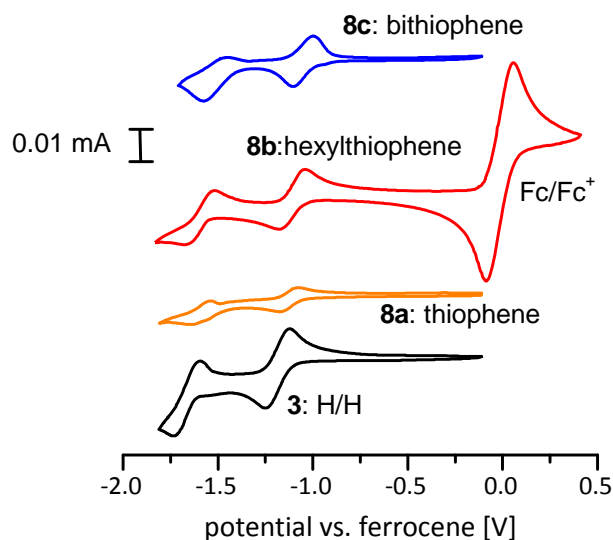


Figure 3: Cyclic voltammograms for the compounds **3**, **8a**, **8b** and **8c** with ferrocene as internal standard (0.1 M TBAF₆P, 50 mV/s, room temperature).

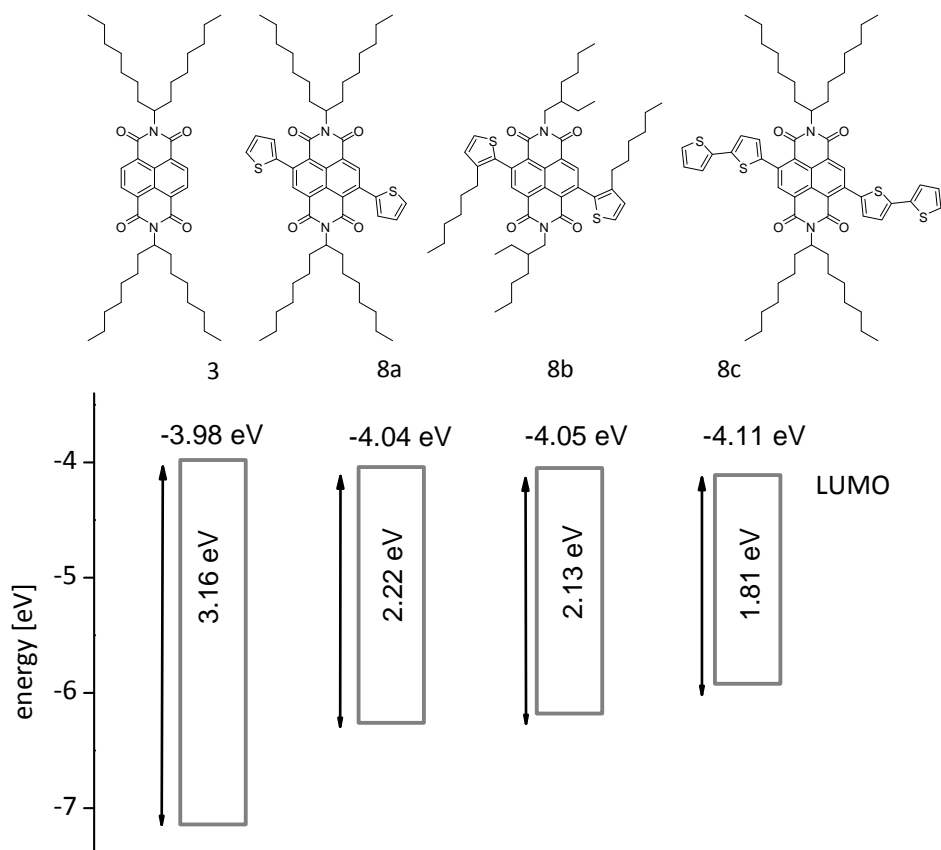
As seen in Figure 3, the electrochemistry of compounds **3**, **8a-c** is characterized by two well-resolved reversible one-electron reduction steps at potentials between -1 and -1.6 eV. The half wave potentials of the first and second reduction steps are in the same range for all four derivatives **3**, **8a-c**. This implies that the electrochemical reduction and thus the LUMO energy levels are not significantly affected by the attached thiophene units. But these donor substituents have strong influence on the HOMO values, as expected. The introduction of thiophene units in **8a-c** drastically reduce the optical gap and therefore move the HOMO energy level up compared to the unsubstituted compound **3**. Moreover, increasing the conjugation length of the donor from monothiophene (**8a**, **b**) to bithiophene (**8c**) the HOMO energy level is further shifted. As expected, the introduction of an alkyl substituent on the thiophene unit in **8b** has only a slight influence on the electrochemical properties.

On going from unsubstituted NDI **3** to substituted derivatives **8a-c** the optical gap is reduced from 3.16 to 1.81 eV. This shifts the HOMO energy level considerably. The electrochemical data in Table 1 clearly demonstrate that the band gap reduction is caused by raising the HOMO energy level by introducing increasing thiophene units. Otherwise the electron-withdrawing naphthalene diimide core is responsible for the reduction potential. Figure 4 illustrates the lowering of the optical gap with the corresponding changes in LUMO energy levels.

Table 1. Electrochemical data of compounds **3**, **8a**, **8b** and **8c**.

| | $E_{1/2}/V$ (1. red.) | $E_{1/2}/V$ (2. red.) | LUMO/eV | Optical gap/eV |
|-----------|--------------------------|--------------------------|---------|-------------------|
| 3 | -1.18 | -1.66 | -3.98 | 3.16 |
| 8a | -1.12 | -1.59 | -4.04 | 2.22 |
| 8b | -1.11 | -1.62 | -4.05 | 2.13 |
| 8c | -1.05 | -1.51 | -4.11 | 1.81 |

Electrochemical potentials (vs. Fc/Fc^+) in CH_2Cl_2 containing 0.1 M TBAPF₆. LUMO energy values are obtained by cyclic voltammetry.

**Figure 4:** LUMO energy levels and values for the optical gap of compounds **3**, **8a**, **8b** and **8c**.

Thermal Properties

The thermal properties of compounds **3**, **8a-c** were investigated by differential scanning calorimetry (DSC) as well as thermogravimetric analysis (TGA) in a nitrogen atmosphere. The TGA and DSC thermograms are shown in Figure 5 and 6. TGA revealed that all derivatives exhibit high thermal stability. Five percent weight loss was observed at 372 °C for NDI **3**, 388 °C for **8a**, 418 °C for **8b** and 392 °C for **8c**. Thus TGA analysis showed that the 2,6-substituted NDIs are thermally more stable than the unsubstituted NDI. Among these, **8b** is the most stable compound.

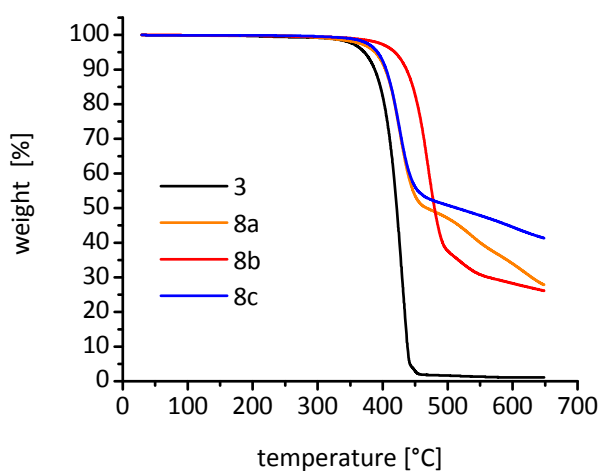


Figure 5: TGA thermograms of samples **3**, **8a-c** conducted at a temperature ramp rate of 10 Kmin⁻¹ under nitrogen atmosphere.

For DSC analysis three heating/cooling cycles were recorded for each sample to eliminate artifacts arising from residual solvent and/or H₂O. Figure 7 shows the second heating and the first cooling curves for each compound. The DSC thermogram of the unsubstituted NDI **3** does not show any transitions in the positive temperature region up to 250 °C, in which the compound is thermally stable. Due to this reason, NDI **3** was also analyzed in the low temperature region from -50 °C to 0 °C at a heating rate of 40 Kmin⁻¹. Here a glass transition at -30 °C could be observed. However, **8a-c** exhibit clear thermal transitions during the heating and/or cooling cycles. Sample **8a** was analyzed with a scan rate of 5 Kmin⁻¹. The corresponding thermogram shows a melting point at 98 °C. No recrystallization is observed in the cooling cycle. Instead, the recrystallization occurred at 55 °C in the next heating cycle. NDI **8b** shows more complex DSC thermograms with recrystallization at 54 °C in the cooling run and at 44 °C in the heating run. Furthermore **8b** reveals two endothermic peaks at 94 °C and at 138 °C in

the heating trace. In the case of bithiophene substituted derivative **8c**, single endothermic and exothermic transitions were observed at temperatures of 182 °C and 141 °C under heating and cooling cycles respectively. Interestingly, **8c** carrying bithiophenes exhibit higher transition temperatures. On comparing **8a**, **8b** and **8c**, the melting points are increasing from 98 °C for **8a** to 138 °C for **8b** to 182 °C for **8c**. The clear melting and recrystallization transitions of the substituted derivatives (**8a-c**) reveal that all compounds are crystalline.

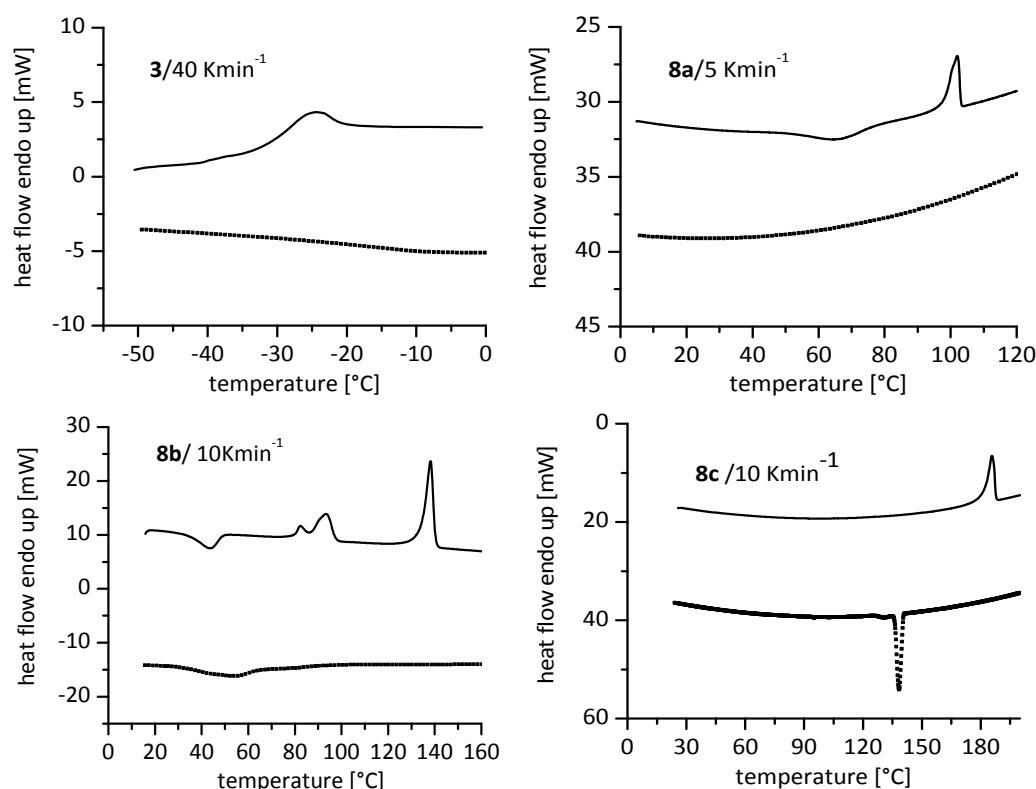


Figure 6: DSC thermograms of samples **3**, **8a-c** under nitrogen. The top solid line is from second heating and the bottom dot line is from first cooling run. The temperature ramp rate is shown inside, respectively.

Charge Carrier Mobility Measurements

A key parameter of the performance of devices like polymer solar cells or organic field effect transistors is the charge carrier mobility of the active material. Space-charge-limited current (SCLC) measurements were carried out to investigate carrier mobility of acceptor material NDI **8b**. The SCLC theory has been well established for mobility measurements.^[21, 22] We have estimated the electron mobility by in electron-

only device according to a procedure published.^[23] Due to unfavorable film forming properties of compound **8b**, 8 wt% of a high molecular weight polystyrene was added as a processing additive. The I - V characteristic of the device was recorded at room temperature in inert gas atmosphere and the experimental data was fitted according to Mott Gurney equation modified for field dependence.^[21]

$$J = \frac{9}{8} \cdot \epsilon_r \cdot \epsilon_0 \cdot \mu_0 \cdot e^{0.89 \cdot \gamma \cdot \sqrt{E}} \cdot \frac{V^2}{L^3} \quad (1)$$

where J is the current density, ϵ_r is the dielectric constant of the polymer (assumed to be 3^[24]), ϵ_0 is the permittivity of free space, μ_0 is the zero-field charge carrier mobility, γ is the field activation parameter, E is the electric field, L is the thickness of the active layer and V is the voltage drop across the device. The experimental data and the corresponding fit are depicted in Figure 7. The applied voltage (V_{ap}) was corrected for the built-in voltage (V_{bi}) from the differences in work-function of Calcium (2.9 eV) and ITO/PEDOT:PSS (5.1 eV).

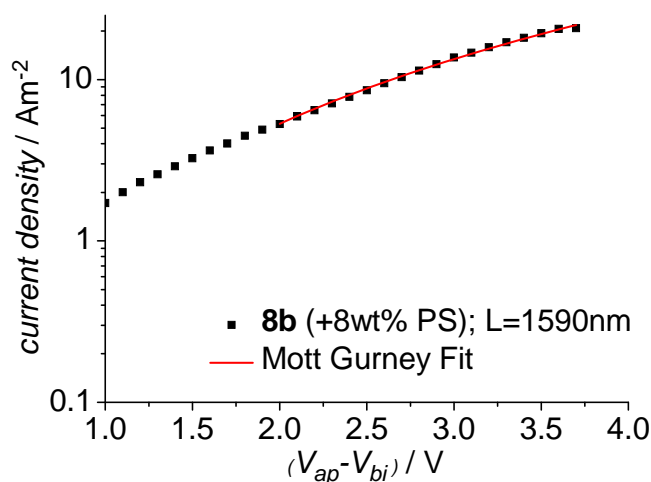


Figure 7: Current density J versus Voltage V plot for NDI **8b** at room temperature. The fit follows a V^2 dependence of current.

At high voltages the current is space charge limited only, assuming ohmic contacts to the injecting electrode. In this regime, the current density approximately scales with $J \sim V^2$, so the charge carrier mobility at zero-field μ_0 and the field activation parameter γ can be extracted using equation 1. The mobility at the maximum applied electric field within the device can be calculated using equation 2.

$$\mu = \mu_0 \cdot e^{\gamma \cdot \sqrt{E}} \quad (2)$$

The zero field electron mobility μ_{0e} is found to be $1.1 \times 10^{-3} \text{ cm}^2\text{V}^{-1}\text{s}^{-1}$ with a field activation parameter γ of $5 \times 10^{-4} \text{ cm}^{0.5}\text{V}^{-0.5}$ and an electron mobility of $2.3 \times 10^{-3} \text{ cm}^2\text{V}^{-1}\text{s}^{-1}$ for the maximum applied electric field.

Conclusion

In conclusion, three novel, soluble naphthalenediimide (NDI) derivatives with different thiophene (T) donor substituents at 2,6-positions were prepared and their optical and electrochemical properties were investigated. The results clearly correlate the structure of the T-NDI-T systems and their donor-acceptor properties. The naphthalenediimide core is responsible for the LUMO energy level and the thiophene donor units for the variation of HOMO level. The HOMO energy level shifts upward with increasing number of thiophene substituents, whereas the LUMO energy level is nearly constant. Thus, we are able to decrease the band gap selectively by raising the HOMO energy level, while keeping the LUMO energy level constant. The suitable energy levels and its strong absorption in the visible range and remarkable electron mobility make NDIs **8a-c** a highly promising candidates to be applied in organic electronics like photovoltaic devices or field-effect transistors.

Experimental Section

General Methods

All reactions were carried out in dry glassware and under inert atmosphere of purified argon using Schlenk techniques. The starting materials, naphthalene-1,4,5,8-tetracarboxylic acid dianhydride (**1**), 2-isopropoxy-4,4',5,5'-tetramethyl-1,3,2-dioxaborolane, 3-hexylthiophene, 8-pentadecanone, 4,4',5,5'-tetramethyl-1,3,2-dioxaborolan-2-yl-thiophene **7b**, cyanuric acid, 2-ethylhexylamine, ammonium acetate, zinc acetate and solvents were purchased from Aldrich, Fluka, Acros or TCI and were used as received. Dibromoisocyanuric acid (DBI) **4** was synthesized according to the literature.^[25] Solvents used for precipitation and column chromatography were distilled under normal atmosphere. ¹H spectra (300 MHz) were recorded on a Bruker AC 300 spectrometer at room temperature. Chemical shifts for ¹H-NMR spectra are referenced relative to residual protons in the deuterated solvents (CDCl₃ δ=7.26 ppm, CD₂Cl₂ δ=5.32 ppm, DMSO δ=2.50 ppm). Abbreviations used for splitting patterns are s = singlet, d = doublet, t = triplet, m = multiplet. Mass spectroscopic data (MS) were obtained from a FINNIGAN MAT 8500 instrument. UV-vis spectra were recorded with a Perkin Elmer Lambda 90 spectrophotometer. The thermal degradation was studied using a Mettler Toledo TGA/SDTA 851e with a heating rate of 10 Kmin⁻¹ under nitrogen atmosphere. Differential scanning calorimetry (DSC) was carried out with a Perkin Elmer differential scanning calorimeter (Diamond) under nitrogen atmosphere with heating and cooling rates of 10 Kmin⁻¹ unless otherwise noted. The instrument was calibrated with indium standards. Cyclic voltammetry (CV) measurements were carried under moisture and oxygen free conditions at room temperature using a standard three-electrode assembly connected to a potentiostat (model 263A, EG&G Princeton Applied Research) at a scanning rate of 50 mVs⁻¹. A Pt milli-electrode was used as working electrode. A platinum wire in CH₂Cl₂ plus conducting salt (tetra-*n*-butylammoniumhexafluorophosphate, 0.1 M) was used as counter electrode. The quasi-reference electrode consisted of an Ag-wire in a AgNO₃/acetonitrile solution. All measurements were calibrated with the internal standard ferrocene/ferrocenium couple (Fc/Fc⁺). The LUMO energy levels were calculated using the empirical relation: $E_{\text{LUMO}}(x) = [-e(E^{1/2}(x \text{ vs. Ag/AgNO}_3) - E^{1/2}(\text{Fc/Fc}^+ \text{ vs. Ag/AgNO}_3))] - 5.16 \text{ eV}$. The oxidation potentials of 5.16 eV for ferrocene/ferrocenium oxidation versus zero vacuum level are obtained from solvent dependent redox potentials.^[20] Column chromatography was performed on silica gel (Silica Gel 60, mesh size 0.02-0.063 mm). SCLC electron-only devices were fabricated

using the following structure: glass/ITO/PEDOT:PSS/active layer/Ca/Al. Commercial ITO coated glass substrates with a sheet resistance 13 Ohms per sq were cleaned using following sequence in an ultrasonic bath: water, acetone and 2-propanol. Each ITO substrate was patterned using photolithography techniques. After ozone treatment of the substrates for 5 min, PEDOT:PSS was spin-coated on the ITO surface and dried at 130 °C for 30 min. All following steps were carried out under nitrogen atmosphere. The active layer was blade coated at 80 °C from a 60 mg/mL toluene solution of NDI **8b** and 8 wt% of polystyrene ($M_n = 15.000.000$ g/mol). Afterwards the substrate was dried for 3 minutes at 80 °C. The top electrode (30 nm Ca/ 100 nm Al) was evaporated under high vacuum (1×10^{-6} mbar) through a shadow mask (active area of 4.5 mm²). The current-voltage characteristics of the devices was measured using a Keithley 2420 (I-V) Digital SourceMeter at room temperature. The film thickness used in the SCLC fit was determined using an Alphastep 500 surface profilometer.

1-Heptyloctylamine (**2**)

In a 1 L Schlenk flask 8-pentadecanone (25.0 g, 0.11 mol), ammonium acetate (84.78 g, 1.1 mol) and sodium cyanoborohydride (4.83g, 0.077 mol) were dissolved in dry MeOH (290 mL). This mixture was stirred at room temperature for 26 h. Then the reaction was terminated through drop wise addition of concentrated HCl (12 mL) and concentrated in vacuum. The yellow crude product was extracted with CHCl₃ (400 mL) two times. The combined extracts were dried with Na₂SO₄ and the solvent was evaporated in vacuum. Vacuum distillation led to colourless oil. Yield: 19.92g (80 %).

$R_f = 0.48$ (CHCl₃);

¹H NMR (300 MHz, CDCl₃, 25°C): $\delta = 2.66$ (s, 1 H, CH-NH₂), 1.44-1.12 (m, 26 H; CH₂), 0.86 ppm (t, ³J(H/H) = 6.3 Hz, 6 H; CH₃);

MS (EI): m/z (%): 226 (50) [M⁺] (calcd 227.4).

N,N'-Bis-(1-heptyloctyl)naphthalene-1,4,5,8-tetracarboxylic acid diimide (**3**)

In a 50 mL Schlenk flask 1,4,5,8-naphthalenetetracarboxylic acid dianhydride (**1**) (536.4 mg, 2.0 mmol) and zinc acetate (275.0 mg, 1.5 mmol) were dissolved in 16 mL dry pyridine. 1-heptyloctylamine (**2**) (1.638 g, 7.2 mmol) was added drop wise and the reaction mixture was stirred under reflux for 2 days. After cooling to room

temperature CH_2Cl_2 (100 mL) was added. The mixture was filtered through a short Celite column and was washed with CH_2Cl_2 . The organic phase was washed with H_2O (3 x 70 mL), dried with Na_2SO_4 and evaporated under reduced pressure. The crude orange product was purified by column chromatography (chloroform/methanol = 95:5, silica gel). Yield: 1.05 g (76 %).

$R_f=0.9$ ($\text{CHCl}_3/\text{MeOH}$ 95:5);

^1H NMR (300 MHz, CDCl_3 , 25°C): $\delta=8.73$ (s, 4 H; Ar-H), 5.23-5.08 (m, 2 H; N-CH), 2.30-2.11 (m, 4 H; CH_2), 1.91-1.75 (m, 4 H; CH_2), 1.41-1.09 (m, 40 H; CH_2), 0.82 ppm (t, $^3J(\text{H}/\text{H})=7.1$ Hz, 12 H; CH_3);

UV/Vis (CHCl_3): λ_{max} (ϵ)=382 (12389), 361 nm (10293 $\text{mol}^{-1}\text{dm}^3\text{cm}^{-1}$);

MS (EI): m/z (%): 686 (67) [M^+] (calcd 687.0).

2,6-Dibromonaphthalene-1,4,5,8-tetracarboxylic acid dianhydride (5)

1,4,5,8-Naphthalenetetracarboxylic acid dianhydride (**1**) (1.07 g, 3.99 mmol) was dissolved in fuming sulfuric acid (20 % SO_3 , 50 mL) under slight heating (60 °C) for 20 min. Then a solution of dibromoisocyanuric acid (**4**) (2.85 g, 9.93 mmol) in fuming sulphuric acid (20 % SO_3 , 90 mL) was added slowly (over a period of 6 hours) at room temperature. The resulting mixture was stirred for 1 h and then cautiously poured onto ice (600 g). Water (1 L) was added and the mixture was allowed to stand for 15 h at room temperature. The precipitated bright yellow solid was collected on a Büchner funnel, washed with HCl (0.5 M, 50 mL), H_2O (50 mL) and MeOH (40 mL) and dried under vacuum. The yellow crude product was used without further purification. Yield: 1.68g (98 %).

^1H NMR (300 MHz, $[\text{D}_6]\text{DMSO}$, 25°C): δ 8.79 (s, 2 H; Ar-H),

MS (EI): m/z (%): 426 (100) [M^+] (calcd 425.9).

N,N'-Bis-(1-heptyloctyl)-2,6-dibromonaphthalene-1,4,5,8-tetracarboxylic acid diimide (6a)

In a 50 mL Schlenk flask 2,6-dibromonaphthalene-1,4,5,8-tetracarboxylic acid dianhydride (**5**) (1.0g, 2.35 mmol) was dissolved in *o*-xylene (12 mL) and propionic acid (4 mL). Then 1-heptyloctylamine (**2**) (1.34 g, 5.9 mmol) was added. The mixture was stirred for 3 h at 140 °C. After cooling to room temperature the solvents were

removed in vacuum. The crude product was purified by column chromatography (hexane/ethyl acetate = 25:1, silica gel). After freeze drying from benzene a yellow solid was gained. Yield: 30 mg (2 %).

$R_f=0.67$ (petroleum ether/DCM 2:1);

m.p. 125.6°C;

$^1\text{H NMR}$ (300 MHz, CDCl_3 , 25°C): $\delta=8.97$ (s, 2 H; Ar-H), 5.20-5.05 (m, 2 H; N-CH), 2.29-2.06 (m, 4 H; CH_2), 1.93-1.75 (m, 4 H; CH_2), 1.41-1.09 (m, 40 H; CH_2), 0.83 ppm (t, $^3\text{J}(\text{H}/\text{H})=6.9$ Hz, 12 H; CH_3);

UV/Vis (CHCl_3): $\lambda_{\text{max}}(\epsilon)=406$ (10402), 386 (9414), 364 nm (14812 $\text{mol}^{-1}\text{dm}^3\text{cm}^{-1}$);

MS (EI) m/z : 844 (100) [M^+] (calcd 844.8).

***N,N'*-Bis-(2-ethylhexyl)-2,6-dibromonaphthalene-1,4,5,8-tetracarboxylic acid diimide (6b)**

In a 50 mL Schlenk flask 2,6-dibromonaphthalene-1,4,5,8-tetracarboxylic acid dianhydride (**5**) (1.0g, 2.35 mmol) was suspended in acetic acid (30 mL). The reaction mixture was stirred under reflux for 30 min. Then 2-ethylhexylamine (1.25 g, 9.7 mmol) was added drop wise. The mixture was stirred under reflux for further 2 h. After cooling to room temperature the mixture was concentrated under vacuum. The crude product was purified by column chromatography (DCM, silica gel). After freeze drying from benzene a yellow solid was gained. Yield: 470 mg (30 %).

$R_f=0.84$ (DCM);

$^1\text{H NMR}$ (300 MHz, CDCl_3 , 25°C): $\delta=8.99$ (s, 2 H; Ar-H) 4.22-4.07 (m, 4 H; N- CH_2), 2.01-1.84 (m, 2 H; CH), 1.48-1.18 (m, 16 H; CH_2), 0.99-0.80 (m, 12 H; CH_3);

MS (EI) m/z : 648 (100) [M^+] (calcd 648.4).

4,4',5,5'-Tetramethyl-1,3,2-dioxaborolan-2-yl-2-thiophene (7a)

n-BuLi (6.25 mL, 10.0 mmol) was added drop wise to a solution of thiophene (8.41 g, 10 mmol) in THF (20 mL) at -78 °C. The solution was stirred for 30 min at room temperature. After cooling to -78 °C 2-isopropoxy-4,4',5,5'-tetramethyldioxoborolane (1.86 g, 10.0 mmol) was added and the reaction mixture was stirred for 20 min at room temperature. The solvent was removed under vacuum and the residue was taken up in CHCl_3 . Under vigorous stirring, aqueous 5N HCl (50 mL) was added. The

organic phase was dried with MgSO_4 and evaporated in vacuum. The product (**7a**) was recrystallized from pentane. Yield: 1.21 g (58 %).

^1H NMR (300 MHz, CDCl_3 , 25 °C): δ =7.66 (dd, $J(\text{H}/\text{H})=3.4$, 0.8 Hz, 1 H; 3-thiophene), 7.64 (dd, $J(\text{H}/\text{H})=4.7$, 1.0 Hz, 1 H; 5-thiophene), 7.19 (dd, $^3J(\text{H}/\text{H})=4.8$, 3.5 Hz, 1 H; 4-thiophene), 1.35 ppm (s, 12 H; CH_3);

MS (EI) m/z : 210 (55) [M^+] (calcd 210.1).

***N,N'*-Bis-(1-heptyloctyl)-2,6-di(thien-2-yl)naphthalene-1,4,5,8-tetracarboxylic acid diimide (8a)**

To a solution of 4,4',5,5'-tetramethyl-1,3,2-dioxaborolan-2-yl-2-thiophene (**7a**) (28.6 mg, 0.136 mmol) and *N,N'*-bis-(1-heptyloctyl)-2,6-dibromonaphthalene-1,4,5,8-tetracarboxylic acid diimide (**6a**) (50 mg, 0.059 mmol) in toluene: THF (12 mL, 1:1), a solution of potassium carbonate (65mg, 0.47 mmol) in H_2O (2 mL) was added. The reaction mixture was degassed for 30 min by bubbling with $\text{Ar}_{(\text{g})}$. Then tetrakis(triphenylphosphine) palladium(0) (6.82 mg, 10 mol-%, 0.0059 mmol) was added and the mixture was stirred under reflux for 48 h. After cooling to room temperature, the crude product was filtered through a short Celite column, which was washed with THF (80 mL). The filtrate was dried over MgSO_4 and evaporated under reduced pressure to give a red solid. Then MeOH (50 mL) was added. The product was isolated by filtration, washed with MeOH and dried under vacuum. The product was purified by gradually column chromatography (petroleum ether/dichloromethane = 6:1 – 2:1, silica gel). After freeze drying from benzene a red solid was obtained. Yield: 41.0 mg (81 %).

$R_f=0.8$ (petroleum ether/DCM 2:1);

m.p. 98°C;

^1H NMR (300 MHz, CDCl_3 , 25°C): δ = 8.73 (s, 2 H; Ar-H), 7.55 (dd, $J(\text{H}/\text{H})=5.1$, 1.1 Hz, 2 H; thiophene), 7.30 (d, $^3J(\text{H}/\text{H})=3.3$ Hz, 2 H; thiophene), 7.19 (dd, $J(\text{H}/\text{H})=5.2$, 3.6 Hz, 2 H; thiophene), 5.18- 4.90 (m, 2 H; N-CH), 2.28-2.05 (m, 4 H; CH_2), 1.87-1.68 (m, 4 H; CH_2), 1.37-1.09 (m, 40 H; CH_2), 0.83 (t, $^3J(\text{H}/\text{H})=6.6$ Hz 12 H; CH_3);

UV/Vis (CHCl_3): λ_{max} (ϵ)=475 (4813), 383 (10640), 363 nm (8735 $\text{mol}^{-1}\text{dm}^3\text{cm}^{-1}$);

MS (EI): m/z (%): 850 (100) [M^+] (calcd 851.3).

***N,N'*-Bis-(2-ethylhexyl)-2,6-di-(3-hexylthien-2-yl)naphthalene-1,4,5,8-tetracarboxylic acid diimide (8b)**

To a solution of 4,4',5,5'-tetramethyl-1,3,2-dioxaborolan-2-yl-2-(3-hexyl)thiophene (**7b**) (568 mg, 1.93 mmol) and *N,N'*-bis-(2-ethylhexyl)-2,6-dibromonaphthalene-1,4,5,8-tetracarboxylic acid diimide (**6b**) (500 mg, 0.77 mmol) in toluene: THF (24 mL, 1:1), a solution of potassium carbonate (0.85 g, 6.16 mmol) in H₂O (4 mL) was added. The reaction mixture was degassed for 30 min by bubbling with Ar_(g). Then tetrakis(triphenylphosphine) palladium(0) (89 mg, 10 mol-%, 0.077 mmol) was added and the mixture was stirred under reflux for 21 h. After cooling to room temperature, the crude product was filtered through a short Celite column and washed with THF (100 mL). The filtrate was dried over MgSO₄ and evaporated under vacuum to give a dark red solid. Then MeOH (50 mL) was added. The product was isolated by filtration, washed with MeOH and dried under vacuum. The product was purified by column chromatography (DCM/ petroleum ether = 2:1, silica gel). After freeze drying from benzene a red solid was obtained. Yield: 458 mg (72 %).

R_f=0.83 (petroleum ether/DCM 1:3); m.p. 138°C;

¹H NMR (300 MHz, CDCl₃, 25°C): δ= 8.70 (s, 2 H; Ar-H), 7.45 (d, ³J(H/H)=5.1 Hz, 2 H; thiophene), 7.08 (d, ³J(H/H)=5.1 Hz, 2 H; thiophene), 3.99-4.14 (m, 4 H; N-CH₂), 2.41 (t, ³J(H/H)=7.5 Hz, 4 H; thiophene-CH₂), 1.98-1.81 (m, 2 H; N-CH), 1.60-1.44 (m, 4 H; CH₂), 1.43-1.06 (m, 28 H; CH₂), 0.95-0.82 (m, 12 H; CH₃), 0.77 ppm (t, ³J(H/H)=6.6 Hz, 6 H; thiophene-CH₃);

UV/Vis (CHCl₃): λ_{max} (ε)=483 (4540), 380 (18076), 360 nm (15050 mol⁻¹dm³cm⁻¹);

MS (EI) m/z: 648 (100) [M⁺] (calcd 648.4).

***N,N'*-Bis-(1-heptyloctyl)-2,6-di(2,2'-bithien-5-yl)-naphthalene-1,4,5,8-tetracarboxylic acid diimide (8c)**

To a solution of 5-(4,4',5,5'-tetramethyl-1,3,2-dioxaborolan-2-yl)-2,2'-bithiophene (**7c**) (46.1 mg, 0.158 mmol) and *N,N'*-bis-(1-heptyloctyl)-2,6-dibromonaphthalene-1,4,5,8-tetracarboxylic acid diimide (**6a**) (60 mg, 0.071 mmol) in toluene: THF (16 mL, 1:1), was added a solution of potassium carbonate (1.10 g, 7.96 mmol) in H₂O (4 mL). The reaction mixture was degassed for 30 min by bubbling with Ar_(g). Then tetrakis(triphenylphosphine) palladium(0) (1.6 mg, 2 mol-%, 1.47 μmol) was added and the mixture was stirred under reflux for 48 h. After cooling to room temperature, the crude product was filtered through a short Celite column and washed with THF (50

mL). The filtrate was dried over MgSO_4 and evaporated under reduced pressure to give a purple solid. Then EtOH (50 mL) was added. The product was isolated by filtration, washed with EtOH and dried under vacuum. The product was purified by gradual column chromatography (petroleum ether/DCM = 6:1 – 2:1, silica gel). After freeze drying from benzene a purple solid was obtained. Yield: 40.0 mg (56 %).

$R_f=0.8$ (petroleum ether/DCM 2:1);

m.p. 182°C;

^1H NMR (300 MHz, CDCl_3 , 25°C): $\delta=8.72$ (s, 2 H; Ar-H), 7.32 (dd, $J(\text{H}/\text{H})=5.1, 1.1$ Hz, 2 H; thiophene), 7.30-7.23 (m, 6 H; thiophene), 7.08 (dd, $J(\text{H}/\text{H})=5.3, 3.6$ Hz, 2 H; thiophene), 4.96-5.16 (m, 2 H; N-CH), 2.06-2.26 (m, 4 H; CH_2), 1.86-1.70 (m, 4 H; CH_2), 1.41- 1.12 (m, 40 H; CH_2), 0.82 ppm (t, $^3J(\text{H}/\text{H})=6.8$ Hz 12 H; CH_3);

UV/Vis (CHCl_3): λ_{max} (ϵ)=564 (16616), 338 nm (45992 $\text{mol}^{-1}\text{dm}^3\text{cm}^{-1}$);

MS (EI): m/z (%): 1014 (100) [M^+] (calcd 1015.5).

Acknowledgments

Financial support from DFG (GRK 1640 and SFB 840) is kindly acknowledged.

References

- [1] X. Guo, M. Baumgarten and K. Müllen, *Progress in Polymer Science* **2013**, *38*, 1832-1908; W. Li, R. Qin, Y. Zhou, M. Andersson, F. Li, C. Zhang, B. Li, Z. Liu, Z. Bo and F. Zhang, *Polymer* **2010**, *51*, 3031-3038; H.-J. Jhuo, P.-N. Yeh, S.-H. Liao, Y.-L. Li, Y.-S. Cheng and S.-A. Chen, *Journal of the Chinese Chemical Society* **2014**, *61*, 115-126.
- [2] Y. Liang, Z. Xu, J. Xia, S. T. Tsai, Y. Wu, G. Li, C. Ray and L. Yu, *Advanced Materials* **2010**, *22*, E135-E138.
- [3] A. J. Heeger, *Advanced Materials* **2014**, *26*, 10-28.
- [4] X. Zhan and D. Zhu, *Polymer Chemistry* **2010**, *1*, 409-419; Y. Zou, D. Gendron, R. Neagu-Plesu and M. Leclerc, *Macromolecules* **2009**, *42*, 6361-6365; R. A. J. Janssen and J. Nelson, *Advanced Materials* **2013**, *25*, 1847-1858.
- [5] Y.-J. Hwang, N. M. Murari and S. A. Jenekhe, *Polymer Chemistry* **2013**, *4*, 3187-3195; J. E. Anthony, A. Facchetti, M. Heeney, S. R. Marder and X. Zhan, *Advanced Materials* **2010**, *22*, 3876-3892; M. Sommer, *Journal of Materials Chemistry C* **2014**, *2*, 3088-3098.
- [6] H. Yan, Z. Chen, Y. Zheng, C. Newman, J. R. Quinn, F. Dotz, M. Kastler and A. Facchetti, *Nature* **2009**, *457*, 679-686.
- [7] Y. Wei, Q. Zhang, Y. Jiang and J. Yu, *Macromolecular Chemistry and Physics* **2009**, *210*, 769-775; H. Krüger, S. Janietz, D. Sainova, D. Dobрева, N. Koch and A. Vollmer, *Advanced Functional Materials* **2007**, *17*, 3715-3723; S. V. Bhosale, M. B. Kalyankar, S. V. Bhosale, S. J. Langford, E. F. Reid and C. F. Hogan, *New Journal of Chemistry* **2009**, *33*, 2409-2413; E. Ahmed, G. Ren, F. S. Kim, E. C. Hollenbeck and S. A. Jenekhe, *Chemistry of Materials* **2011**, *23*, 4563-4577.
- [8] Y.-J. Cheng, S.-H. Yang and C.-S. Hsu, *Chemical Reviews* **2009**, *109*, 5868-5923.
- [9] S. Chopin, F. Chaignon, E. Blart and F. Odobel, *Journal of Materials Chemistry* **2007**, *17*, 4139-4146.
- [10] C. Thalacker, C. Röger and F. Würthner, *The Journal of Organic Chemistry* **2006**, *71*, 8098-8105.
- [11] X. Guo and M. D. Watson, *Organic Letters* **2008**, *10*, 5333-5336; W. Gottardi, *Monatshefte für Chemie / Chemical Monthly* **1968**, *99*, 815-822.
- [12] Z. Chen, Y. Zheng, H. Yan and A. Facchetti, *Journal of the American Chemical Society* **2009**, *131*, 8-9.

- [13] R. F. Borch, M. D. Bernstein and H. D. Durst, *Journal of the American Chemical Society* **1971**, *93*, 2897-2904.
- [14] N. Miyaura and A. Suzuki, *Chemical Reviews* **1995**, *95*, 2457-2483; P. Piyakulawat, A. Keawprajak, A. Chindaduang, M. Hanusch and U. Asawapirom, *Synthetic Metals* **2009**, *159*, 467-472.
- [15] M. Murata, T. Oyama, S. Watanabe and Y. Masuda, *The Journal of Organic Chemistry* **1999**, *65*, 164-168.
- [16] Y. Dienes, S. Durben, T. Kárpáti, T. Neumann, U. Englert, L. Nyulászi and T. Baumgartner, *Chemistry - A European Journal* **2007**, *13*, 7487-7500.
- [17] D. Gosztola, M. P. Niemczyk, W. Svec, A. S. Lukas and M. R. Wasielewski, *The Journal of Physical Chemistry A* **2000**, *104*, 6545-6551; F. Würthner, S. Ahmed, C. Thalacker and T. Debaerdemaeker, *Chemistry - A European Journal* **2002**, *8*, 4742-4750.
- [18] A. Karolewski, T. Stein, R. Baer and S. Kümmel, *Journal of Chemical Physics* **2011**, *134*, 151101.
- [19] A. Wicklein, P. Kohn, L. Ghazaryan, T. Thurn-Albrecht and M. Thelakkat, *Chemical Communications* **2010**, *46*, 2328-2330; Z. Chen, V. Stepanenko, V. Dehm, P. Prins, L. D. A. Siebbeles, J. Seibt, P. Marquetand, V. Engel and F. Würthner, *Chemistry – A European Journal* **2007**, *13*, 436-449.
- [20] K. Gräf, M. A. Rahim, S. Das and M. Thelakkat, *Dyes and Pigments* **2013**, *99*, 1101-1106.
- [21] P. W. M. Blom, C. Tanase, D. M. d. Leeuw and R. Coehoorn, *AIP*, **2005**, p. 092105.
- [22] P. N. Murgatroyd, *Journal of Physics D: Applied Physics* **1970**, *3*, 151; Z. An, J. Yu, B. Domercq, S. C. Jones, S. Barlow, B. Kippelen and S. R. Marder, *Journal of Materials Chemistry* **2009**, *19*, 6688-6698.
- [23] M.-A. Muth, M. Carrasco-Orozco and M. Thelakkat, *Advanced Functional Materials* **2011**, *21*, 4510-4518.
- [24] C. Goh, R. J. Kline, M. D. McGehee, E. N. Kadnikova and J. M. J. Fréchet, **2005**, *86*, 122110.
- [25] H. G. O. Becker, *Organikum*, Wiley, Weinheim, **2000**, p. 371; W. Gottardi, *Monatshefte für Chemie / Chemical Monthly* **1967**, *98*, 507-512.

DANKSAGUNG

Ich möchte mich bei allen ganz herzlich bedanken, die direkt oder indirekt zum Gelingen dieser Arbeit beigetragen haben.

Mein erster Dank gilt hierbei meinem Doktorvater *Prof. Dr. Mukundan Thelakkat* für die Bereitstellung eines äußerst interessanten und abwechslungsreichen Themas. Seine immerwährende Bereitschaft zu anregenden Diskussionen, sowie die große Freiheit die er mir während des Forschungsprojektes gewährte, haben zum Gelingen dieser Arbeit beigetragen. Die Möglichkeit zur Teilnahme an nationalen und internationalen Fachtagungen und diversen Soft-Skills Seminaren war für mich sowohl fachlich als auch persönlich eine große Bereicherung. Vielen Dank für das entspannte Miteinander und die vielen Kochabende innerhalb unserer Gruppe!

Für die Bereitstellung eines sehr gut ausgestatteten Lehrstuhls bedanke ich mich bei dem Lehrstuhlinhaber *Prof. Dr. Hans-Werner Schmidt*.

Ein herzliches Dankeschön auch an *Prof. Dr. Peter Strohmriegl* für die begleitende Beratung als Mentor.

Vielen Dank an *Prof. Dr. Stephan Kümmel* aus der theoretischen Physik IV, der mir als Mentor beratend zur Seite stand und durch viele fachliche Diskussionen meinen Horizont erweitert hat. Ein großes Dankeschön an ihn und *Dr. Andreas Karolewski* für unsere erfolgreiche Kooperationsarbeit. Es hat Spaß gemacht mit euch an der Verringerung diversester „Lücken“, ob Bandlücke oder Sprachbarriere, zu arbeiten!

Ein großes Dankeschön an meine vielen Praktikanten für ihre tatkräftige Unterstützung bei der Synthese und der Durchführung zahlreicher Messungen: *Christian David Heinrich, Bodo Knörnschild, Tina Borke, Bernhard Glatz, Georg Lochner, Joseph Lange, Sonja Lippert* und *Mareike Stenglein*.

Ich möchte mich bei allen ehemaligen und aktuellen Mitarbeitern der MC I ganz herzlich bedanken. Dank eurer Hilfsbereitschaft, Unterstützung in fachlichen Belangen und die tolle Arbeitsatmosphäre bin ich immer wieder gerne zur Arbeit gegangen. Danke im speziellen an diejenigen, die für mich relevante Messgeräte betreuten: *Dr. Jayasundera Bandara* für die Einführung in die Solarzellenpräparation, *Dr. Katja Gräf* für die Einweisung und Unterstützung bei der Cyclovoltammetrie, *Dr. Ruth Lohwasser* für die Einweisung in den Transistormessstand, *Martin Hufnagel* für die MALDI-Messungen und *Dr. Mathis-Andreas Muth* für die SCLC Messungen. Vielen Dank dem GPC-Team für die Messung meiner Proben: *Dr. Klaus Kreger, Dr. Robin Pettau, Dr.*

Andreas Lang und im speziellen *Katharina Neumann* für die Einweisung in die präparative GPC. Vielen Dank an unsere Techniker/-innen für die literweise Bereitstellung destillierter Lösemittel sowie der generellen Unterstützung am Lehrstuhl. Großer Dank gilt *Petra Weiß* und *Christina Wunderlich*, die bei organisatorischen Angelegenheiten eine sehr große Hilfe sind. Ein großes Dankeschön an *Dr. Florian Wieberger*, *Dr. Andreas Ringk*, *Katharina Neumann* und *Tina Weller* für das genaue Korrekturlesen und eure Unterstützung.

Ein herzliches Dankeschön gilt auch allen Mitgliedern der AFuPo-Arbeitsgruppe. Neben dem Fachlichen ist auch das Soziale nicht zu kurz gekommen und unsere diversen Unternehmungen (Golf, Plätzchen backen, etc.) waren immer eine Bereicherung. Ein herzliches Dankeschön geht an *Helga Wietasch* die mit ihrer lockeren und lieben Art nicht nur bei der Synthese sondern auch bei anderen Problemen geholfen hat. Spezieller Dank gilt Christian David Heinrich, mit dem ich in einer sehr netten Arbeitsatmosphäre die letzte Zeit im Labor verbringen durfte.

Vielen Dank allen GraKo 1640 Mitgliedern. Durch unsere unterschiedlichen Blickwinkel auf verschiedene Themen und Diskussionen konnte ich viel dazulernen.

Einen großen Anteil zum Gelingen dieser Arbeit hatte neben dem Fachlichen auch das soziale Miteinander: die Motivation, Unterstützung und der Feierabend mit lieben Kollegen aber auch außeruniversitären Freunden. Ihnen allen möchte ich ein riesen Dankeschön aussprechen!

Ein besonderes Dankeschön an *Dr. Andreas Lang*, der mir in meiner ersten Zeit im Labor zur Seite stand. Nicht nur mit deinem fachlichen Rat sondern auch mit deiner direkten Art hast du das Laborleben enorm bereichert. Danke für unsere schöne (Labor-)zeit.

Bei *Katharina Neumann* möchte ich mich besonders bedanken. Ohne dich wäre die Zeit nur halb so schön gewesen. Vielen Dank für zahlreiche fachliche Hilfestellungen, Laborlachattacken sowie Rat und Tat in allen Lebenslagen.

Ein ganz großes Dankeschön an alle meine Freunde: ob noch von Daheim, aus der Schulzeit oder aus der Studienzeit, ihr habt mich immer wieder aufgeheitert, motiviert und abgelenkt. Danke!

Meiner ganzen Familie gebührt der größte Dank. Ohne eure Unterstützung und euer Vertrauen wäre ich wohl nicht so weit gekommen. Euch ist diese Arbeit gewidmet.

Ganz besonders möchte ich Thomas danken. Vielen lieben Dank für deine unermüdliche Unterstützung, deine Geduld und den grenzenlosen Rückhalt, den du mir gibst.



ERKLÄRUNG

Hiermit erkläre ich, dass ich die vorliegende Arbeit selbstständig verfasst und keine anderen als die angegebenen Quellen und Hilfsmittel verwendet habe. Die Arbeit wurde weder in gleicher noch in ähnlicher Form bei anderen Prüfungsbehörden zur Erlangung eines akademischen Grades vorgelegt.

Des Weiteren erkläre ich, dass ich keine Hilfe von gewerblichen Promotionsberatern bzw. -vermittlern oder ähnlichen Dienstleistern in Anspruch genommen habe und auch nicht beabsichtige diese zukünftig in Anspruch zu nehmen.

Weiterhin erkläre ich, dass ich bisher keinen anderweitigen Promotionswunsch unternommen habe.

Bayreuth, den 14. Mai 2014

Anne Neubig

